In presenting the dissertation as a partial fulfillment of the requirements for an advanced degree from the Georgia Institute of Technology, I agree that the Library of the Institute shall make it available for inspection and circulation in accordance with its regulations governing materials of this type. I agree that permission to copy from, or to publish from, this dissertation may be granted by the professor under whose direction it was written, or, in his absence, by the Dean of the Graduate Division when such copying or publication is solely for scholarly purposes and does not involve potential financial gain. It is understood that any copying from, or publication of, this dissertation which involves potential financial gain will not be allowed without written permission.

_____

_____

7/25/68

AN EXPERIMENTAL INVESTIGATION OF COMPRESSIBLE JET WALL ATTACHMENT AT LOW REYNOLDS NUMBERS

A THESIS

Presented to

The Faculty of the Graduate Division

by

Daniel Charles Anderson, Jr.

In Partial Fulfillment

of the Requirements for the Degree

Doctor of Philosophy in the School of Mechanical Engineering

Georgia Institute of Technology

March, 1969

AN EXPERIMENTAL INVESTIGATION OF COMPRESSIBLE JET

WALL ATTACHMENT AT LOW REYNOLDS NUMBERS

Approved:

Chairman

Date approved by Chairman: 5/9/67

ACKNOWLEDGMENTS

The author is very grateful to the faculty and staff of the School of Mechanical Engineering whose assistance and advice were invaluable throughout the course of this investigation and his studies at Georgia Tech.

The author is especially grateful to his advisor, Dr. Stephen L. Dickerson, who first suggested the use of the Knudsen number for modeling attaching jets and whose guidance, encouragement, and unlimited patience during this study is greatly appreciated. A special note of thanks goes to Dr. Walter O. Carlson, Dr. Gene T. Colwell, Dr. Prateen V. Desai, and Dr. Roger P. Webb, for their very special efforts and assistance as members of the thesis committee.

The author is indebted to Dale E. Jensen, a fellow student and co-designer of the experimental apparatus, and to Clifford R. Bannister, David W. Kiebel, John W. Davis and Joseph G. Doyal for their aid in construction and assembly of the equipment.

Finally, the author is very grateful to his wife, Freddie, who typed the first copy of the thesis and whose loving encouragement and sacrifice were instrumental in making this undertaking possible.

TABLE OF CONTENTS

Page

ACKNOWLEDGMENTS ii

LIST OF TABLES v

LIST OF ILLUSTRATIONS vii

SUMMARY x

NOMENCLATURE xii

Chapter

I. INTRODUCTION 1

Historical Background
Definition of Problem
Objectives

II. ANALYSIS OF ATTACHMENT POINT 13

Preliminary Free Jet Description
Olson's Attachment Model
Free Jet Analysis
Adaptation of the Model
Simplified Jet Attachment Model

III. EQUIPMENT AND INSTRUMENTATION 29

Wall Attachment Model
Vacuum Pump
Support Equipment
Probes
Instrumentation

IV. PROCEDURE 44

Preliminary Considerations and Adjustment of Flow Conditions
Measurements
Jet Attachment Experiments
Unattached Jet Experiments
Analytical Comparison

Page

V. DISCUSSION OF RESULTS 51

Data
Wall Attachment Results
Unattached Jet Results
Comparison to Olson's Analysis
Correlation Between x_c and L_R
Simplified Attachment Model

VI. CONCLUSIONS AND SUGGESTIONS FOR FURTHER RESEARCH . . . 83

Conclusions
Suggestions for Further Research

Appendix

A. EXAMINATION OF MODEL SIMILITUDE 88

B. COMPUTER PROGRAM FOR f_1 and f_2 92

C. DATA 96

Desired Flow Conditions
Data from Jet Attachment Experiments
Unattached Jet Experimental Data

D. SAMPLE CALCULATIONS 139

Calculation of Jet Velocities
Calculation of K_2

E. EQUIPMENT CAPABILITIES 146

F. EXPERIMENTAL ERRORS 150

LITERATURE CITED 153

OTHER REFERENCES 155

VITA 157

LIST OF TABLES

Table		Page
1.	Desired Flow Pressure Settings	97
2.	Actual Flow Pressure Settings, Jet Attachment	99
3.	Jet Attachment Distance $\left(\frac{L_R}{W}\right)$	100
4.	Attachment Wall Static Pressure Coefficient, $M_o = 0.5$	101
5.	Attachment Wall Static Pressure Coefficient, $M_o = 0.8$	102
6.	Attachment Wall Static Pressure Coefficient, $M_o = 1.94$	103
7.	Attachment Wall Static Pressure Coefficient, $M_o = 2.71$	105
8.	Control Volume Location Coefficient (K_1)	106
9.	Pressure Force Coefficient at Attachment (K_2)	106
10.	Actual Flow Pressure Settings Unattached Jet	108
11.	Unattached Jet Impact Pressure Measurements, $M_o = 0.5$, $K_n = 10^{-4}$	109
12.	Unattached Jet Impact Pressure Measurements, $M_o = 0.5$, $K_n = 5 \times 10^{-4}$	110
13.	Unattached Jet Impact Pressure Measurements, $M_o = 0.5$, $K_n = 10^{-3}$	111
14.	Unattached Jet Impact Pressure Measurements, $M_o = 0.5$, $K_n = 4 \times 10^{-3}$	112
15.	Unattached Jet Impact Pressure Measurements, $M_o = 0.8$, $K_n = 10^{-4}$	113
16.	Unattached Jet Impact Pressure Measurements, $M_o = 0.8$, $K_n = 5 \times 10^{-4}$	114

Page

17. Unattached Jet Impact Pressure Measurements, $M_o = 0.8$, $K_n = 10^{-3}$ 115

18. Unattached Jet Impact Pressure Measurements, $M_o = 0.8$, $K_n = 4 \times 10^{-3}$ 116

19. Unattached Jet Impact Pre-sure Measurements, $M_o = 1.94$, $K_n = 10^{-4}$ 117

20. Unattached Jet Impact Pressure Measurements, $M_o = 1.94$, $K_n = 5 \times 10^{-4}$ 118

21. Unattached Jet Impact Pressure Measurements, $M_o = 1.94$, $K_n = 10^{-3}$ 119

22. Unattached Jet Impact Pressure Measurements, $M_o = 1.94$, $K_n = 4 \times 10^{-3}$ 120

23. Unattached Jet Impact Pressure Measurements, $M_o = 2.71$, $K_n = 10^{-4}$ 121

24. Unattached Jet Impact Pressure Measurements, $M_o = 2.71$, $K_n = 5 \times 10^{-4}$ 122

25. Unattached Jet Impact Pressure Measurements, $M_o = 2.71$, $K_n = 10^{-3}$ 123

26. Unattached Jet Impact Pressure Measurements, $M_o = 2.71$, $K_n = 4 \times 10^{-3}$ 124

27. Dimensionless Free Jet Core Length $\left(\frac{x_c}{w}\right)$ 125

28. Centerline Velocity Decay Constant (m) 125

LIST OF ILLUSTRATIONS

Figure		Page
1.	Submerged Jet Adjacent to Wall	2
2.	Submerged Jet Attached to Wall	2
3.	Bistable Wall Attachment Fluid Amplifier Sketch	4
4.	Flow Ranges Investigated	7
5.	Single Wall Model Geometry	11
6.	Sketch of Free Jet and Centerline Velocity	14
7.	Attachment Model	16
8.	Free Jet Analytical Sketch	20
9.	Simplified Jet Attachment Model	24
10.	Experimental Model Sketch	30
11.	Representative Nozzle Blocks	32
12.	Apparatus Diagram	34
13.	Upstream Tank	36
14.	Static Pressure Probes	38
15.	Impact Probes	40
16.	Thermocouple Probe	41
17.	Flag Probe	41
18.	Equipment Photographs	43
19.	Static Pressure on Attachment Wall, $K_n = 10^{-4}$	52
20.	Static Pressure on Attachment Wall, $K_n = 5 \times 10^{-4}$	53
21.	Static Pressure on Attachment Wall, $K_n = 10^{-3}$	54
22.	Static Pressure on Attachment Wall, $K_n = 4 \times 10^{-3}$	55

Page

23. Attachment Distance and Mach Number 57

24. Attachment Distance and Reynolds Number 59

25. Assumed Eddy Viscosity and Reynolds Number Relationship . . . 62

26. Variation of "Apparent" Reynolds Number with Reynolds Number 63

27. Dimensionless Velocity Profiles, Core Region 65

28. Dimensionless Velocity Profiles, Developed Region 66

29. Dimensionless Core Length Variation with Reynolds Number, Centerline Decay Constant Variation with Reynolds Number . . 69

30. Control Volume Location Constant (K_1) 71

31. Pressure Force Constant (K_2) 72

32. Correlated Attachment Distance 75

33. Attachment Bubble Leakage Parameter 77

34. Simplified Model and Data from This Investigation 78

35. Simplified Model and Experimental Data, Several Geometries, Large R_e 79

36. Simplified Model, Laminar Incompressible Jet, $\frac{S}{w} = 0$ 81

37. Unattached Jet Centerline Velocity, $M_o = 0.5$, $K_n = 10^{-4}$ . . . 126

38. Unattached Jet Centerline Velocity, $M_o = 0.5$, $K_n = 5 \times 10^{-4}$ 127

39. Unattached Jet Centerline Velocity, $M_o = 0.5$, $K_n = 10^{-3}$ . . . 128

40. Unattached Jet Centerline Velocity, $M_o = 0.5$, $K_n = 4 \times 10^{-3}$ 129

41. Unattached Jet Centerline Velocity, $M_o = 0.8$, $K_n = 10^{-4}$ . . . 130

42. Unattached Jet Centerline Velocity, $M_o = 0.8$, $K_n = 5 \times 10^{-4}$ 131

43. Unattached Jet Centerline Velocity, $M_o = 0.8$, $K_n = 10^{-3}$ . . . 132

Page

44. Unattached Jet Centerline Velocity, $M_o = 0.8$, $K_n = 4 \times 10^{-3}$ 133

45. Unattached Jet Centerline Velocity, $M_o = 1.94$, $K_n = 10^{-4}$ . . 134

46. Unattached Jet Centerline Velocity, $M_o = 1.94$, $K_n = 5 \times 10^{-4}$ 135

47. Unattached Jet Centerline Velocity, $M_o = 1.94$, $K_n = 10^{-3}$ . . 136

48. Unattached Jet Centerline Velocity, $M_o = 1.94$, $K_n = 4 \times 10^{-3}$ 137

49. Unattached Jet Centerline Velocities, $M_o = 2.71$ 138

50. Distance to Discriminating Streamline, $M_o = 0.5$ 142

51. Beach-Russ Model 1000RP Typical Pumping Speed Curve 147

52. Envelope of Equipment Capabilities ($T_t = 537°R$, $w = 0.20$ inch) 149

SUMMARY

The subject of this research is the experimental investigation of steady state attachment of compressible jets to an adjacent offset inclined wall for jet Reynolds numbers well below those of previous research in the subject. The Reynolds numbers for this investigation were defined at the nozzle exit. Experiments were conducted for fixed values of Mach number and Knudsen number which was defined as the ratio of molecular mean free path at the jet nozzle exit to the nozzle exit width. The Knudsen number is proportional to the ratio of Mach number to Reynolds number. Previous compressible jet investigations have been limited to Knudsen numbers below 10^{-5} corresponding to Reynolds numbers above 10^{5}. The limits of this investigation are:

$$10^{-4} < K_n < 4 \times 10^{-3}$$

$$0.5 < M < 2.71$$

$$150 < R_e < 5 \times 10^{4}$$

A flow model one inch thick with 0.20 inch wide nozzle exit and an adjacent wall offset 0.30 inches from the nozzle lip and inclined at 10° to the nozzle centerline was constructed for the experiments. Sixteen flow conditions were investigated by providing rarefied flow of air through the model with a high displacement vacuum pump.

Adjacent wall static pressure measurements confirm that jet attachment occurred throughout the flow range. Attachment distance

along the wall was shown to be independent of Reynolds numbers for large values of Reynolds number and to have a maximum value in the lower Reynolds number range with other conditions fixed.

Unattached jet velocity profiles and centerline velocity variations were obtained with the adjacent wall removed from the model. A correlation between centerline velocities and distance along the jet centerline was empirically developed. A standard Gaussian correlation between jet mixing zone velocity and position exhibited fairly good agreement with experiment with some scatter of the data.

A very simple empirical correlation between unattached jet core length and attachment distance along the adjacent wall was developed and showed good agreement with experiment in this study although the variation of the correlation with changes in wall geometry was not determined.

Comparison of a semi-empirical method of establishing attachment distance that was developed in an earlier study was found to be unsuitable without modification for the range of flow in this investigation.

A simplified jet attachment model was proposed for estimating attachment distance. The model was found to agree well with experiments for both compressible and incompressible flow and a variety of wall geometries. In addition, computation procedures were found to be relatively simple.

NOMENCLATURE

A	turbulent eddy viscosity
a	speed of sound
B	velocity profile coefficient (equation 14, Chapter II)
C_p	constant pressure specific heat
d	depth of the nozzle (nozzle aspect ratio = d/w)
e	base of natural logarithms
f_1	momentum function (equation 16)
f_2	mass function (equation 17)
$g(M_o)$	attachment bubble leakage parameter
h	jet potential core half-width
I_o	initial forward jet momentum flux
I_1	forward jet momentum flux external to discrimination streamline
I_2	reversed jet momentum flux of fluid returned to attachment bubble
J_1	dimensionless momentum flux $\left(\frac{I_1}{\rho_o u_o^2 w}\right)$
K_1	Olson's empirical control volume location constant
K_2	Olson's empirical pressure force coefficient at attachment
K_n	Knudsen number
L	distance from nozzle exit plane along attachment wall
ℓ	setback geometry dimension $\left(\ell = \frac{w/2 + S}{\tan\theta}\right)$
M	Mach number
m	centerline velocity decay constant

P	absolute pressure
r	radius of curved jet centerline
R	gas constant
R_e	Reynolds number
S	setback of attachment wall
T	absolute temperature
U	velocity ratio
u	velocity in the jet centerline direction
w	nozzle width
x	distance along jet centerline
x_c	jet core length
y	distance perpendicular to jet centerline
α	angle measured from nozzle exit plane
γ	ratio of specific heats
Δ	distance perpendicular from jet centerline to attachment wall
δ	distance perpendicular from jet centerline to discriminating streamline
θ	angle between attachment wall and nozzle centerline
λ	mean free path of gas molecules
ξ	displaced y coordinate within the mixing zone (see Figure 8)
ρ	mass density
μ	coefficient of viscosity

Subscripts

c	denotes conditions on the jet centerline
e	denotes ambient conditions of fluid reservoir

i denotes conditions within the separation bubble

o denotes conditions at nozzle exit

R denotes conditions at attachment point

s denotes stagnation conditions on discriminating streamline

t denotes stagnation conditions

w denotes conditions on the attachment wall

* denotes conditions where $u = 0.5u_c$

τ denotes fully turbulent jet conditions (large R_e)

Superscripts

' denotes conditions along a line perpendicular to jet centerline and passing through point on attachment wall where $P = P_e$

Underlined symbols denote vector quantities.

CHAPTER I

INTRODUCTION

Historical Background

The Coanda Effect is the name given to the phenomenon of a submerged fluid jet attaching to a solid wall which is adjacent to the jet. It is named after Henri Coanda, a Rumanian engineer, who utilized the phenomenon in numerous inventions (1).

The Coanda Effect is a consequence of the natural entrainment of surrounding fluid by a submerged jet. Figure 1 is a sketch of a two-dimensional jet submerged in a non-moving reservoir of the same fluid and an adjacent wall. As the jet progresses through the reservoir it spreads by entraining the surrounding fluid which is swept along in the downstream direction. Prior to attachment the surrounding fluid will flow into the void left by the entrained fluid that is swept away. The free side of the jet which is opposite the wall side exists with no restriction of the replacement flow from the surroundings, but replacement flow on the wall side is restricted by the presence of the wall. This replacement flow restriction and continuing entrainment of fluid by the jet will result in a lowering of the pressure between the jet and the wall. The absence of replacement flow restrictions on the free side permits the pressure on that side to remain essentially equal to ambient pressure. Thus the pressure difference across the jet deflects it toward the wall. As the jet moves closer to the wall, the restric-

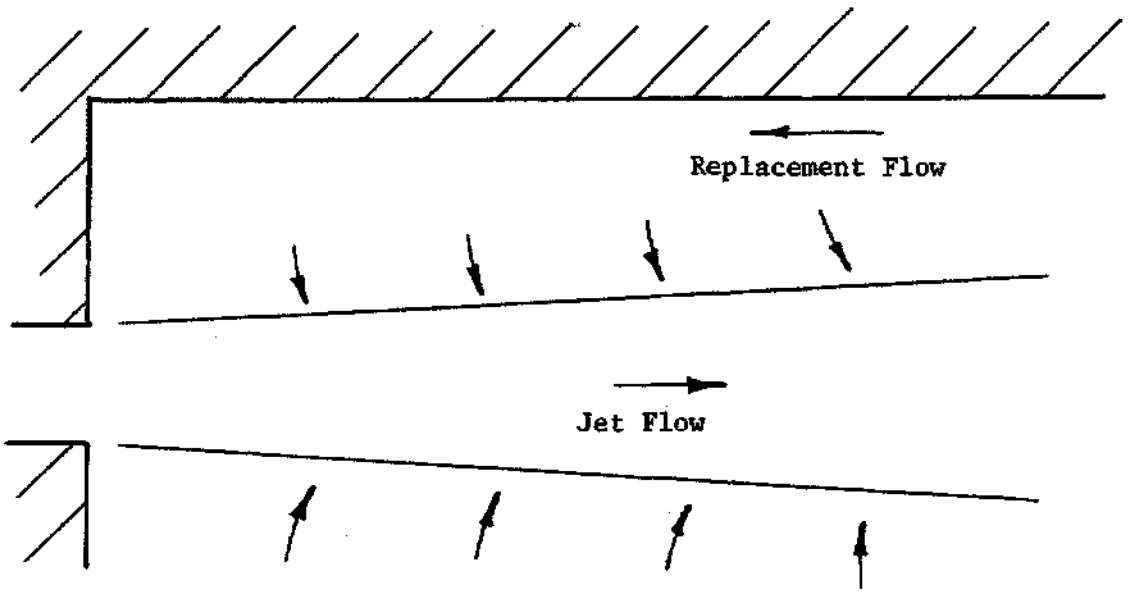

Figure 1. Submerged Jet Adjacent to Wall

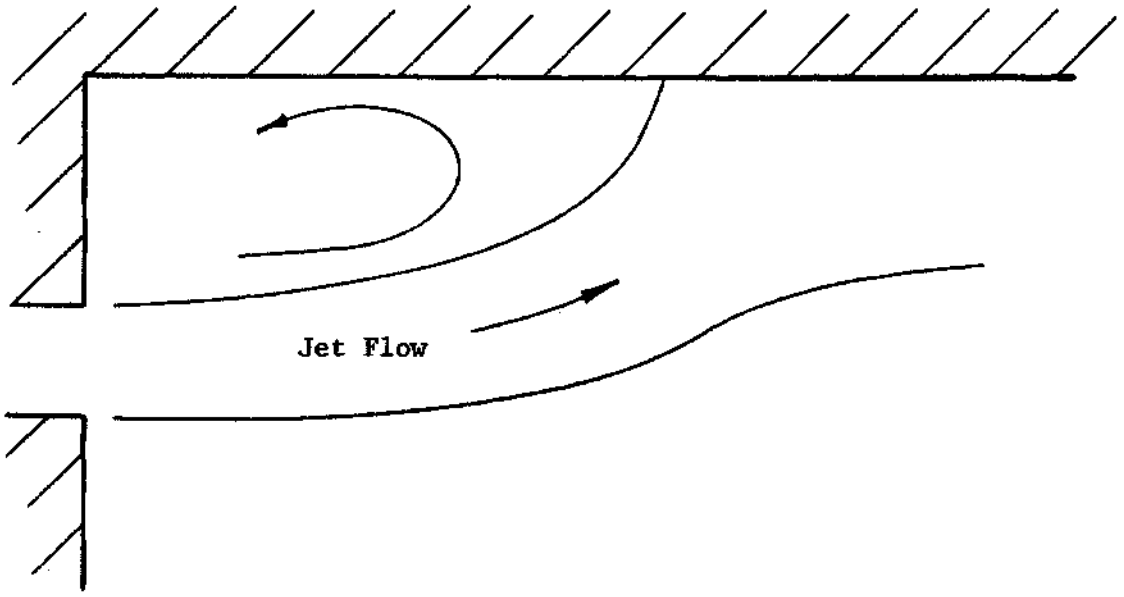

Figure 2. Submerged Jet Attached to Wall

tion of the replacement fluid flow next to the wall is increased, and the pressure between the jet and wall is further reduced. Eventually the jet will contact the wall and enclose a region between the jet and wall that is called the attachment bubble. Fluid will be constantly entrained from the bubble region by the jet and returned at a position upstream from the attachment point. In this way a lower bubble pressure than ambient is maintained. Eventually the change in radial momentum flux due to the jet curvature will just balance the pressure force across the jet, and a stable steady state attachment of the jet to the wall at some point on the wall is achieved as illustrated in Figure 2. In this manner a fluid jet will spontaneously attach to an adjacent wall (2).

The primary motivation of this investigation is the use of the Coanda Effect as the operating principle of the bistable fluidic amplifier. Figure 3 is a simple sketch of this device with the important parts labled. Jet attachment to either wall of the amplifier is determined by the control jets. The geometry of the sketched device is typical of bistable amplifiers with the attachment walls offset from the nozzle lip and inclined to the nozzle centerline. This bistable fluidic amplifier geometry and previously established amplifier design parameters were influencing factors in the flow model design and the data accumulation.

Three of the most important parameters of attaching jets are the location of the attachment point on the attachment wall, the static pressure variation along the wall, and the description of the jets upstream of attachment. Bourque and Newman (3) have developed an

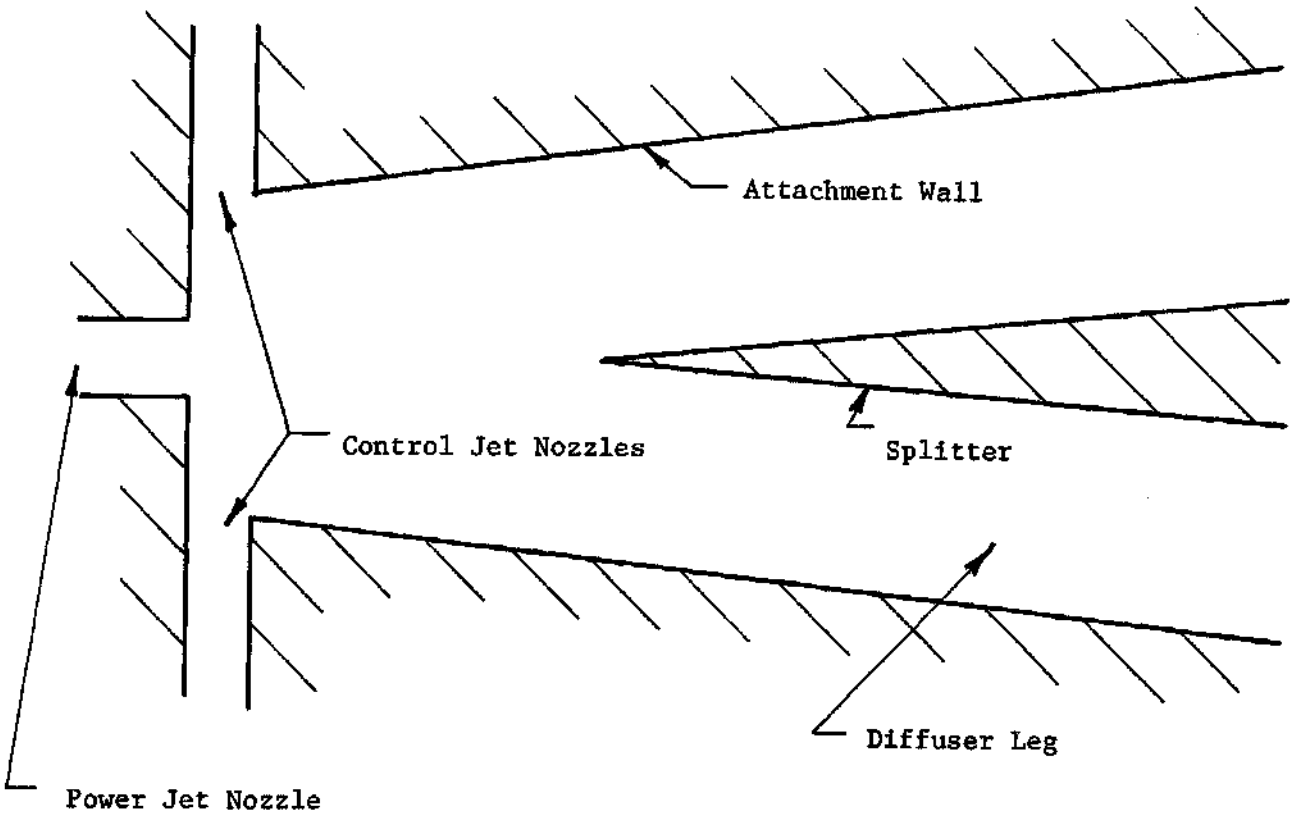

Figure 3. Bistable Wall Attachment Fluid Amplifier Sketch

analytical method of predicting the attachment point of a two-dimensional incompressible jet on an adjacent wall, and more recently Bourque (4) presented an improved analysis. Both of these analytical investigations have exhibited good agreement with experimental data. Perry (5) and McRee and Moses (6) have verified that the analytical model of Bourque and Newman is suitable for the design of bistable amplifiers with incompressible power jets. Numerous investigations of compressible jet attachment have been conducted including the behavior of overexpanded, underexpanded, and fully expanded supersonic jets. Olson, et al, (7, 8, 9, 10, 11, 12) have conducted extensive investigations dealing with the description of submerged compressible jets and the determination of attachment points for various wall geometries. He has presented a semi-empirical analytical determination of compressible jet attachment (10) that has been shown to agree well with experiments for highly turbulent jets. A method of examining this analysis to determine its suitability for use in describing the range of flow in this investigation is presented in the next chapter.

Past research in fluidics has provided valuable qualitative knowledge of attachment wall geometry effects on attachment as well as the effects of flow parameters such as the Mach number and Reynolds number which is usually based on the nozzle exit conditions. Small (13) has indicated that a definite value of Reynolds number exists for incompressible flow below which attachment will not occur for a given fluid amplifier geometry. Comparin, Jenkins, and Moore (14), however, have reported incompressible jet attachment at Reynolds numbers much lower than the limit of 1500 suggested by Small. This inconsistency is

very important when viewed from the standpoint of fluidic device performance. Small devices which correspondingly operate at low Reynolds numbers have higher switching frequencies and lower gas consumption than large ones and therefore perform better in fluidic logic circuits. For this reason the present trend is to miniaturize fluidic devices. Two major problems make miniaturization difficult. The reliable manufacture of flow passages smaller than 0.004 inches in width has not yet been achieved, and no previous investigation has been conducted to describe the attachment of very small or low density compressible submerged jets. The subject of this investigation may be considered to be an examination of models of very small compressible jets attaching to an adjacent wall with a wall geometry typical of fluidic devices.

The range of jet flow that was examined in this study is presented in Figure 4 where the range of flow examined by previous investigations is also denoted for comparison purposes. The previous investigators examined a wide variety of wall geometries for reasonably restricted flow ranges, and this study differs from previous ones in that only one wall geometry was used with a wide variety of jet flow conditions. Equipment limitations are responsible for the flow range boundaries for this investigation in Figure 4.

Definition of Problem

The subject of this investigation is the study of the Coanda Effect for compressible low Reynolds number jets. Experiments were designed utilizing the Knudsen number and Mach number as variables. The Knudsen number (K_n) is defined as the dimensionless number equal

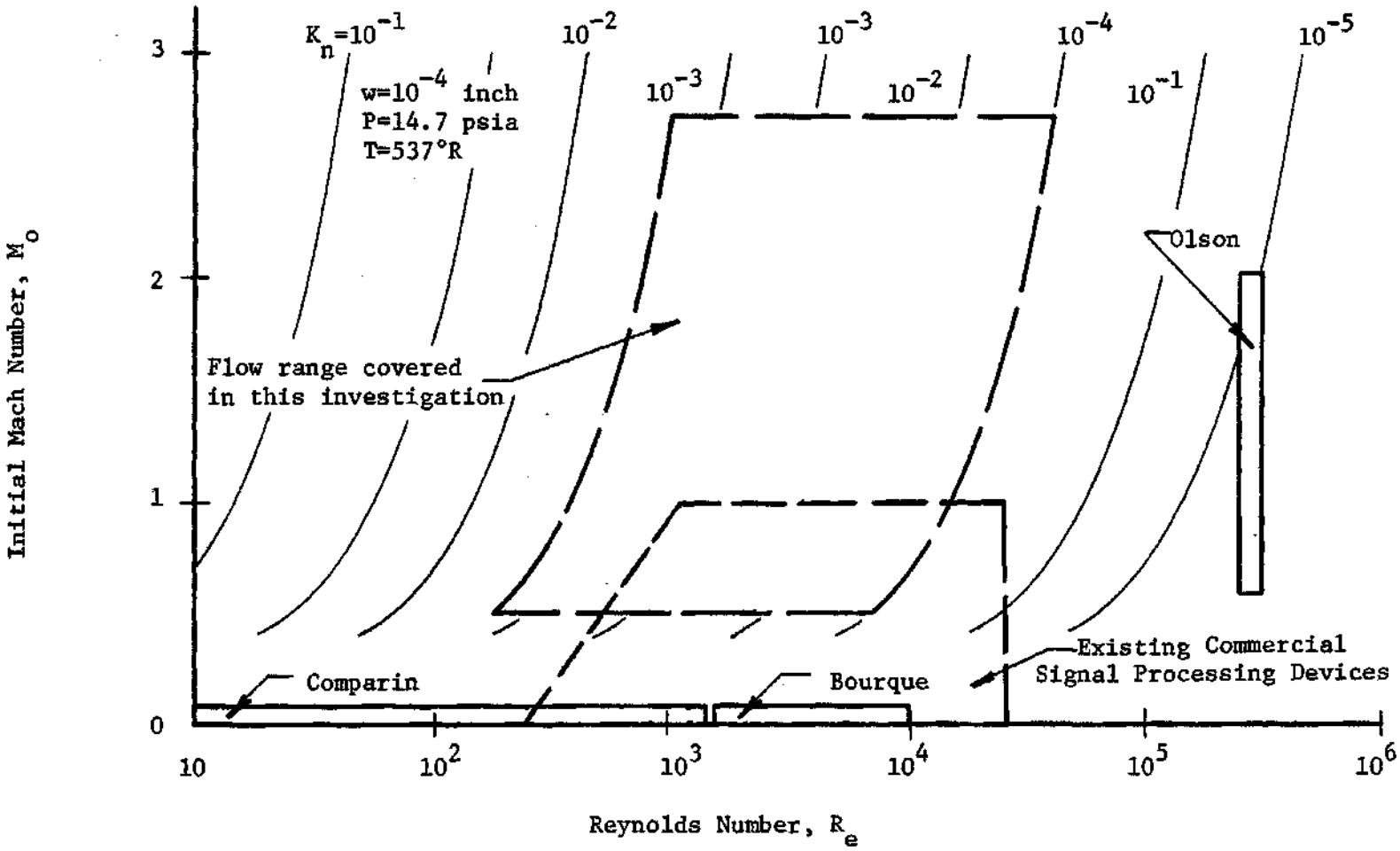

Figure 4. Flow Ranges Investigated

to the ratio of the mean free path of the gas molecules to some significant physical dimension of the flow. In this investigation the nozzle exit width is taken as that dimension. Therefore:

$$K_n = \frac{\lambda}{w} \tag{1}$$

Dry air is the compressible fluid used, and only steady state attachment is studied.

A well known relation from the kinetic theory of gases is that the product of density and mean free path are constant for a given gas (15) or:

$$\rho\lambda = \text{constant} \tag{2}$$

This relation and the perfect gas equation of state

$$\frac{P}{\rho} = RT \tag{3}$$

can be used to eliminate λ from (1) to obtain:

$$K_n = \frac{RT}{Pw}\,(\text{constant}) \tag{4}$$

The constant for air was determined from experimental evidence (15) to be approximately $1.58 \times 10^{-8}\ \frac{lbm}{ft^2}$. From equation (4) the Knudsen number of a typical small fluid amplifier with 0.020 inch power nozzle exit and air at atmospheric pressure and 77°F is determined to be:

$$K_n \approx 10^{-4}$$

The Knudsen number range for this study was chosen to be:

$$10^{-4} \leq K_n \leq 4 \times 10^{-3}$$

This range of Knudsen numbers falls within the continuum flow regime of gases and borders on the slip flow regime (16). Continuum gas dynamics theory is considered valid for this study as well as relations from molecular gas dynamics.

One of the classical results of the kinetic theory of gases (16) relates the Knudsen number, Mach number (M), and Reynolds number (R_e). The relation is as follows:

$$K_n = 2\sqrt{\frac{\pi}{8}}\sqrt{\gamma}\ \frac{M}{R_e} \tag{5}$$

Where γ is the ratio of specific heats of the gas. The relation applies for flow in the continuum regime with the Knudsen number and Reynolds number based on the same significant flow dimension. The Mach number range of the jets that was investigated is

$$0.5 \leq M \leq 2.71$$

which is broad enough to cover the range of Mach numbers of previously studied compressible jet attachment. Therefore, the range of Reynolds numbers investigated is by equation (5) approximately:

$$150 < R_e < 5 \times 10^4$$

Specific values of jet Mach numbers that are investigated are 0.5, 0.8, 1.94, and 2.71 because simple nozzles were easily designed for these values. To limit the number of types of flow, only fully expanded supersonic jets were considered. Specific Knudsen number values in-

vestigated are 10^{-4}, 5×10^{-4}, 10^{-3}, and 4×10^{-3}.

A relatively large, single wall attachment model shown in Figure 5 was constructed for this investigation in order to reduce flow measurement problems associated with small models. The model consists of a geometry which is typical of setback and wall angle of previous investigations. Desired flow conditions are achieved with a high displacement vacuum pump.

Analysis of the ability to model small fluid jet attachment with rarefied power jets in the Knudsen number range above 10^{-4}, with a scaled up model is presented in Appendix A.

Objectives

The primary objective of this study was to experimentally investigate attachment of compressible jets to an adjacent wall for a range of Reynolds numbers much smaller than the range of previous investigations. To properly evaluate the desired range of flow it was necessary to develop an understanding of the flow field and compare the results of this study with previous investigations. The analytical method of compressible jet attachment location on an adjacent wall developed by R. E. Olson (10) has shown close agreement with experimental results of Reference (10) and was chosen for comparison purposes in this investigation. Olson's analytical development is presented in Chapter II.

The experiments were designed for the purpose of establishing whether jets at large Knudsen numbers actually attach to the wall and of obtaining values of experimental attachment parameters that

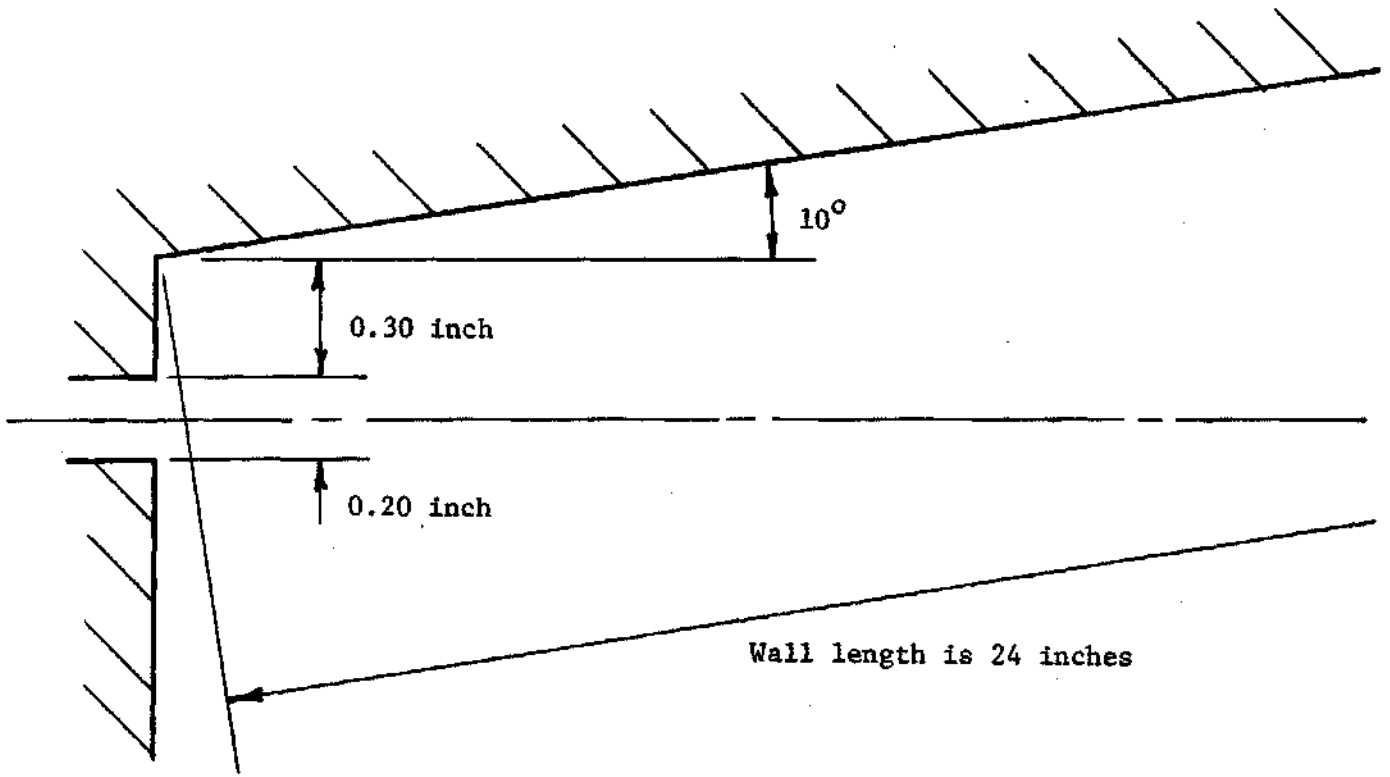

Figure 5. Single Wall Model Geometry

were easily compared with results of other investigations. The attachment parameters that were investigated are wall static pressure and attachment distance along the adjacent wall. In addition, an attempt was made to obtain a description of the flow field near the wall. In order to achieve a reasonably thorough qualitative examination of the range of flow with a reasonable expenditure of effort only one adjacent wall geometry was used in the study.

CHAPTER II

ANALYSIS OF ATTACHMENT POINT

Preliminary Free Jet Description

Olson's compressible jet attachment analysis (10) is based on the knowledge of the characteristics of a free jet of fluid issuing from a nozzle into a reservoir of the same fluid with no boundary restrictions. A sketch of a two-dimensional free jet in Figure 6 illustrates the assumed geometry and centerline velocity of the unattached two-dimensional jet. For purposes of analysis the velocity profile at the nozzle exit is assumed uniform. A potential core region of length x_c exists in which the velocity remains equal to the nozzle exit velocity. The core region width is assumed to decrease linearly with distance along the jet centerline from the nozzle exit width to x_c. At distances along the jet centerline greater than x_c the centerline velocity is assumed to decay in a manner that is determined in Appendix C. Within the core region the flow is assumed inviscid.

On each side of the core and downstream of x_c mixing regions exist where surrounding fluid is entrained and swept away causing the jet to spread downstream. The velocity profiles in the mixing region may be considered to approximate a Gaussian distribution function (8). The jet spreading is described by the locus of positions at which the jet velocity is one-half the jet centerline velocity.

In the attachment analysis Olson assumes that the description

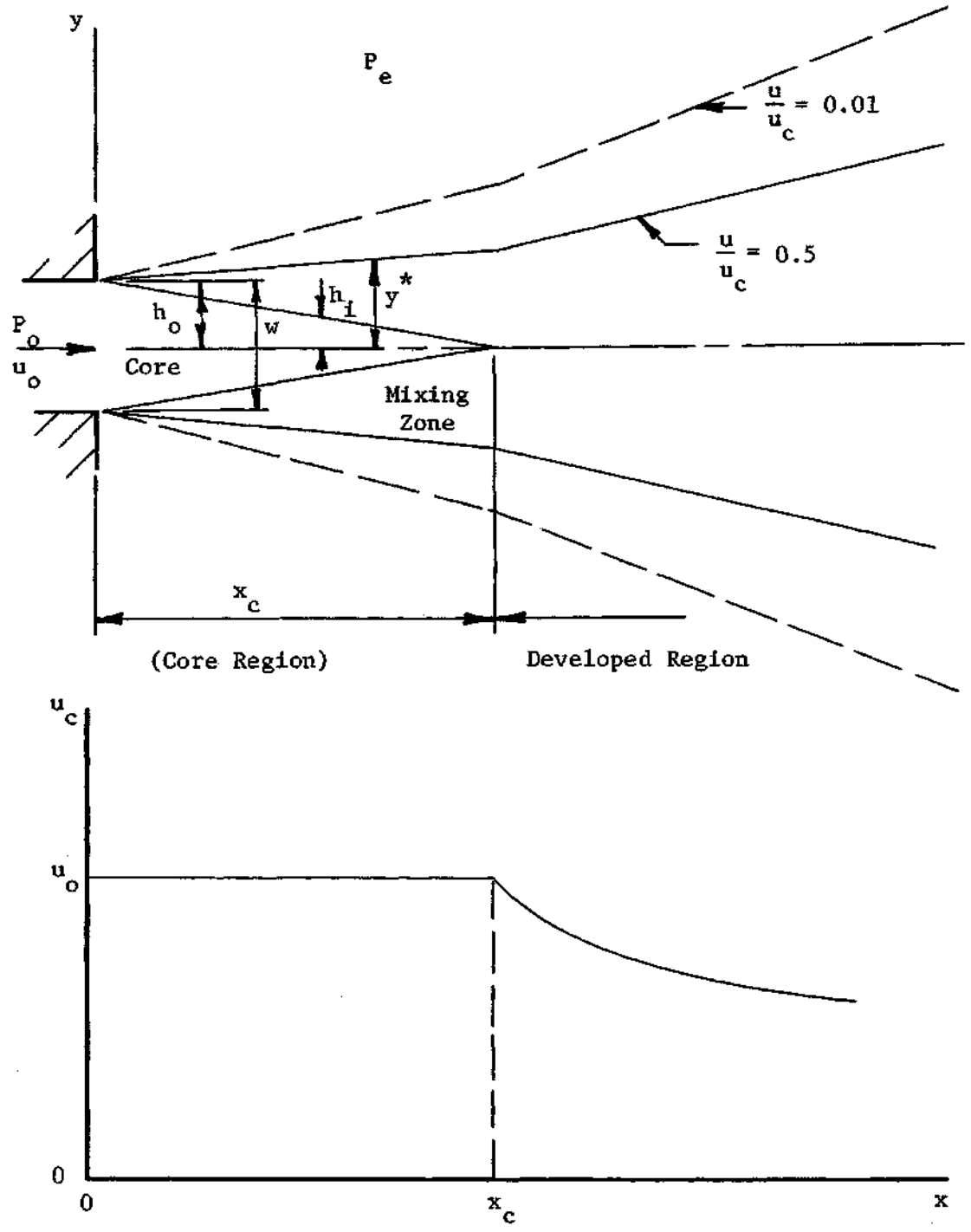

Figure 6. Sketch of Free Jet and Centerline Velocity

of the free jet closely approximates the description of the attaching jet. This assumption has been proven essentially correct in previous studies in the case of the velocity profile although spreading rates for the attaching supersonic jets are somewhat larger than for free supersonic jets (7).

Olson's Attachment Model

Figure 7 is a sketch of Olson's attachment model. The model consists of a nozzle to supply the jet and a straight wall inclined at some angle away from the nozzle centerline and offset from the nozzle exit wall. Pertinent dimensions and nomenclature are included on the sketch. The separation or discriminating streamline is the locus of stations within the jet that divides the flow that proceeds downstream subsequent to attachment from the flow that recirculates into the attachment bubble under steady state conditions. The attachment point is the intersection of the discriminating streamline and the wall.

The attachment point location analysis is based on four principal assumptions. The forward jet momentum in the downstream jet centerline direction remains constant upstream of the attachment point. The jet upstream of the attachment point may be treated as a free submerged jet at the same pressure as the surroundings excluding the attachment bubble. The pressure within the attachment bubble is constant and the jet centerline is approximately a circular arc between the nozzle exit and the attachment point. The radius of the jet centerline arc is large in comparison with the width of the jet.

A detailed derivation of the equations presented in this chapter

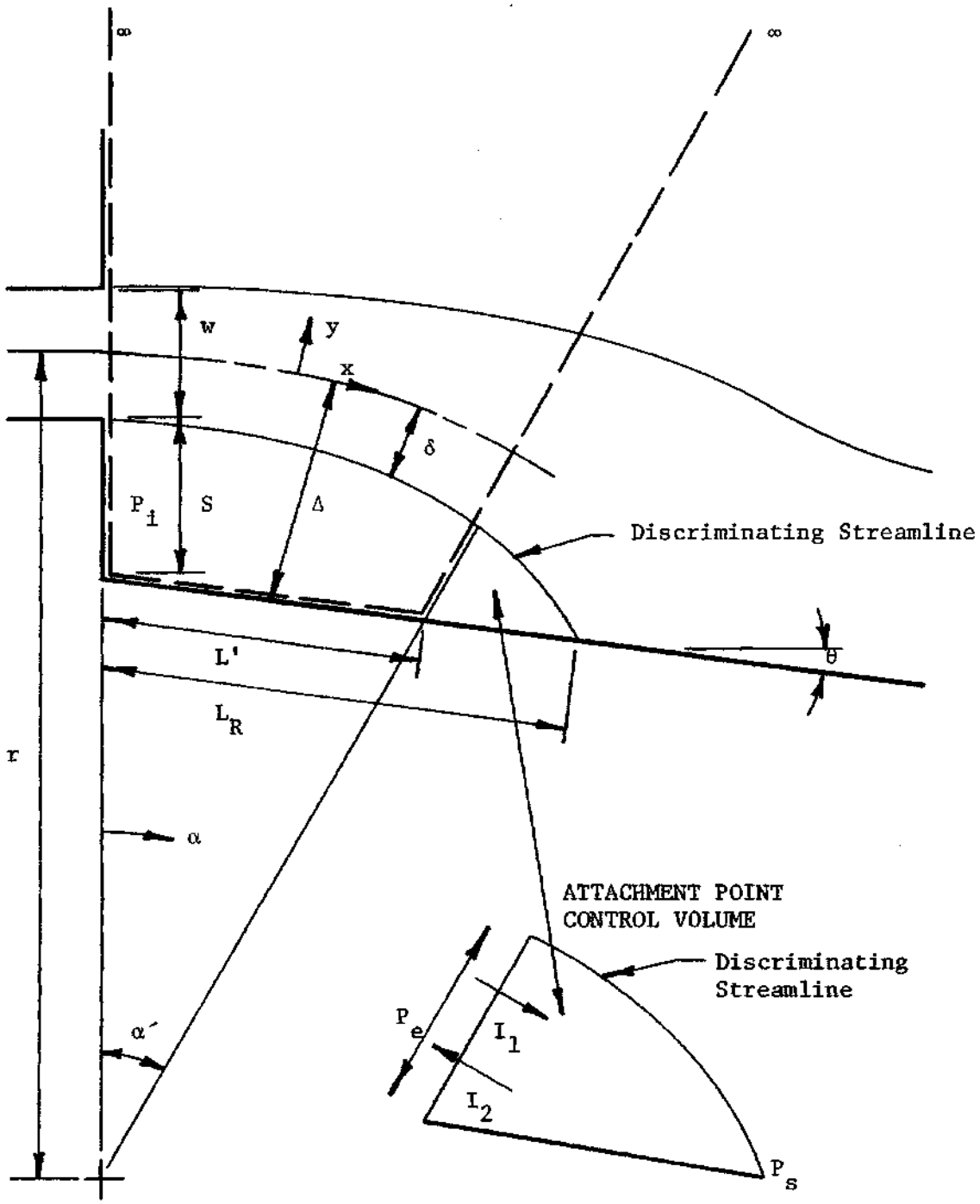

Figure 7. Attachment Model

is found in Reference (10). The pertinent results and the underlying principals are considered here.

From the assumptions listed above and the approximate equation of motion of the jet and perfect gas relations, the jet radius of curvature non-dimensionalized with respect to the nozzle width may be expressed as:

$$\frac{r}{w} = \frac{\gamma M_o^2}{1 - \frac{p_i}{p_e}} \tag{6}$$

Therefore the radius of jet curvature is essentially a function of initial jet Mach number and the average pressure within the separation bubble. Reference to Figure 7 will yield the following geometric relations in non-dimensional form:

$$\frac{\Delta}{w} = \frac{r}{w} - \sqrt{\left(\frac{L}{w}\cos\theta\right)^2 + \left[\frac{r}{w} - \left(\frac{1}{2} + \frac{S}{w} + \frac{L}{w}\sin\theta\right)\right]^2} \tag{7}$$

$$\frac{x}{w} = \frac{r}{w}\,\alpha \tag{8}$$

where

$$\alpha = \tan^{-1}\left[\frac{\frac{L}{w}\cos\theta}{\frac{r}{w} - \left(\frac{L}{w}\sin\theta + \frac{S}{w} + \frac{1}{2}\right)}\right] \tag{9}$$

If the position of the separation streamline is determined from free jet considerations, the position of the jet centerline for jet attachment can be determined from the criterion that

$$\frac{\Delta}{w} = \frac{\delta}{w} \tag{10}$$

at attachment. According to Olson the attachment point is determined by trial and error. Equations (6), (7), (8), (9), and (10) are solved simultaneously using an assumed value of P_i/P_e in equation (6) and free jet data to determine $\frac{\delta}{w}$ in terms of $\frac{x}{w}$. Once the attachment position is determined for the assumed value of P_i/P_e the attachment bubble geometry is determined, and the value of P_i/P_e can be checked by a semi-empirical examination of the momentum in the direction of the jet centerline within the attachment bubble. The momentum analysis consists of dividing the separation bubble into two regions as shown in Figure 7. The value of α' in this sketch is determined from experimental measurements of the static wall pressure within the bubble. It is the angle for which the dividing radial line intersects the wall where the static wall pressure equals the ambient pressure (P_e). The pressure along this straight line is assumed constant in this analysis, and the coefficient K_1 is defined as the ratio of the value of L' to the value of L_R at attachment. Reference to Figure 7 shows that x' is the jet centerline position intersected by the radial line that divides the bubble. Another coefficient K_2 is defined as the fraction of the maximum pressure force in the attachment bubble that is effective in reversing the flow in the jet direction back into the attachment bubble. Both coefficients K_1 and K_2 are determined from experimental measurements. Olson assumed that the fluid momentum in the attachment bubble in the jet direction (I_1) and the momentum of the reversed fluid which flows back into the bubble (I_2) is in the direction of the jet centerline at the dividing radial line. He then developed an expression for the ratio of bubble pressure to ambient pressure from momentum considerations

of the divided bubble:

$$\frac{P_1}{P_e} = 1 + \frac{\gamma M_o^2 (1+J_1-\sec\alpha') - K_2(P_s/P_o - 1)\frac{\Delta'-\delta'}{w}}{\left(\frac{S}{w} + \frac{L'}{w}\sin\theta\right)\sec\alpha'} \qquad (11)$$

where

$$J_1 = \frac{I_1}{\rho_o u_o^2 w} \qquad (12)$$

The trial and error analysis is complete if the values of P_1/P_e in equations (6) and (11) are equal.

Free Jet Analysis

The attachment point analysis requires only three non-dimensional quantities from the analysis of the free submerged jet. The quantities are the location of the discriminating streamline relative to the jet centerline $\frac{\delta}{w}$, the stagnation pressure on the discriminating streamline location P_s/P_o, and the free jet momentum external to the discriminating streamline (J_1).

Figure 8 is a sketch of the free jet geometry with the pertinent dimensions included. Only the important results of the analysis are presented in this section. The basic analytical assumptions are the same as those presented in the preliminary free jet description. The momentum flux in the jet centerline direction is assumed constant.

In this analysis, the velocity profiles in the mixing region are assumed to be similar, and in non-dimensional form may be represented as:

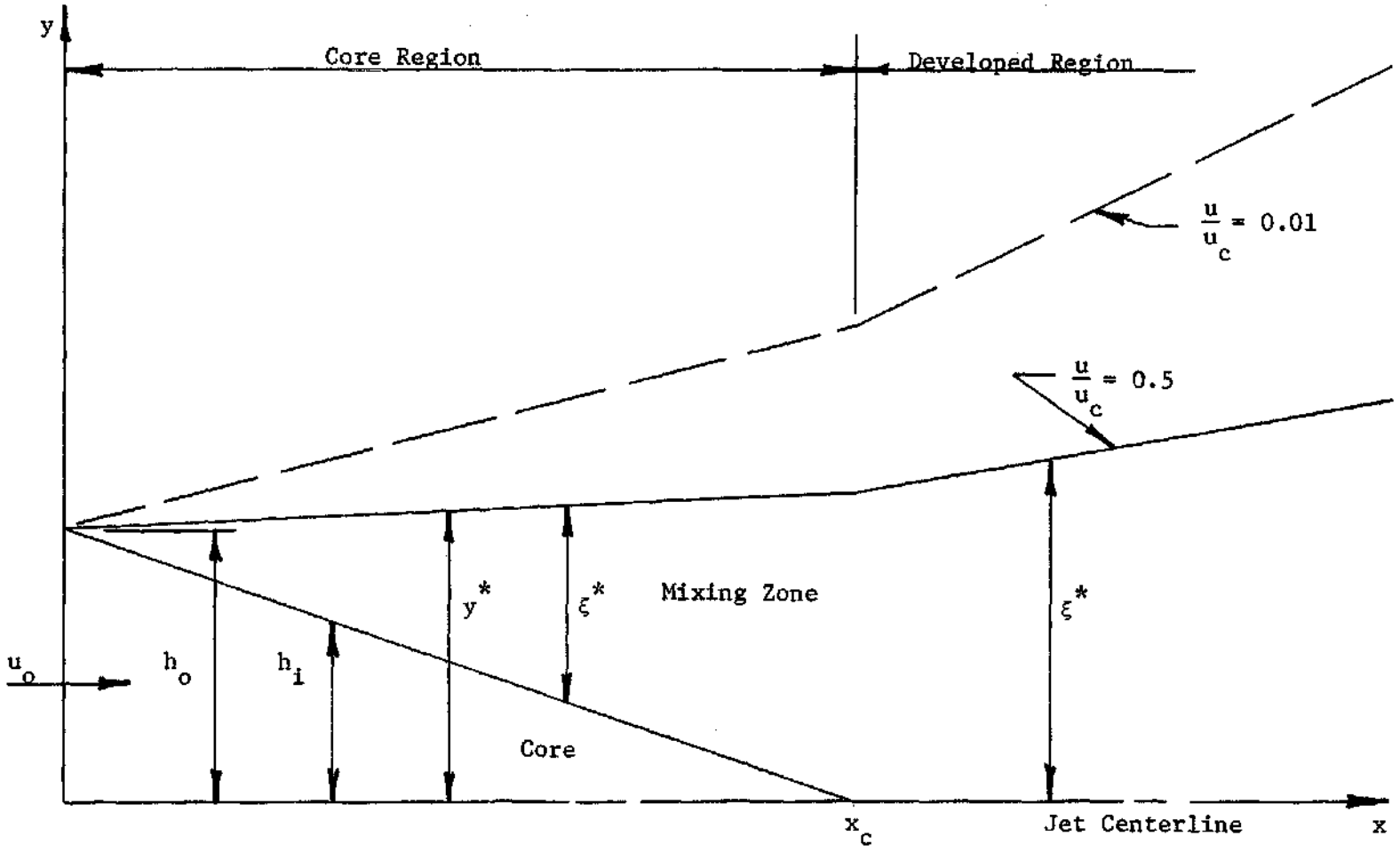

Figure 8. Free Jet Analytical Sketch

$$\frac{u}{u_c} = e^{-B\left(\frac{\xi}{\xi^*}\right)^2} \tag{14}$$

as recommended by Olson. The value of B is determined to be 0.6931 where $\frac{u}{u_c}$ is 0.5 and $\frac{\xi}{\xi^*}$ is one. For this model the pressure throughout the jet is considered to be constant and equal to the ambient pressure. Also, the stagnation temperature throughout the flow is assumed constant as a result of isoenergetic mixing. The energy equation and the perfect gas equation of state may be combined to determine the non-dimensional expression for jet density.

$$\frac{\rho}{\rho_o} = \frac{1}{1 + \frac{\gamma-1}{2} M_o^2 \left[1 - \left(\frac{u}{u_o}\right)^2\right]} \tag{15}$$

for a perfectly expanded jet. A non-dimensional jet momentum function (f_1) may be defined as:

$$\begin{aligned} f_1 &= \int_o^{\frac{\xi}{\xi^*}} \frac{\rho}{\rho_o} \left(\frac{u}{u_o}\right)^2 d\left(\frac{\xi}{\xi^*}\right) \\ &= \int_o^{\frac{\xi}{\xi^*}} \frac{U^2 \left(\frac{u}{u_c}\right)^2}{1 + \frac{\gamma-1}{2} M_o^2 \left[1 - U^2\left(\frac{u}{u_c}\right)^2\right]} d\left(\frac{\xi}{\xi^*}\right) \end{aligned} \tag{16}$$

where $U = \frac{u_c}{u_o}$. Similarly, a jet mass function (f_2) may be defined as:

$$f_2 = \int_o^{\frac{\xi}{\xi^*}} \frac{\rho}{\rho_o} \frac{u}{u_c} d\left(\frac{\xi}{\xi^*}\right) \tag{17}$$

$$f_2 = \int_0^{\frac{\xi}{\xi^*}} \frac{U\left(\frac{u}{u_c}\right)}{1 + \frac{\gamma-1}{2} M_o^2 \left[1 - U^2 \left(\frac{u}{u_c}\right)^2\right]}$$

The remaining information required for a complete free jet description is the empirically determined core length and the centerline velocity curve in the developed region. These quantities are approximately determined from measurements of unattached jet centerline velocities.

The value of $\frac{\xi^*}{w}$ is determined by conservation of jet momentum and equation (16). The value of $\frac{\delta}{w}$ is then determined using equation (17). The value of P_s/P_o may then be determined from momentum considerations and the assumption of constant jet pressure. The value of J_1 is determined for any value of U or $\frac{x}{w}$ from conservation of momentum considerations and equation (16).

Comparison of the Model

In reference (10) empirically determined values of K_1 and K_2 are presented for jets having Reynolds number values larger than 10^5. The values of these coefficients are selected in the reference to yield good agreement between theory and experimental results. In an attempt to compare the theory to the low Reynolds number or high Knudsen number case new values of the coefficients are empirically determined for each case considered in this investigation.

Simplified Jet Attachment Model

The model proposed by Olson has been shown to exhibit good agreement with experimental results when applied to jets with initial

Reynolds numbers above 10^5. No provision is made for variation in the jet attachment distance with Reynolds number, however, since reference (10) assumes a fixed free jet description determined solely by the initial jet Mach number. In addition, the calculations required to estimate the attachment distance are tedious and time consuming.

A jet attachment model that requires much simpler calculations and compensates for Reynolds number is devised in this section by assuming that variation in attachment distance with Reynolds number is determined only by the variation of the unattached jet descriptions with Reynolds number. Figure 9 illustrates the important geometry and nomenclature of the simplified model. The basic assumptions are the same as the ones for Olson's model. The attaching jet velocity profile and density relations are assumed to be the same as the ones used in Olson's model, and the jet centerline velocities are determined experimentally for each jet flow condition.

Conservation of jet momentum in the jet centerline direction upstream of attachment may be expressed as

$$I_o = \int_{-\infty}^{\infty} \rho u^2 dy \tag{18}$$

The approximate Equation of motion may then be written

$$\frac{I_o}{r} = P_e - P_1 \tag{19}$$

From the model geometry, the following relations are obvious

$$1 - \cos\frac{x_w}{r} = \left(\frac{\ell}{r} + \sin\frac{x_w}{r}\right)\sin\theta \tag{20}$$

where

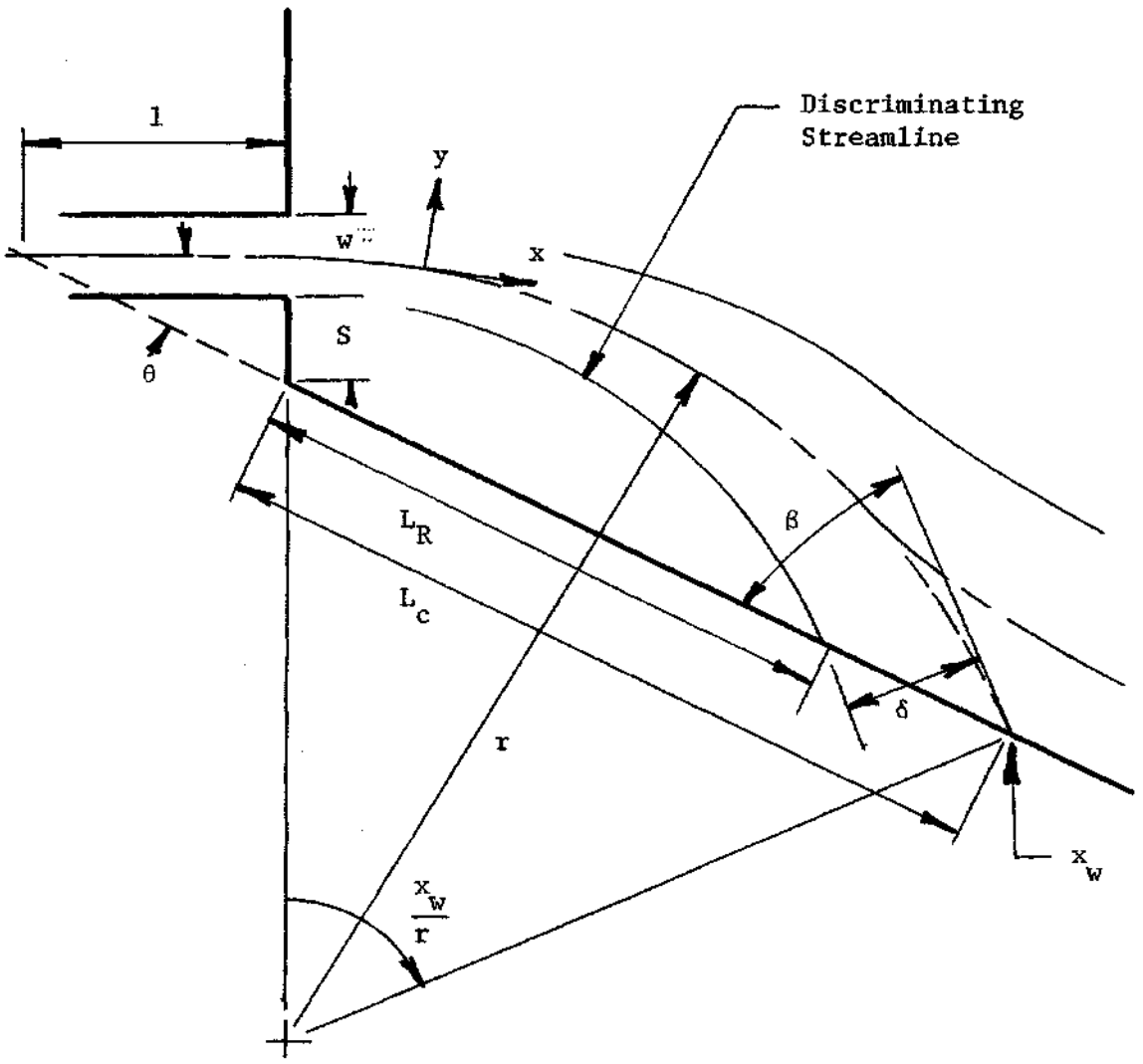

Figure 9. Simplified Jet Attachment Model

$$\ell = \frac{S + \frac{w}{2}}{\tan\theta} \tag{21}$$

$$\beta = \frac{x_w}{r} - \theta \tag{22}$$

$$\frac{L_c}{w} = \frac{\frac{r}{w} \sin \frac{x_w}{r}}{\cos\theta} \tag{23}$$

Bourque and Newman (3) have obtained good comparison between experiment and theory by writing the jet momentum equation in the wall direction near the attachment point neglecting pressure forces in that region. The values of δ at x_R and x_w are assumed equal since the difference between x_R and x_w is relatively small. The momentum flux returned to the attachment bubble in the wall direction is equal to I_1. The momentum equation neglecting pressure forces is

$$I_o \cos\beta + \int_{-\infty}^{-\delta} \rho u^2 dy = \int_{-\delta}^{\infty} \rho u^2 dy \tag{24}$$

Conservation of mass between the jet centerline and the wall upstream of the attachment point may be written as

$$\frac{\rho_o u_o w}{2} + \frac{Q}{d} = \int_{-\infty}^{o} \rho u dy - \int_{-\infty}^{-\delta} \rho u dy \tag{25}$$

where Q is the leakage flow into the attachment bubble due to three-dimensional effects. The value of Q must be determined experimentally; however, a form of Q may be estimated in order to better correlate experimental data with a single parameter. The form of Q for the flow range of this investigation is taken to be

$$Q = \frac{1}{2}\rho_o \sqrt{\frac{P_e - P_i}{\rho_o}}\; x_c^2\; g(M_o) \tag{26}$$

where x_c is the appropriate free jet core length and $g(M_o)$ is the leakage flow parameter that is a function of initial jet Mach number and will be determined experimentally.

Equation (25) may be simplified with equation (26) and equations (24) and (25) can be non-dimensionalized to yield

$$f_1\left(U, \frac{\delta}{\xi^*}\right) = f_1(U,\infty)\cos\beta \tag{27}$$

$$f_2\left(U, \frac{\delta}{\xi^*}\right) = f_1(U,\infty)\left[1 + \frac{\left(\frac{x_c}{w}\right)^2}{\frac{d}{w}\sqrt{\frac{r}{w}}}\, g(M_o)\right] \tag{28}$$

for jet centerline positions beyond the core where f_1 and f_2 are defined by equations (16) and (17). Tables of f_1 and f_2 for the Mach numbers of this investigation and numerous values of U and ξ/ξ^* can be tabulated easily with the computer program in Appendix B.

A simple trial and error solution for L_c/w is possible if the geometry and unattached jet centerline velocity relation is given:

1. Assume a value of r/w.
2. Find x_w/r from equation (20) and compute x_w/w.
3. Determine U_w corresponding to $x = x_w$ from the appropriate unattached jet centerline velocity relation.
4. Determine β from equation (22).
5. Determine δ/ξ^* from equation (27) at $U = U_w$ using the tables for f_1 and f_2.
6. Determine δ/ξ^* from equation (28) at $U = U_w$ with the

appropriate value of x_c/w and $g(M_o)$.

If the values of δ/ξ^* are not equal a new estimate of r may be made by multiplying the original estimate by the ratio of δ/ξ^* from step 6 to δ/ξ^* from step 5. When the values of δ/ξ^* are sufficiently close to one another the value of L_c/w is computed from equation (23). The approximate value of L_R/w may be computed from the relation

$$\frac{L_R}{w} \simeq \frac{L_c}{w} - \frac{\frac{\delta}{\xi^*}}{2f_1(U_w,\infty)\cos\beta} \tag{29}$$

The values of $g(M_o)$ were determined from the experimental data and the procedure outlined above to best fit the data obtained in this investigation. The $g(M_o)$ curve and a comparison of the simplified model to data from this investigation and from References (3), (10), and (14) are found in Chapter V.

The relationship of the simplified model to Olson's model is easily determined by direct comparison of the sections in this chapter. The simpler method of computation of attachment point location with the simplified model is readily apparent.

The first model of Bourque and Newman (3) is essentially the same as the simplified model with the exception that the turbulent incompressible jet velocity profile from Reference (18) is used in the place of the velocity profiles used in this investigation. Reference (3) considers wall geometries of setback with no wall angle and large wall angles with no setback. For the case of large wall angles and no setback the geometry relations of equations (20) through (23) are simplified by assuming that the nozzle half width is negligible

compared to the jet radius of curvature.

The model used by Comparin, Jenkins, and Moore (14) differs essentially from the ones of Bourque and Newman and the simplified model of this investigation by the use of the laminar incompressible jet velocity profile from Reference (18). Reference (14) considers only wall geometries of large wall angle and no setback, and the nozzle half width is considered to be negligible as in the models of Reference (3) for the same geometry. In addition, the momentum equation was written for a finite control volume around the attachment point rather than for a point near the attachment point as was done in the simplified model.

For a more detailed comparison of the simplified model to previously proposed models of jet attachment refer to References (3), (10), and (14).

CHAPTER III

EQUIPMENT AND INSTRUMENTATION

Wall Attachment Model

Figure 10 is a sketch of the wall attachment model with important dimensions and features labled. The entire model has one inch of thickness as flow space. A two inch pipe into the nozzle stagnation chamber admits the power jet supply air, and a four inch pipe exhaust allows expulsion of the exhaust air from the downstream end of the model. The one inch square steel sides of the model are bolted to the 5/8 inch thick aluminum sidewall base. The aluminum sidewall has scratches approximately 1/32 inch deep in the surface; however, the surface was sanded with a fine grain abrasive paper and polished with crocus cloth to prevent any extension of metal into the flow. A two inch thick plexiglas cover plate which covers the entire surface of the model was held tightly against the model sides with "C" clamps distributed along the edges.

A complete two-dimensional probe traverse of the flow field was obtained by use of a sliding brass bar at the downstream end of the model. The brass bar slides in an aluminum channel which is bolted to the edge of the model. Probe access to the flow from outside the model is achieved through the airtight Swagelok fittings in the brass bar and slotted holes through the aluminum channel and edge of the model. Longitudinal probe traverses were achieved by sliding the probes in and out of the mod-

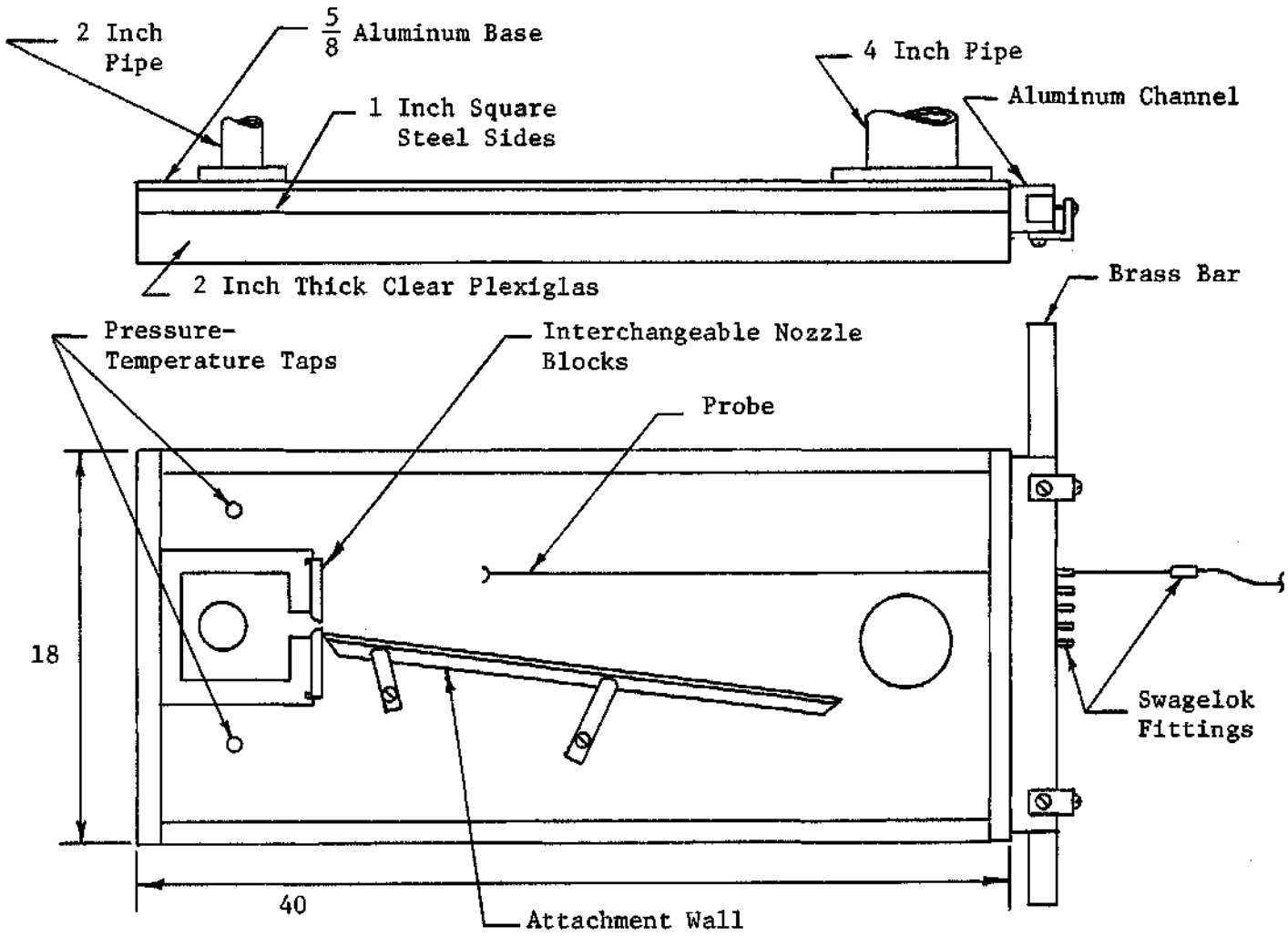

Figure 10. Experimental Model Sketch

el through the Swagelok fittings, and lateral probe traverses of the model were accomplished by sliding the brass bar in the aluminum channel.

Interchangeable nozzle blocks were bolted to the nozzle stagnation chamber to provide the desired Mach number jet while maintaining a 0.02 inch wide nozzle exit dimension or nozzle aspect ratio equal to 5. A representative sketch of the nozzle blocks is found in Figure 11. Supersonic nozzles were designed with circular cylindrical walled throats and plane walled supersonic sections to minimize nozzle length and boundary layer buildup and simplify construction. The radii of the supersonic nozzle throat walls were maintained equal to the throat width, and nozzle supersonic section walls diverged at a total angle of 30°. Subsonic nozzle blocks had a 1/4 inch radius cylindrical walled configuration. The attachment wall was clamped to the aluminum base of the model in the desired position with two simple "L" shaped clamps similar to the type clamp used on milling machine tables. For attachment point visualization one end of a flexible hairlike synthetic fiber fringe was glued to the surface of the wall in such a way that the fringe laid flat against the wall and the 1/2 inch long free end of the fringe was perpendicular to the sidewalls and the flow direction. The wall was located in the model at a setback of 0.3 inches and wall angle of 10° away from the nozzle centerline for all the experiments. The line of contact between the attachment wall and the nozzle block was sealed with a clay-like caulking compound. Most of the mating surfaces of the model component parts were sealed air tight with Glyptol sealant as the model was assembled. The non-

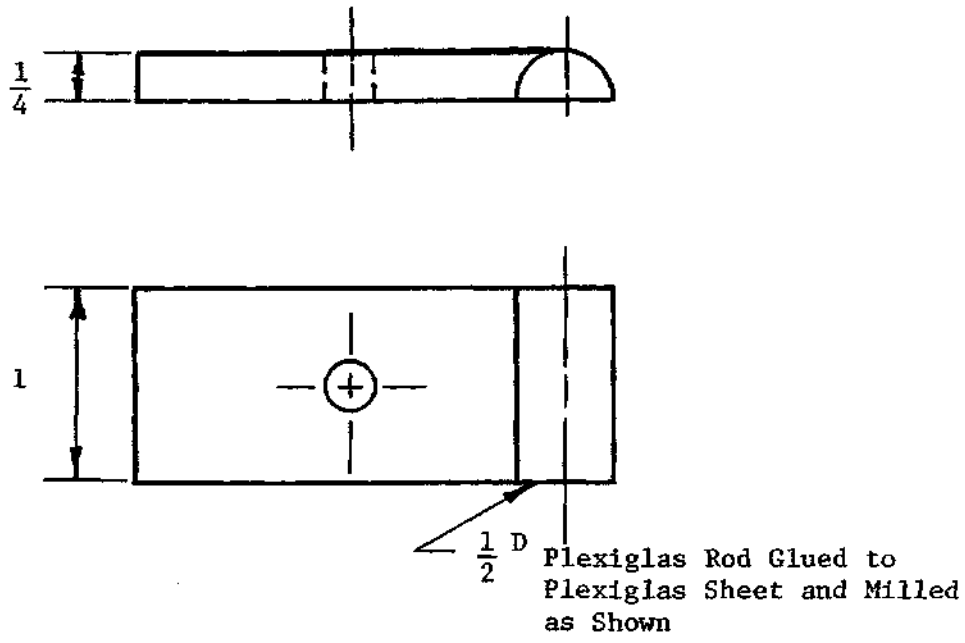

SUBSONIC NOZZLE BLOCK (M_o < 1)

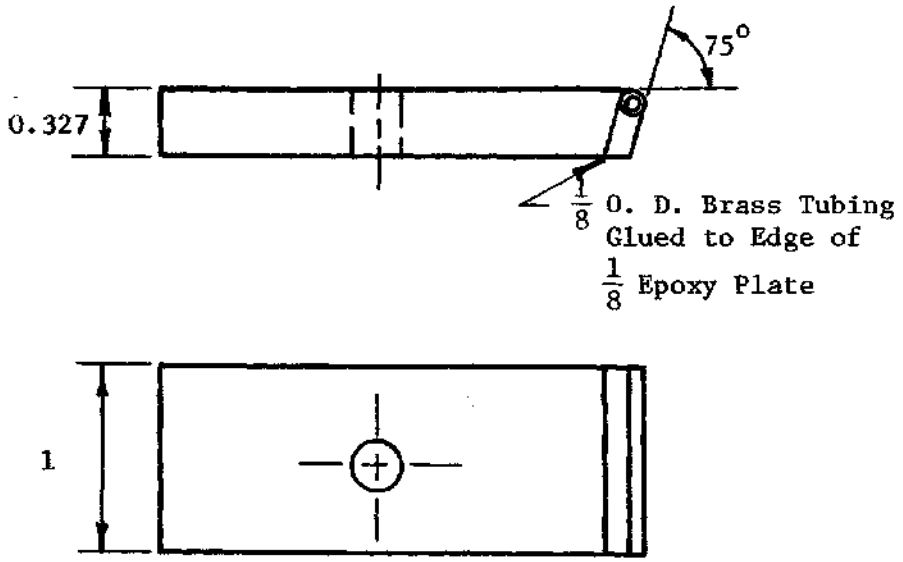

SUPERSONIC NOZZLE BLOCK (M_o = 2.71)

Figure 11. Representative Nozzle Blocks

permanent mating surfaces of the nozzle blocks, attachment wall, sliding brass bar and plexiglass cover were sealed with a Dow Corning High Vacuum Silicone Grease to provide easy entry into the model for changes of nozzle blocks and variation of probe position.

Vacuum Pump

A very high volume vacuum pump was required to pull the air through the model at the desired ambient pressures. The pump used was a Beach Russ rotary piston vacuum pump capable of exhausting 1050 cubic feet of air per minute with atmospheric pressure at the pump intake. The pump was mounted on a metal frame which was bolted to a wooden base composed of four inch by six inch timbers. A cylinder constructed from a five foot length of eight inch pipe sealed off on one end was connected to the pump input manifold for use as a damper of any suction surges caused by the pump. Two short lengths of three inch pipe were welded to the cylinder to provide for the model exhaust flow into it. The vacuum pump exhaust flow was carried to the atmosphere outside the building which housed the pump and model by a line composed of eight inch pipe and sheet metal ducting. The pump coolant water was piped to the upstream air temperature regulation can described in the next section to provide a source of hot water.

Support Equipment

Figure 12 is a diagram of the entire experimental apparatus with the major parts labled. The air entering the apparatus from the high pressure supply is first filtered and dried in a 30 inch thick

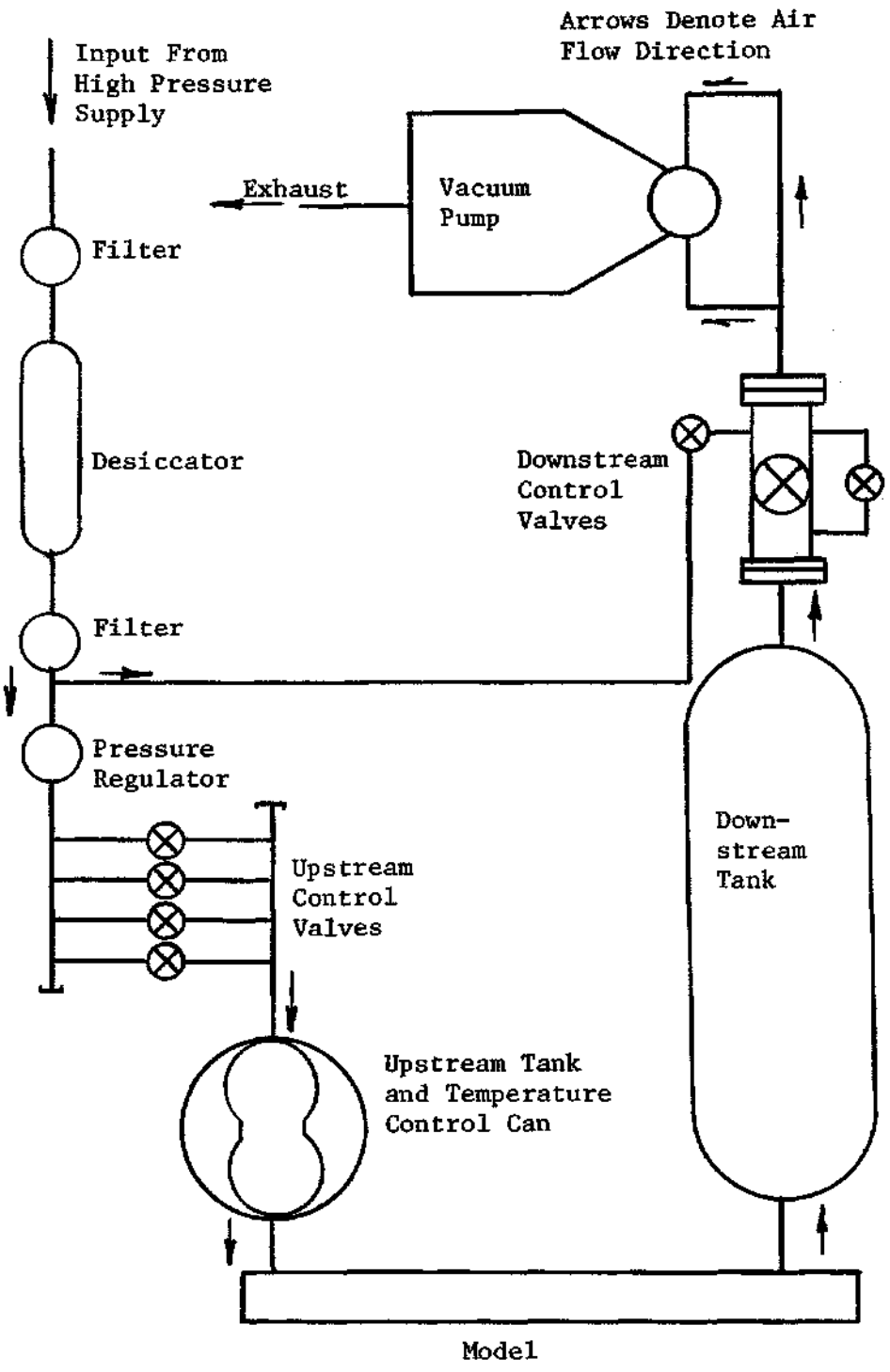

Figure 12. Apparatus Diagram

bed of silica gel with the desiccator. It is filtered a second time to eliminate any silica gel dust that is swept from the bed. A pressure regulator is used to reduce the air supply pressure to an approximately constant value of 35 psig.

The upstream control valves are four manually operated needle valves for regulating the power nozzle supply pressure. The four valves are connected in parallel to provide large volume flowrates with fine flowrate adjustments.

The upstream control valves throttle air into the upstream tank. This tank serves two purposes; it provides enough volume that the nozzle supply pressure can be adjusted manually, and it can channel the supply air through constant temperature water to regulate the gas temperature. Figure 13 is a sketch of the tank and the internal baffling arrangement. The tank is made from two lengths of ten inch pipe, and the baffles are arranged in such a manner that the supply air must make four passes along the length of the pipe. The tank rests in a 50 gallon oil drum through which passes the waste coolant water at approximately 100°F from the vacuum pump and enough cold water to maintain the water temperature in the drum at 77°F.

The supply air expands through the nozzle of the model and passes into the downstream tank. This tank is similar in shape to a standard cylindrical propane tank with domed ends, and it has a volume of approximately 18 cubic feet. The purpose of the tank is to provide enough volume to the model downstream of the nozzle to permit manual adjustment of the ambient pressure with the downstream

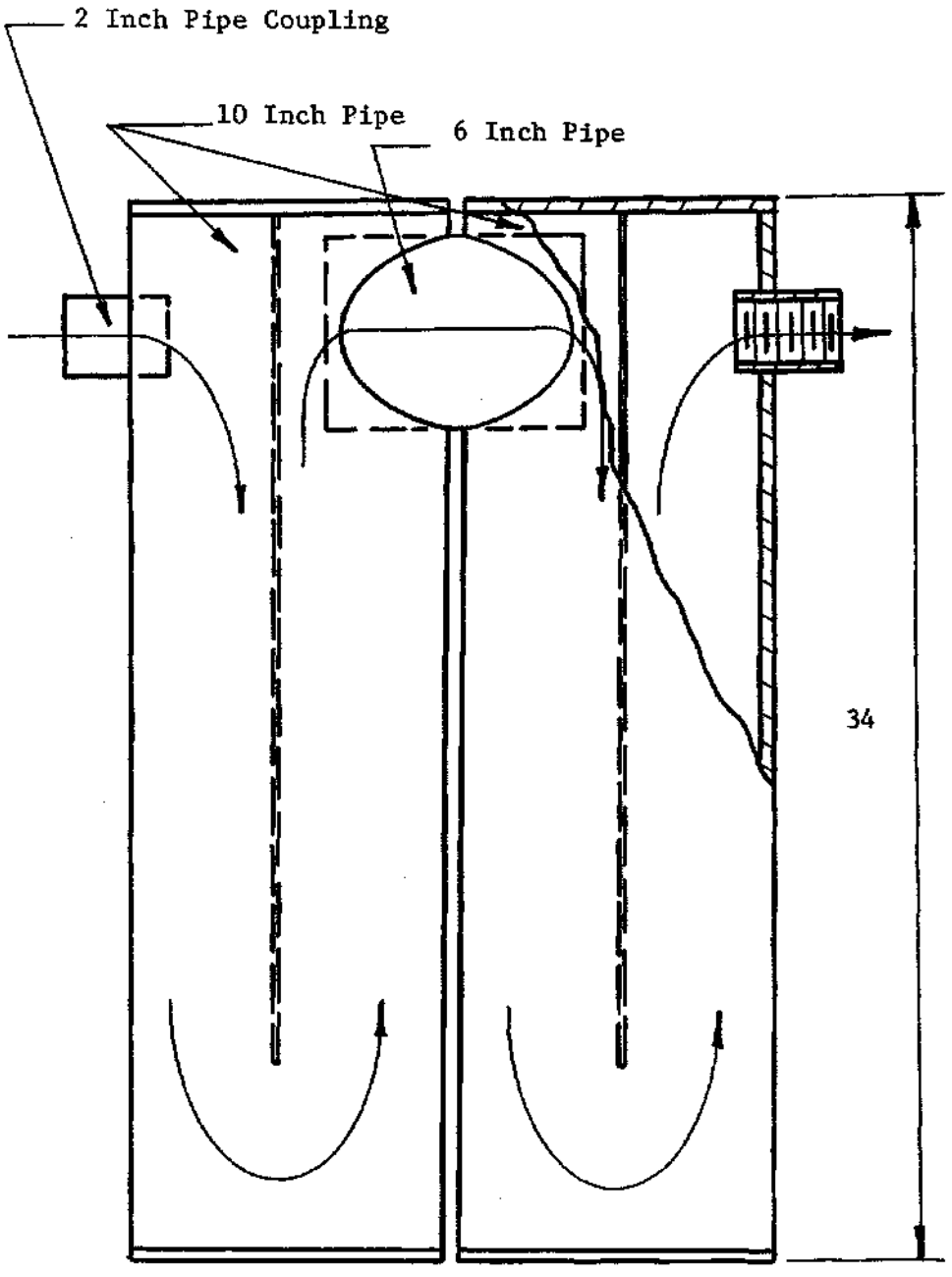

Figure 13. Upstream Tank

control valves.

The downstream control valves consist of a one inch diameter bellows type vacuum valve in parallel with a four inch diameter butterfly type valve. These two valves restrict the flow into the vacuum pump by reducing the effective flow area between the model and pump. A third small needle valve is used to admit air from the high pressure supply at the upstream control valves into the vacuum line downstream of the downstream control valves. This needle valve is used to reduce the volume of flow from the model by admiting high pressure air directly into the pump intake.

Probes

Figure 14 is a sketch of the two static pressure probe heads used to obtain data in this investigation. Both heads were soldered to three foot lengths of 1/4 inch outside diameter, 1/64 inch wall thickness brass tubing. The tubing slipped through Swagelok fittings on the brass bar and was connected to manometers and pressure sensors with flexible tubing. The static wall probe consists of a piece of 3/32 inch square, 1/64 inch wall thickness brass tubing which is bent to the same angle (10°) as the angle between the wall and the nozzle centerline of the model. The static boundary probe was constructed to minimize disturbance of the flow in the model. It consists of a 1/8 inch outside diameter, 1/64 inch wall thickness brass tube flattened to 1/16 inch outside thickness. A flat steel fairing was soldered to the thin edges of the tube and it was tapered from 1/16 inch at the center

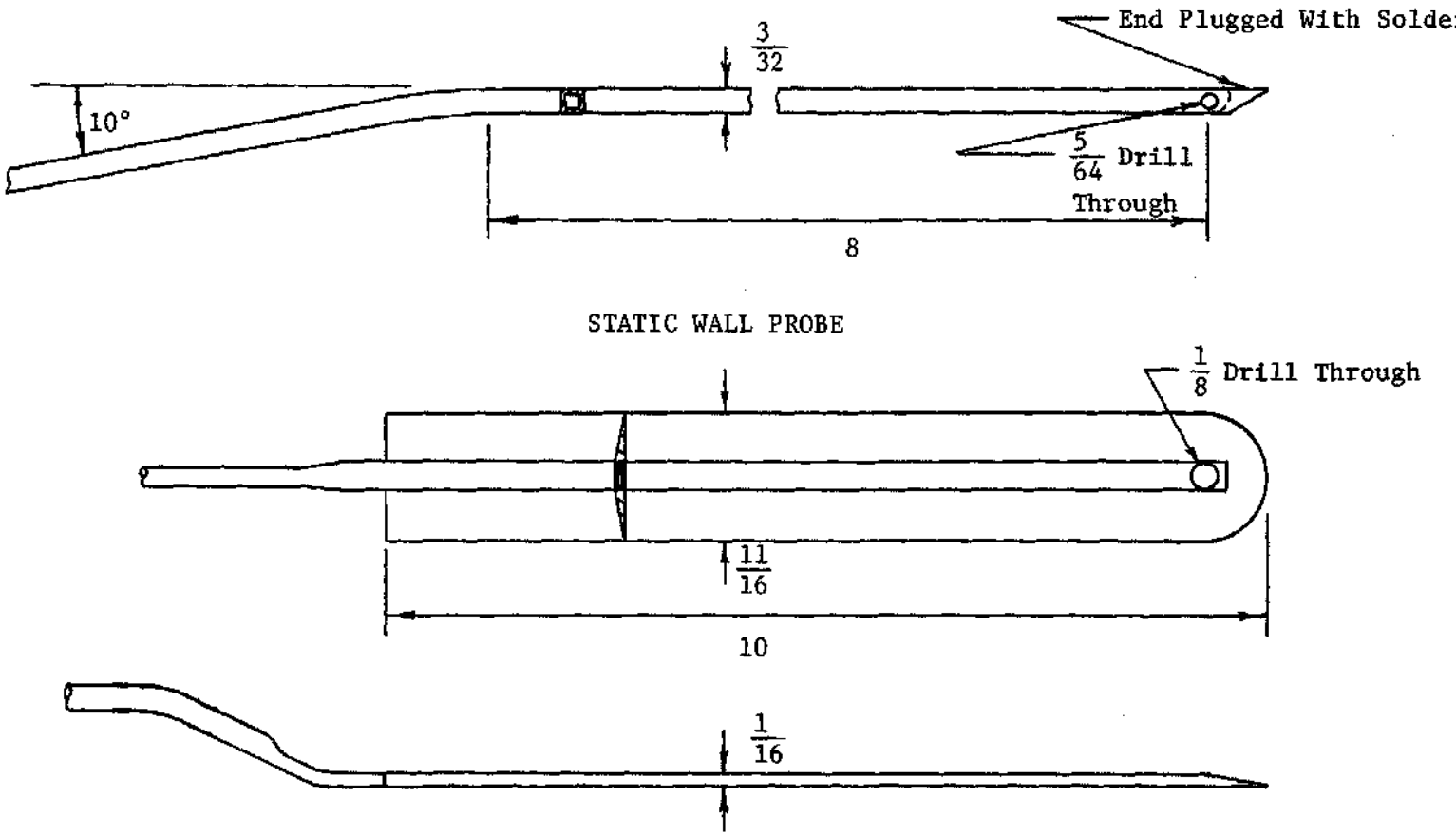

Figure 14. Static Pressure Probes

to a knife edge on the perifery. The entire assembly was polished to a high gloss with jeweler's rouge and a cloth buffing wheel. The very thin probe was to remain in the boundary layer of the flow by resting against the aluminum sidewall of the model. The validity of the probe readings was to be checked by utilizing three 3/32 inch holes drilled into the aluminum base of the model and connected to manometers.

A sketch of the impact probes used to obtain total pressure data in the flow field is shown in Figure 15. One of the impact probe heads was constructed to swivel in the plane of the model in order to be pointed directly into the flow to be measured. Control of the probe position from outside the model was achieved by a string and pulley arrangement. The shape of the probe heads is the internally sharpened shape that yields the most accurate pressure measurements in low Reynolds number flows (17).

Copper-Constantan thermocouples were used to monitor the stagnation temperature of the air in the upstream tank, the model, and the downstream tank. For purposes of analysis and data evaluation the total temperature of the gas was assumed constant, and these temperature measurements provided a check for that assumption. A sketch of the probe used is shown in Figure 16.

In order to determine the approximate direction of the flow at selected points in the model a flag probe as shown in Figure 17 was used. The flow direction is determined visually through the plexiglass as is the position of each of the other probes.

The jet velocity profile at the nozzle exit was qualitatively

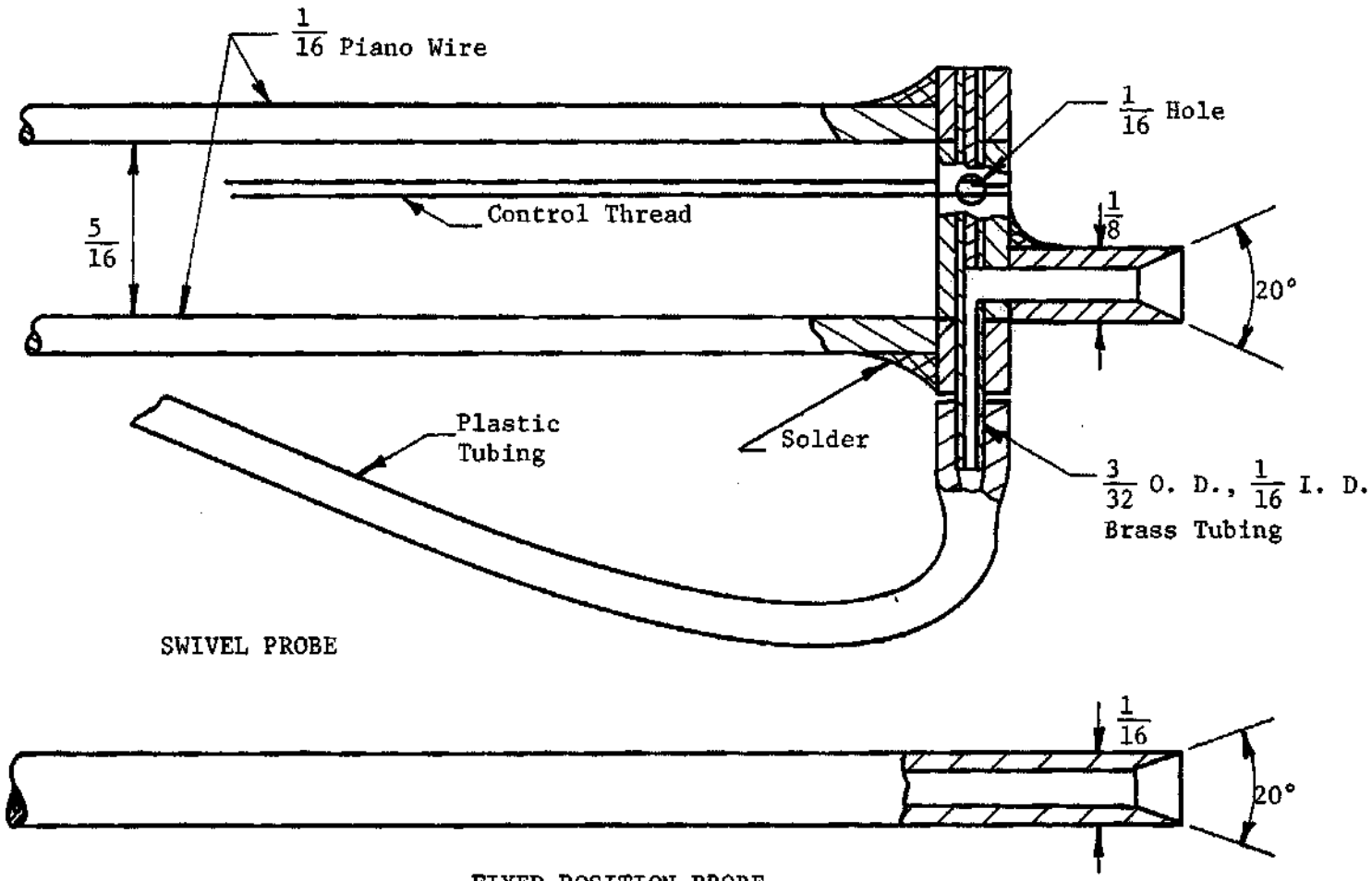

Figure 15. Impact Probes

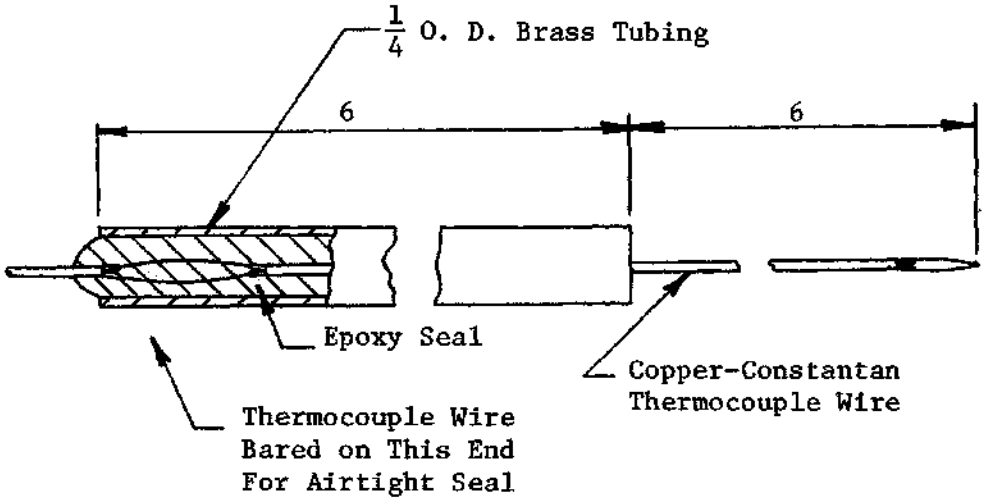

Figure 16. Thermocouple Probe

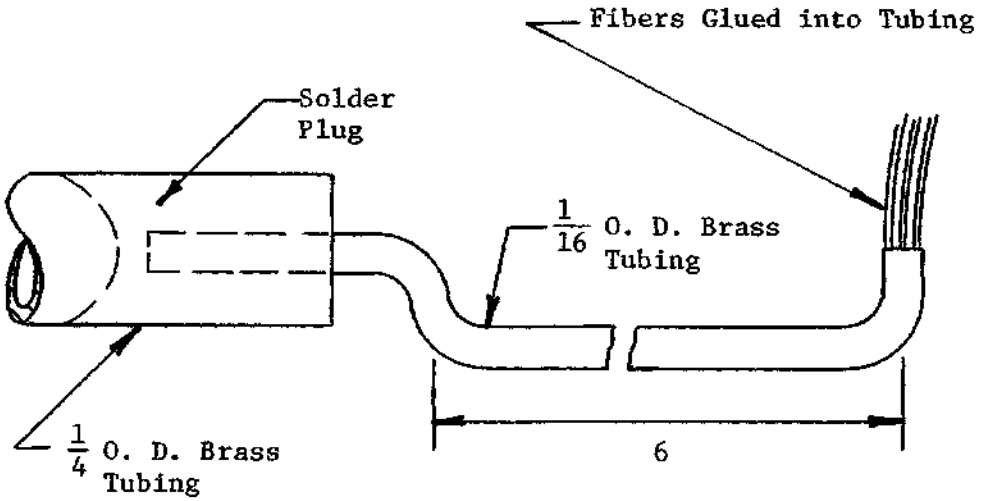

Figure 17. Flag Probe

examined with a probe consisting of a stainless steel tube which is 1/32 inch in outside diameter with 0.006 inch wall thickness.

Instrumentation

Pressure readings were taken from each probe and read from a group of manometers. Mercury manometers open to the atmosphere on one side were used in conjunction with a cathetometer to obtain absolute pressure readings by correcting with barometer readings taken at the time of each experiment. Oil filled manometers inclined at 30° to the horizontal and oil filled "U" tube manometers were used to read differential pressures between the probes and the model ambient pressure for values of differential pressure less than 21 mm of mercury. The oil used was a red Meriam manometer oil with specific gravity of 1.04, and it possessed an extremely low vapor pressure for use specifically in high vacuum applications.

Temperature measurements were made by reading voltages directly with a potentiometer in a thermocouple circuit with cold junction at 32°F in an ice bath. Temperatures were then determined by conversion of voltage readings to temperature with standard thermocouple tables.

Figure 18 shows photographs of the assembled model and instrumentation board.

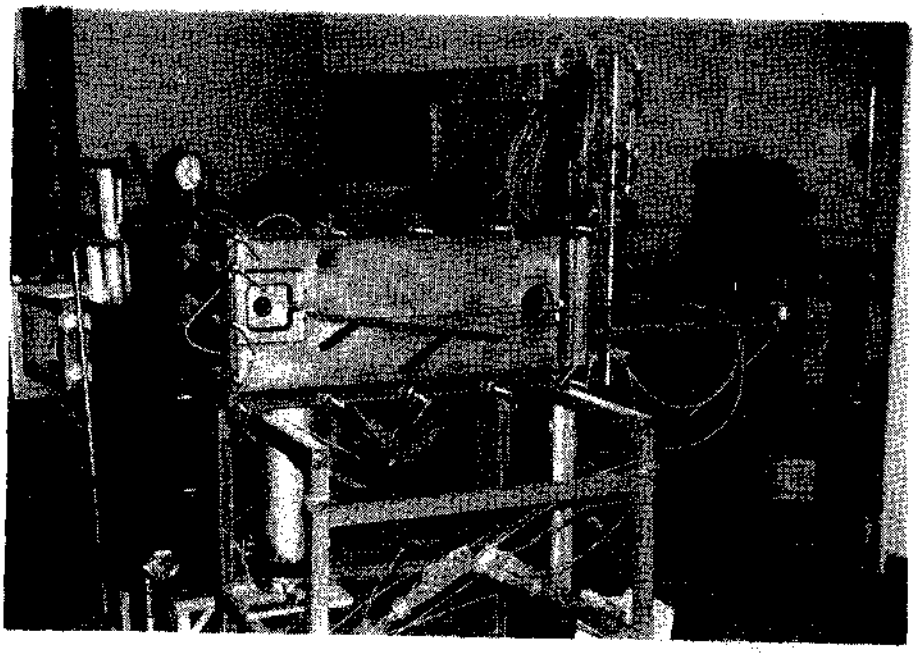

Assembled Model

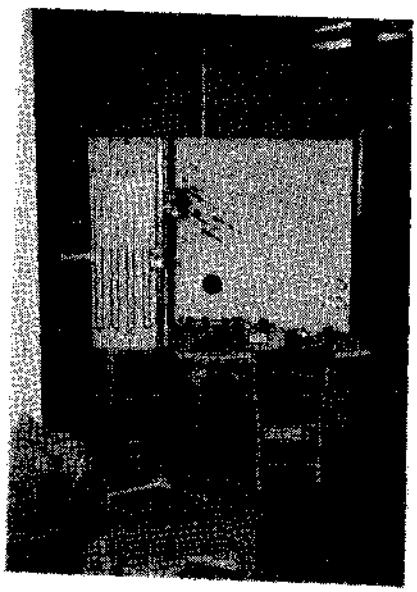

Instrumentation Board

Figure 18. Equipment Photographs

CHAPTER IV

PROCEDURE

Preliminary Considerations and Adjustment of Flow Conditions

The experimental investigation was divided into two segments consisting of jet attachment studies and unattached jet studies. The jet attachment experiments were to determine if jet attachment will occur for the low Reynolds number flow associated with the Knudsen number flow ranges to be examined, and to collect data on attachment distance, attachment wall static pressure, and attempt to fully describe the flow fields encoundered. The unattached jet experiments were to provide data for the purpose of obtaining an approximate model of a free jet in the flow ranges investigated for use in comparing Olson's analysis of attaching jets and the simplified model to the experimental results.

Two flow measuring devices were considered before standard impact and static pressure probes and manometers were selected for use. A corona discharge probe that operated on the principle of varying drift speed of ionized gas particles between highly charged minute electrodes with varying gas velocity was considered. This device was not used because it had been previously demonstrated to have an unpredictable useful life, and it presented calibration difficulties. Hot wire anemometers were considered, but were not used due to insufficient development for use in compressible flow. The accuracy of

these two devices had not been demonstrated for supersonic flow as well as subsonic flow as in the case for the impact pressure probe.

Prior to each experiment the model and pressure sensing instruments were evacuated below 1 mm of mercury for a short time to expell accumulated moisture and contaminants from the apparatus. The model pressure and the nozzle supply pressure were regulated by trial and error by manually adjusting the upstream and downstream control valves simultaneously. Model ambient pressures were determined from equation (4) and perfect gas, isentropic nozzle flow relations for four values of Mach number 0.5, 0.8, 1.94, and 2.71, and for four values of Knudsen number 10^{-4}, 5×10^{-4}, 10^{-3}, and 4×10^{-3}. The upstream tank pressure was determined from the standard isentropic nozzle flow relations for a perfect gas also. Every effort was made to adjust the pressures within the device to the theoretical values presented in Appendix C. Very small variations from desired Mach and Knudsen number pressure settings were unavoidable, however. These slight variations are ignored in the presentation of the results although they are available from the data in the appendix.

Prior to conducting the attachment and unattached jet experiments temperature measurements were made for a variety of flow conditions with air taken from within the surrounding room and without the water bath around the upstream tank. The stagnation temperature of the air varied less than 5°F from room temperature (77°F) in each case, so further temperature measurements were discontinued for the other experiments, and the water bath was not used.

Measurements

All pressure measurements were made with the group of manometers described in the previous chapter. Pressure measurements were obtained by positioning the probe and measuring its position as described in the next section. The very low Reynolds numbers characteristic of some of the flow encountered in the experiments required a waiting period after positioning the probes for the manometers to reach an equilibrium reading. This waiting period varied from fifteen minutes to only a few seconds depending on the flow conditions and type of measurement. The inclined oil manometers were read by visually determining the line on a graph paper background that was tangent to the miniscus. Oil "U" tube and mercury manometers were read with a vertical telescopic lens cathetometer. All probes except the flat boundary layer probe were positioned midway between the sidewalls plus or minus approximately 1/8 inch to minimize the influence of the sidewalls on the pressure measurements.

Jet Attachment Experiments

For each attachment experiment, the pertinent amplifier geometry was drawn on the outer face of the plexiglass cover plate by sighting along one edge forming the right angle of a drawing triangle while the other perpendicular edge was held flat against the plexiglas. The triangle was placed along the plexiglas surface so that desired locations within the model were visually aligned with the edge perpendicular to the model and the location on the plexiglas was marked with a

very fine point pen. This method was used in laying off the model geometry and in marking the position of probes in each experiment that was performed. Accuracy was determined by measurement of the amplifier geometry that was drawn on the plexiglas to be ± 0.01 inches. The positions of the probes were measured on the outer surface of the plexiglas with a vernier caliper.

All of the attachment experiments were conducted with the same model geometry consisting of setback of the attachment wall of 0.30 inches and wall angle of 10°. Since replacement of the removable nozzle blocks required a partial disassembly of the model, all the experiments for a given Mach number were performed before proceeding to a different Mach number experiment.

Jet attachment distance was measured along the attachment wall from the nozzle exit plane by examining the synthetic fibers that were glued to the attachment wall. The location of jet attachment was assumed to be the location on the wall where the direction of bend of the fibers that were deflected by the flow changed from the upstream direction to the downstream flow direction. The change in the direction of the fibers indicated the point where the flow recirculating into the attachment bubble separated from the flow continuing downstream along the wall.

Static pressure along the attachment wall was measured using the probe shown in Figure 14. The probe was moved along the attachment wall to a desired location and its position was measured along the wall by the method previously discussed. The fringe on

the attachment wall was watched carefully to confirm that the attachment point location did not move during the measurements and thereby invalidate the data. Care was taken to position the probe near the center of the wall between the side plates.

Attempts to make impact and static pressure measurements throughout the flow field were unsuccessful. These measurements were not made because the presence of the probes drastically changed the flow field as determined by observation of the hairlike fringe on the attachment wall.

Pressure readings were made using the oil filled manometers whenever possible to assure greater accuracy. Other measurements made with the mercury manometers were subject to minor inaccuracies due to small barometric pressure fluctuations during the course of the experiments.

Unattached Jet Experiments

The unattached jet experiments were conducted with the same nozzle blocks used in the attachment experiments and with the attachment wall removed from the model. Just as in the attachment experiments the experiments for a given Mach number were completed before proceding to the other experiments. The nozzle centerline and nozzle exit plane were drawn on the outer surface of the plexiglas cover plate to establish the x and y coordinates of the probe positions.

Jet impact pressure profile measurements were made using the fixed position probe shown in Figure 15 for two fixed values of x

along the jet centerline. These measurements were made for numerous values of y parallel to the nozzle exit plane in an effort to establish velocity profiles under the assumptions of constant pressure and stagnation temperature within the jet. One of the profile measurements was made within the jet near the nozzle where the potential core was present, and the other profile measurement was made downstream of the core region in the fully developed portion of the jet.

The pressure profiles obtained from the lateral traverses of the impact probe across the jet showed that the jet centerline defined by the locus of maximum velocity locations did not exactly correspond to the nozzle centerline. The slope of the jet centerline was found to be approximately 1/30 or less with respect to the nozzle centerline. Impact pressure measurements were made approximately along the jet centerline as indicated by the profile measurements to obtain the potential core length and jet centerline velocity decay curve.

Impact pressure measurements were made at several positions across the nozzle exit with the 1/32 inch O. D. probe described in the previous chapter. The Reynolds numbers for this small probe and the type of flow encountered is such that the pressure values determined from its use are very inaccurate (17). Furthermore, the probe was not small enough to obtain an accurate impact pressure profile across the 0.2 inch nozzle exit. These measurements were made to qualitatively examine the nozzle exit flow profile for squareness as assumed in Olson's theoretical analysis.

Analytical Comparison

Olson's analysis of jet attachment is dependent on two empirically determined coefficients K_1 and K_2 which have been defined in Chapter II. The comparison of Olson's method to the experimental results of this study is made by determining the constants K_1 and K_2 from the data obtained in this study and comparing them with values of K_1 and K_2 reported by Olson. The method of calculating K_2 is illustrated in Appendix D, "Sample Calculations."

CHAPTER V

DISCUSSION OF RESULTS

Data

A complete collection of the data obtained from the experiments is found in Appendix C. The calculations that were performed to obtain the results are not presented in full, but illustrations of the pertinent calculation procedures are also found in Appendix D as sample calculations.

Wall Attachment Results

Static pressure variations along the attachment wall are presented in Figures 19 through 22 in terms of a dimensionless pressure coefficient, $P_w-P_e/P_{t_o}-P_e$. The pressure coefficient represents the fraction of nozzle supply pressure in excess of the ambient model pressure that is available along the attachment wall as static pressure. The shape of the curves drawn through the data points is characteristic of static wall pressure curves for attaching jets previously investigated by Bourque and Newman and Olson. The shape of the curves confirms that in each case the jet did attach to the wall. The wavy portion of some of the curves indicates the presence of oblique shock waves in the supersonic attaching jets. Shock waves were caused by the simplicity of the nozzle geometry and slight errors in adjustment of nozzle supply pressure. The attachment point locations along the wall are denoted on each curve. The attachment point location was determined for each

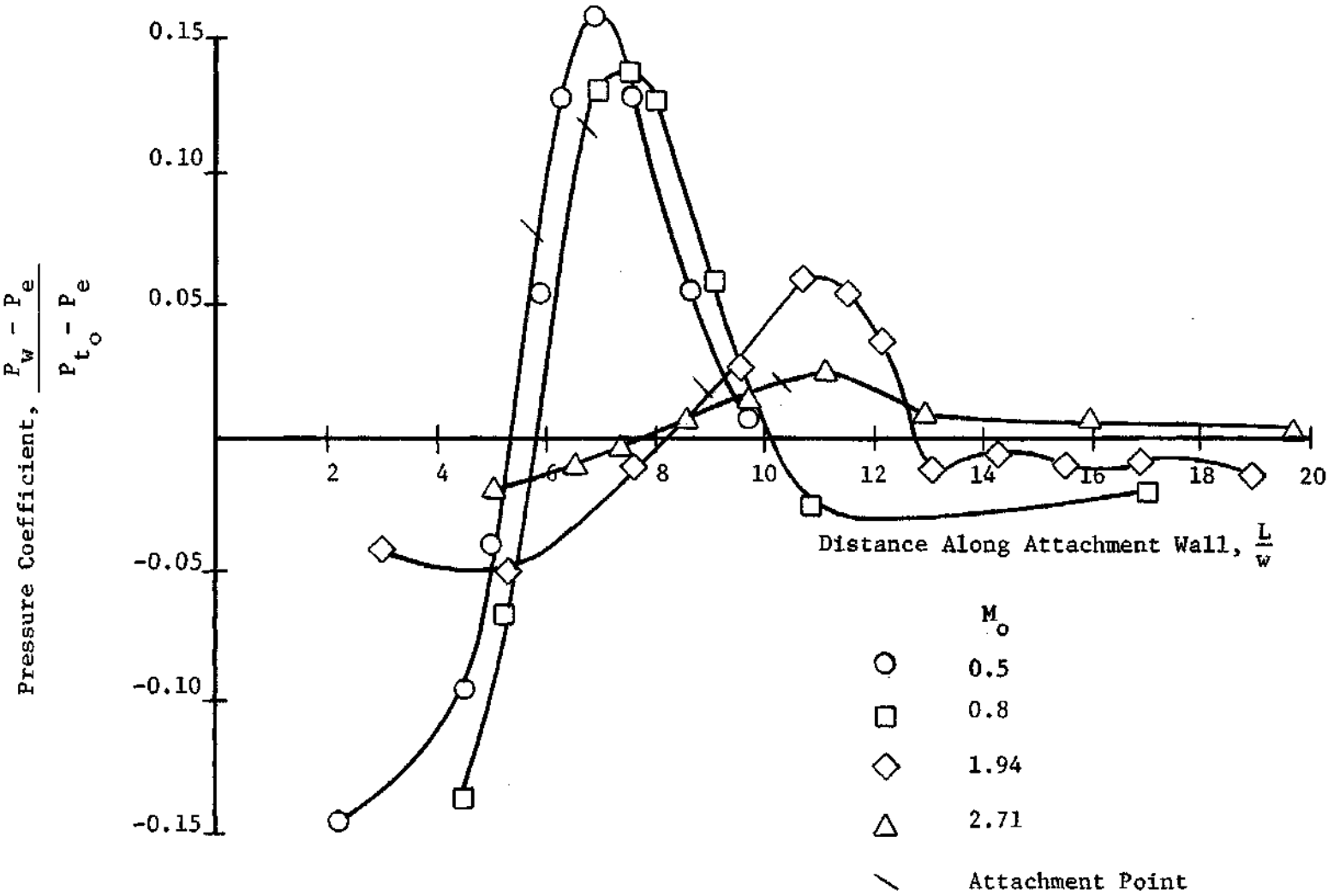

Figure 19. Static Pressure on Attachment Wall, $K_n = 10^{-4}$

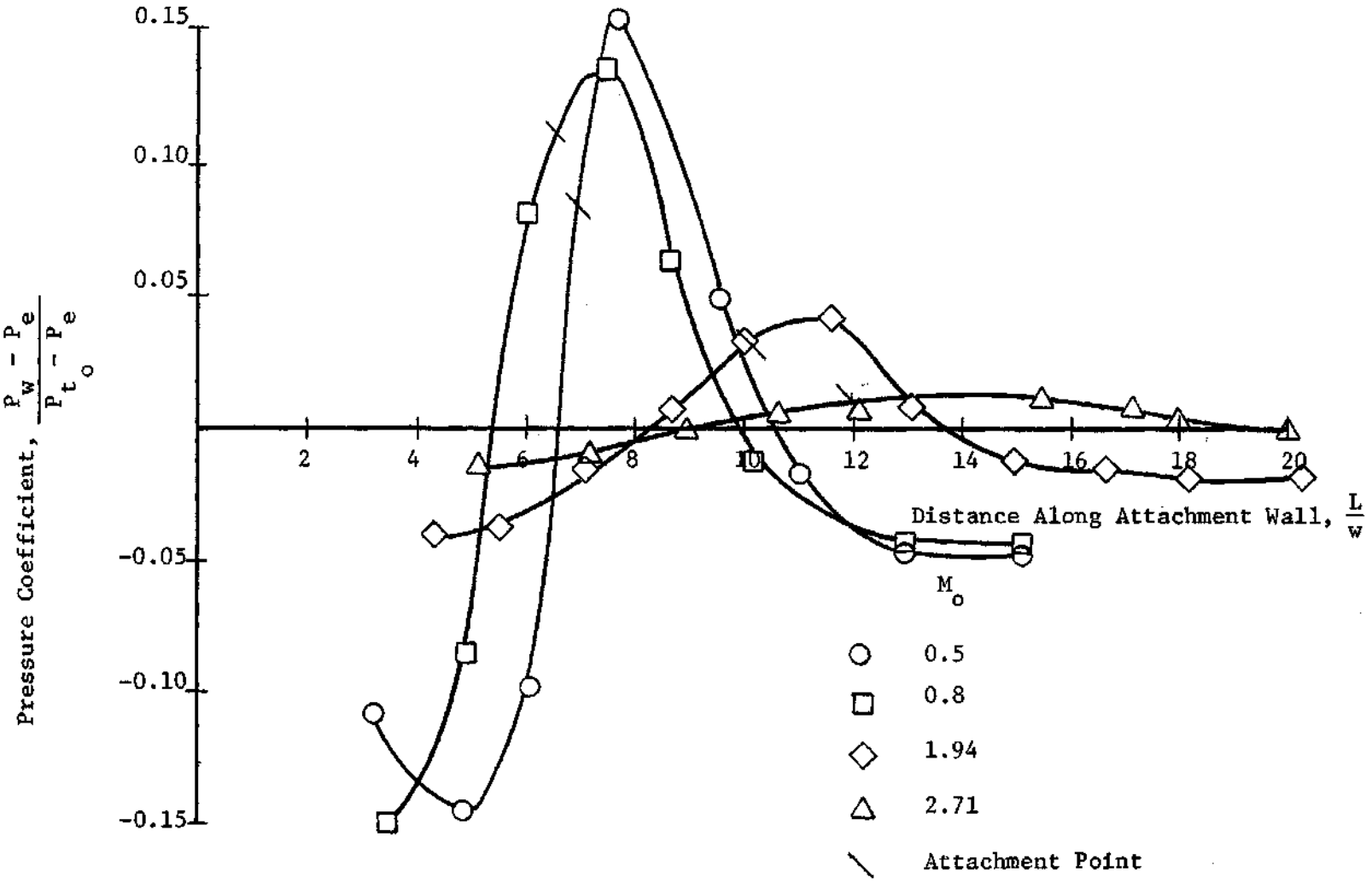

Figure 20. Static Pressure on Attachment Wall, $K_n = 5 \times 10^{-4}$

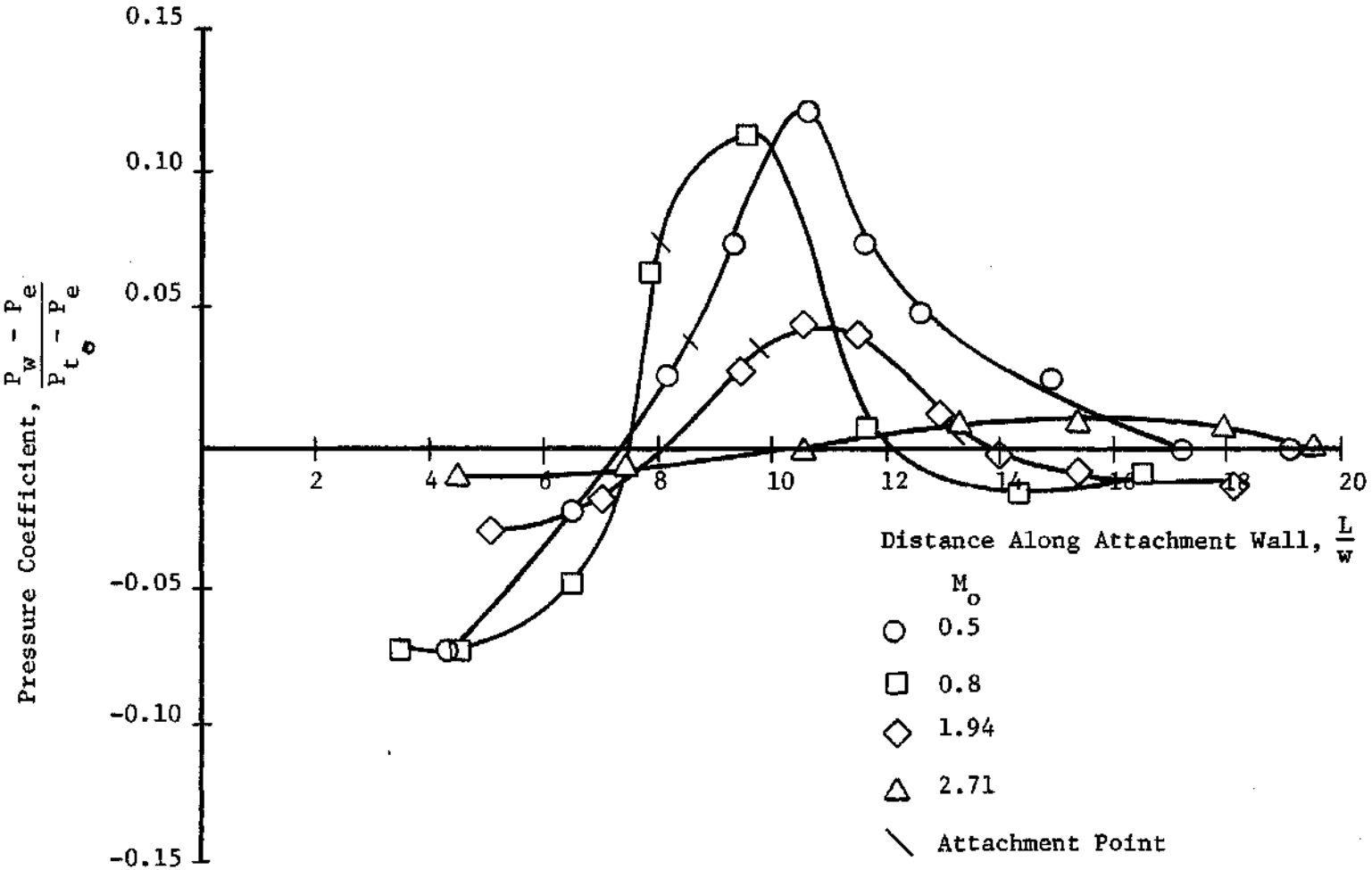

Figure 21. Static Pressure on Attachment Wall, $K_n = 10^{-3}$

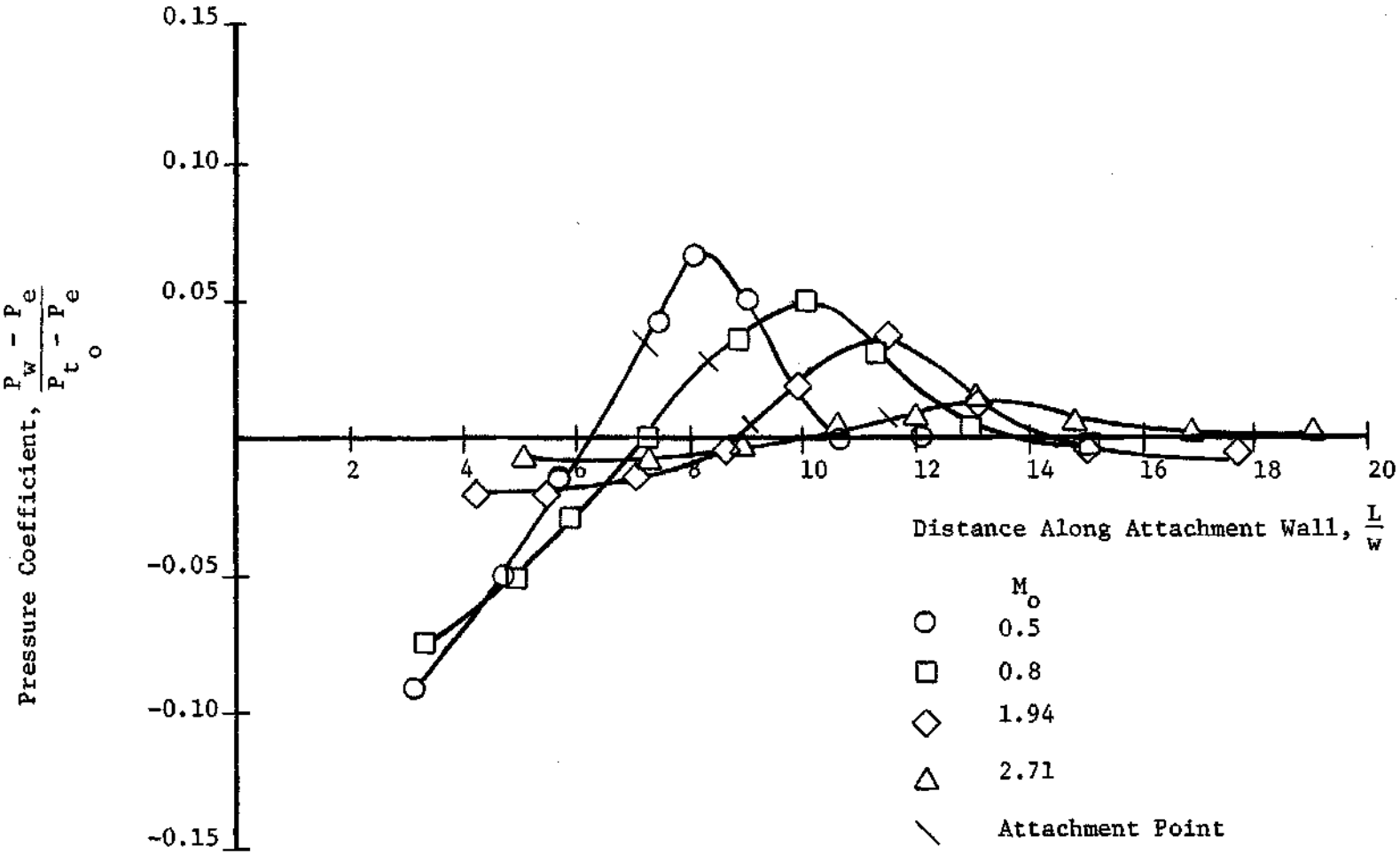

Figure 22. Static Pressure on Attachment Wall, $K_n = 4 \times 10^{-3}$

case by observation of the fibers glued to the attachment wall except for the Mach numbers 0.5 and 0.8 in Figure 22. For these two cases the flow immediately adjacent to the wall was not sufficient to bend the fibers, and the attachment point in each case was assumed to lie near the position on the wall where the static pressure coefficient was one-half its maximum value. All of the measured attachment locations indicated on the static pressure curves are located between the maximum and zero value of the pressure coefficient. This location on the pressure rise portion of the curve in the downstream direction is in agreement with the results of the jet attachment investigations that are referred to above. The relative positions of attachment point locations along the wall correspond with the relative positions of the maximum values of the corresponding curves drawn through the pressure data. Maximum values of pressure coefficient are greater for low Mach numbers than for high Mach numbers because jet momentum varies more than pressure drop due to entrainment resulting in large Mach number jets having large radii of curvature and therefore shallow attachment angles. The maximum values of static pressure coefficient appear to decrease in general with increasing Knudsen number and, in turn, decreasing Reynolds number. This effect is a result of the decrease in jet density and therefore reduction in wall pressure rise required to deflect the jet with reductions in Knudsen number.

The attachment distance along the wall non-dimensionalized with the nozzle width is presented in Figure 23 as a function of Mach number for fixed values of Knudsen number. The data does not exhibit a consistently shaped variation for all Knudsen number values; however,

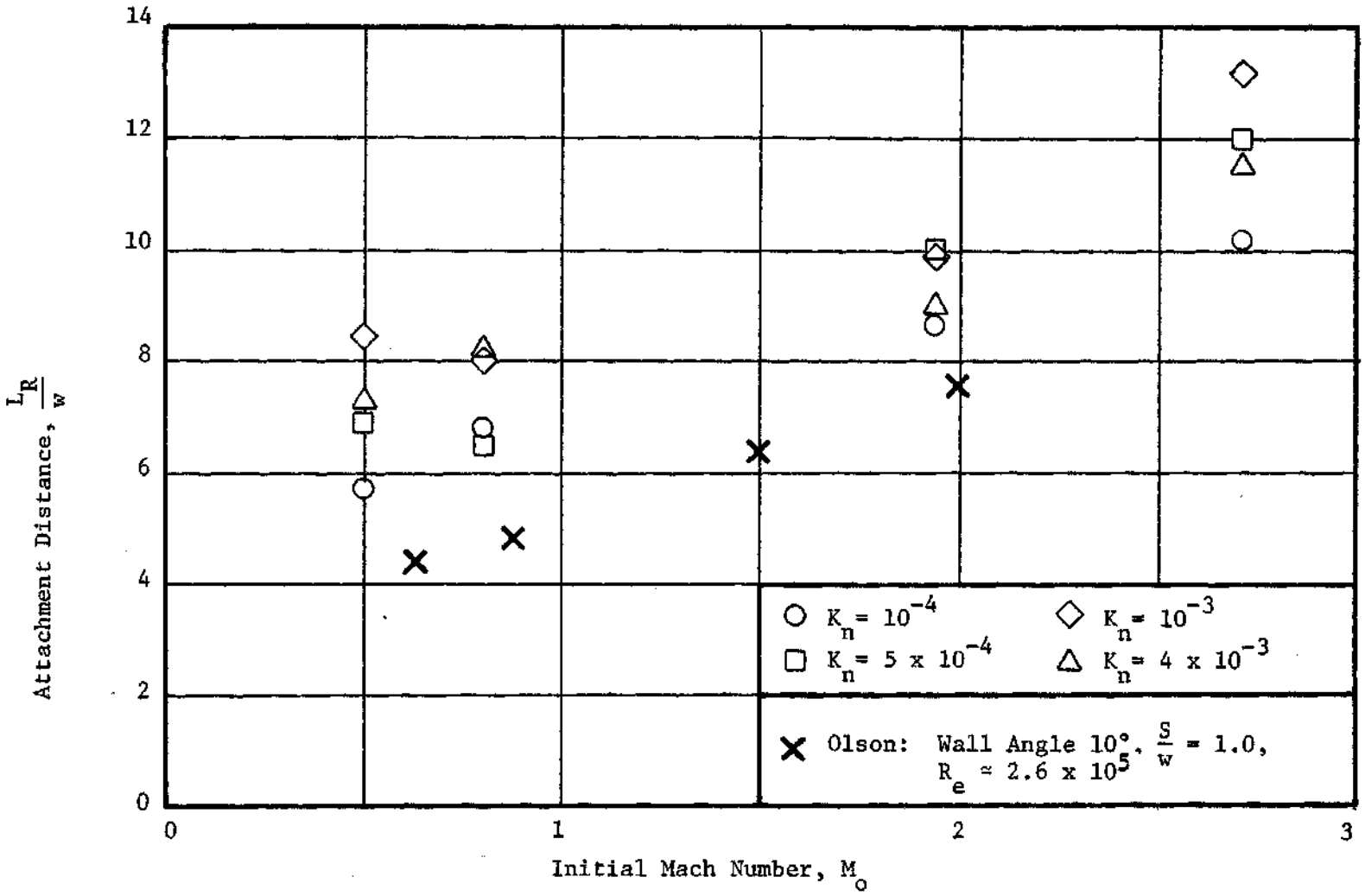

Figure 23. Attachment Distance and Mach Number

it does reflect an increase in attachment distance, generally speaking, with Mach number. The attachment point distance appears to level off or perhaps exhibit a minimum in the subsonic jet region. Data from Reference (10) is plotted in Figure 23 for comparison. The geometry used in Reference (10) is approximately the same as that used in this study; however, the setback was equal to 1.0 nozzle width rather than the setback of 1.5 nozzle widths for this study, and the attaching jet Reynolds numbers were approximately constant and equal to 2.6×10^5. The closer proximity of the wall to the jet results in slightly shorter attachment distances than observed in this study as expected.

The non-dimensionalized attachment distance is plotted as a function of Reynolds number for four Mach number values in Figure 24. Each curve defined by the data for one Mach number value exhibits a maximum. The curves have the same shape qualitatively as the curves that provide similar information in the study by Comparin, Jenkins, and Moore (14) of attaching incompressible jets at very low Reynolds numbers. The data from the study by Comparin exhibited maximums at somewhat lower Reynolds numbers than this study. Comparin's data and analysis did show, however, that for a fully laminar incompressible jet, attachment distance was proportional to Reynolds number, that three-dimensional effects were partly responsible for increased attachment distance with decrease in two-dimensional nozzle aspect ratio for small Reynolds number jets, and that the peak in the attachment distance curves becomes more prominent for increased wall

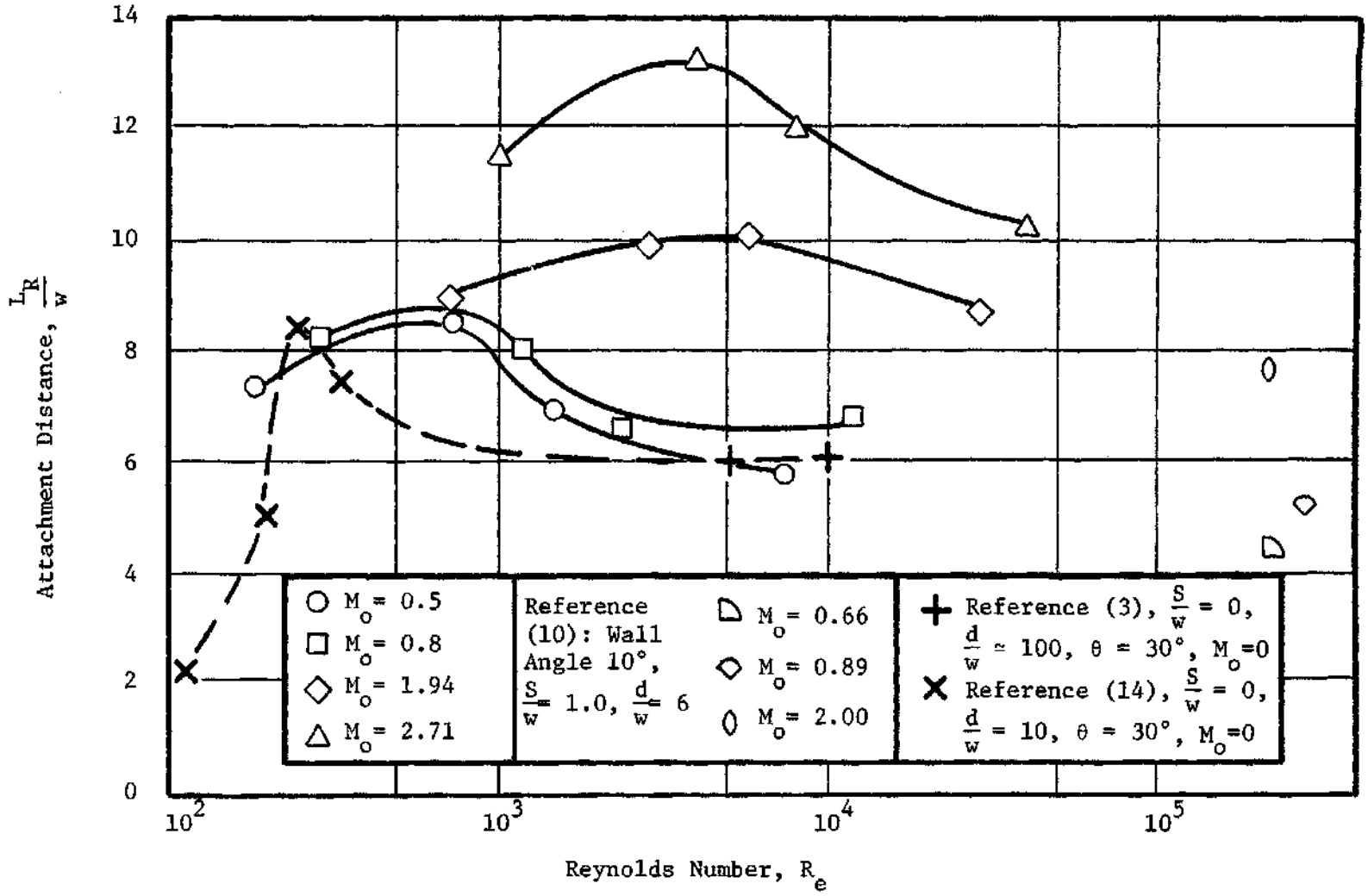

Figure 24. Attachment Distance and Reynolds Number

angle or increased average distance of the wall from the nozzle centerline. According to the results of Bourque and Newman the attachment distance is approximately constant for a fixed geometry and turbulent incompressible jets, and it is independent of Reynolds number. This result appears to be the same for compressible jets as shown in Figure 24 where the attachment distance curves seem to level off as the Reynolds number becomes large. The data by Olson that was previously plotted in Figure 23 is included also in Figure 24. It seems to agree qualitatively with the results when the closer proximity of the wall in Olson's experiments is considered.

The peak in the attachment distance curves is explained by Comparin to be a result of three-dimensional effects. These effects may indeed influence the attachment distance for finite aspect ratio nozzle devices, but a peak in the curve may also be qualitatively explained by considering the effect of the behavior of the turbulent eddy viscosity at various local jet Reynolds numbers. An apparent Reynolds number (R_{e_a}) may be defined locally as:

$$R_{e_a} = \frac{\rho \xi^* u}{\mu + A} \tag{30}$$

where A is the turbulent eddy viscosity and ξ^* is the mixing region width of the jet at some position along the jet centerline. Rewriting equation (30) we have:

$$R_{e_a} = \frac{R_e}{1 + \frac{A}{\mu}} \tag{31}$$

where R_e is the local Reynolds number in the flow field. Assuming

the viscosity (μ) remains approximately constant locally, equation (30) can be differentiated:

$$\frac{\partial R_{e_a}}{\partial R_e} = \frac{1}{1 + \frac{A}{\mu}} - \frac{R_e}{\left(1 + \frac{A}{\mu}\right)^2} \frac{\partial\left(\frac{A}{\mu}\right)}{\partial R_e} \tag{32}$$

The eddy viscosity is considered to be proportional to R_e if Prandtl's mixing length model is considered valid and fully turbulent flow prevails. The eddy viscosity is also known to vanish for some value of R_e where the flow becomes laminar. If the eddy viscosity is then assumed to vary with Reynolds number in the manner shown in Figure 25, it is reasonable to assume that the value of $\partial \frac{A}{\mu} / \partial R_e$ may be large enough somewhere in the region of transition from laminar to turbulent flow to make the negative term in equation (32) predominate. For this case a maximum value of R_{e_a} will occur when the slope of the eddy viscosity curve is large enough to make equation (32) zero. From examination of Figure 25 and equation (31) R_{e_a} is essentially constant for all large values of R_e, and it is equal to R_e for small values. The resulting sketch of R_{e_a} as a function of R_e in Figure 26 is of the same shape as the attachment distance as a function of R_e curves in Figure 24. It is reasonable, then, to surmise that the attachment distance varies in some linear manner with apparent Reynolds number. This intuitive idea agrees qualitatively with the results of all the investigations previously mentioned if the suitable characteristic local Reynolds number for this type of flow is assumed to be the Reynolds number defined at the nozzle exit. Figure 24 indicates that

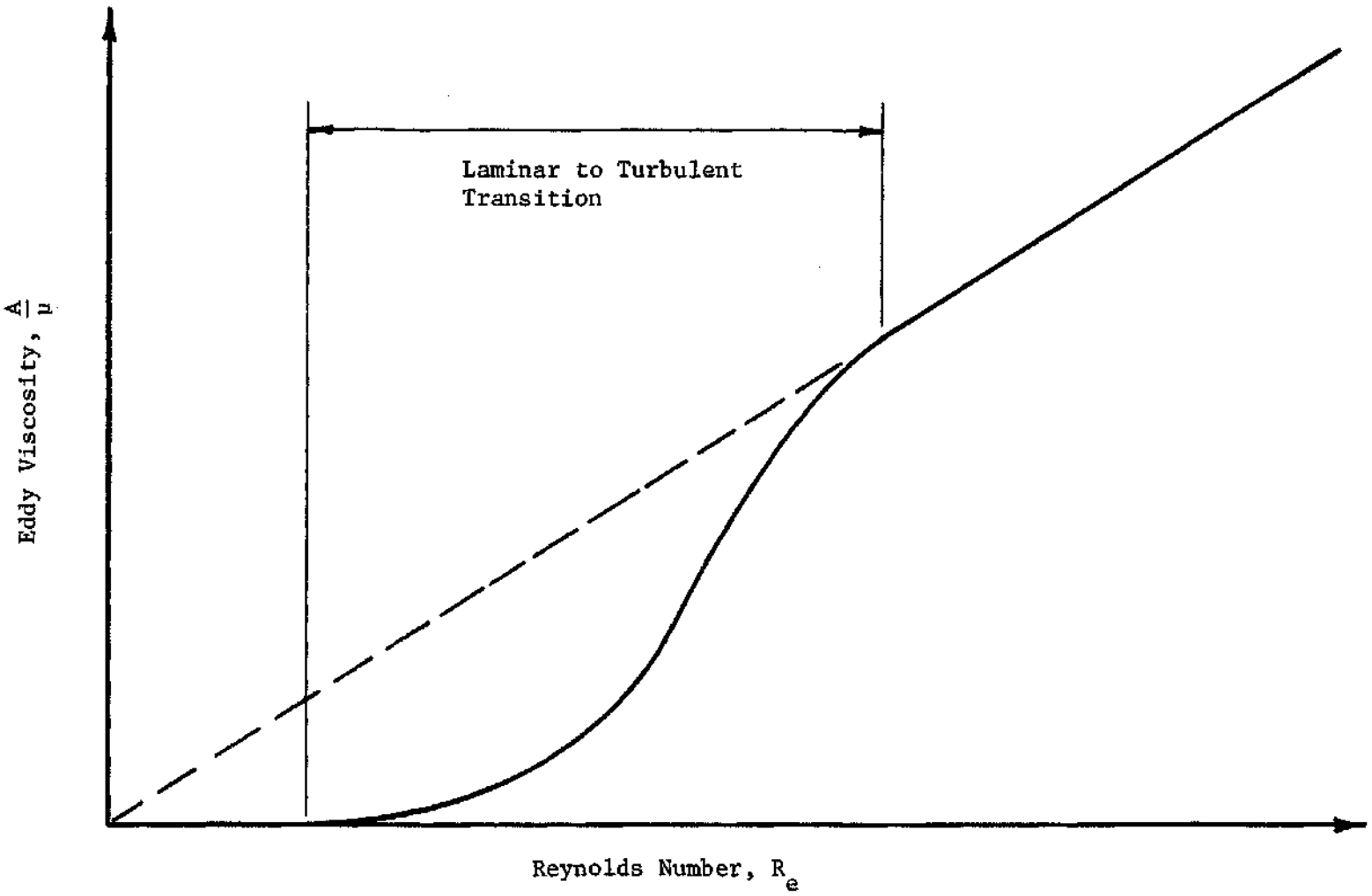

Figure 25. Assumed Eddy Viscosity and Reynolds Number Relationship

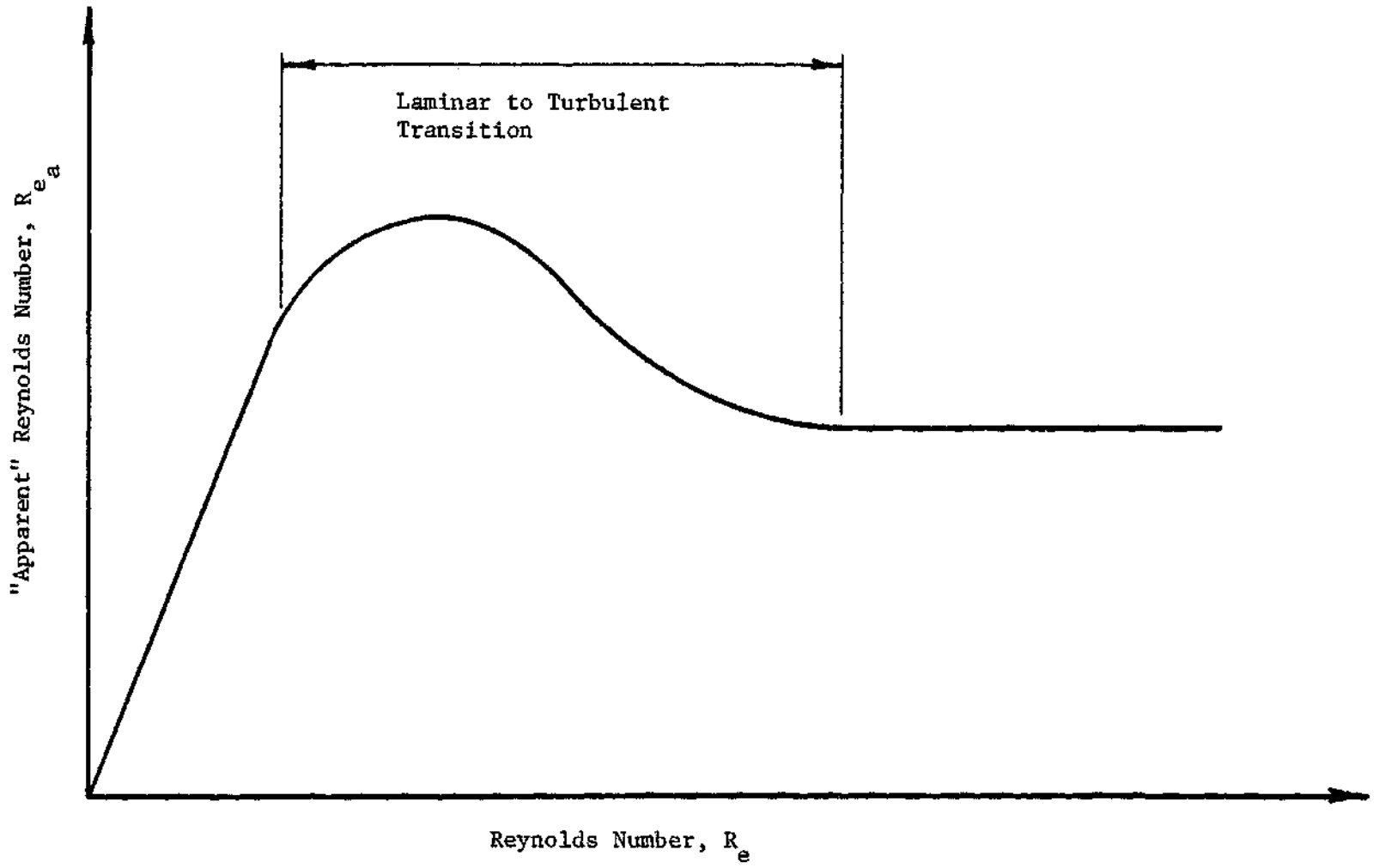

Figure 26. Variation of "Apparent" Reynolds Number with Reynolds Number

for fixed Reynolds numbers, the attachment point will increase with increasing Mach number as expected from the results of Reference (10). Also the maximum attachment point value occurs at larger values of Reynolds numbers for supersonic flow than for subsonic flow. This result might be caused by the influence of shock waves in the supersonic flow.

Efforts to obtain data for complete flow field description within the model were not successful. The presence of any type of probe positioned in the flow field and not adjacent to the attachment wall resulted in a rather large change in the attachment distance along the wall and therefore the flow field was altered. In addition the flat boundary layer type static pressure probe lifted off the model sidewall when in the presence of high velocity flow and was subjected to violent fluttering that threatened to damage the probe and the model. Development of a suitable method of visualizing rarefied flows without positioning a probe in the flow field would simplify a complete flow field analysis near the wall.

Unattached Jet Results

The impact pressure profiles obtained from the unattached jets were not spread precisely around the nozzle centerline, but the approximate axis of symmetry was determined by plotting the calculated velocity profiles and folding them so that each half met. The non-dimensional velocity profiles in Figures 27 and 28 were calculated as illustrated in Appendix D for the core and the developed region of the jet. Although the spread of the data is noticeable around the curve that was

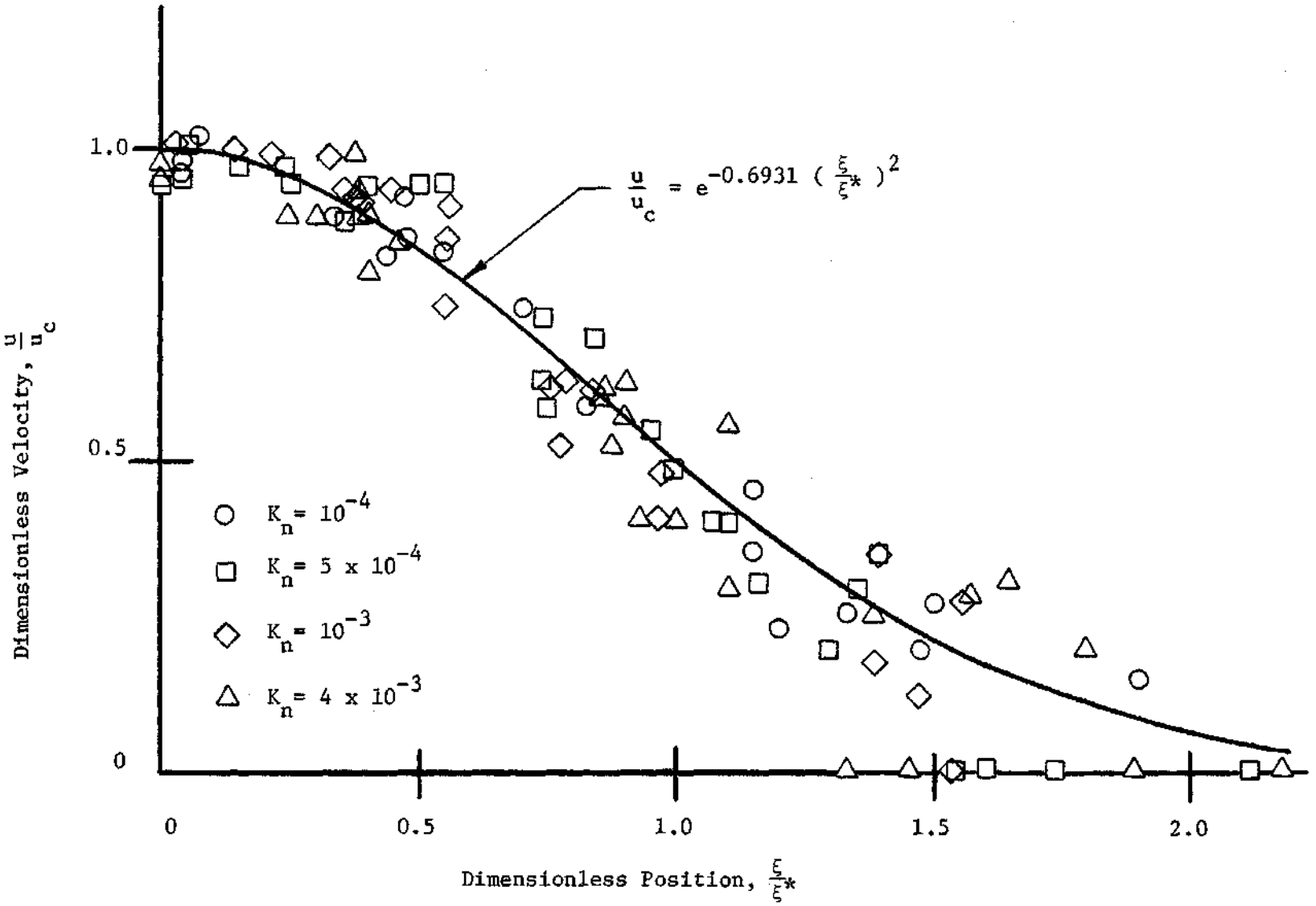

Figure 27. Dimensionless Velocity Profiles, Core Region

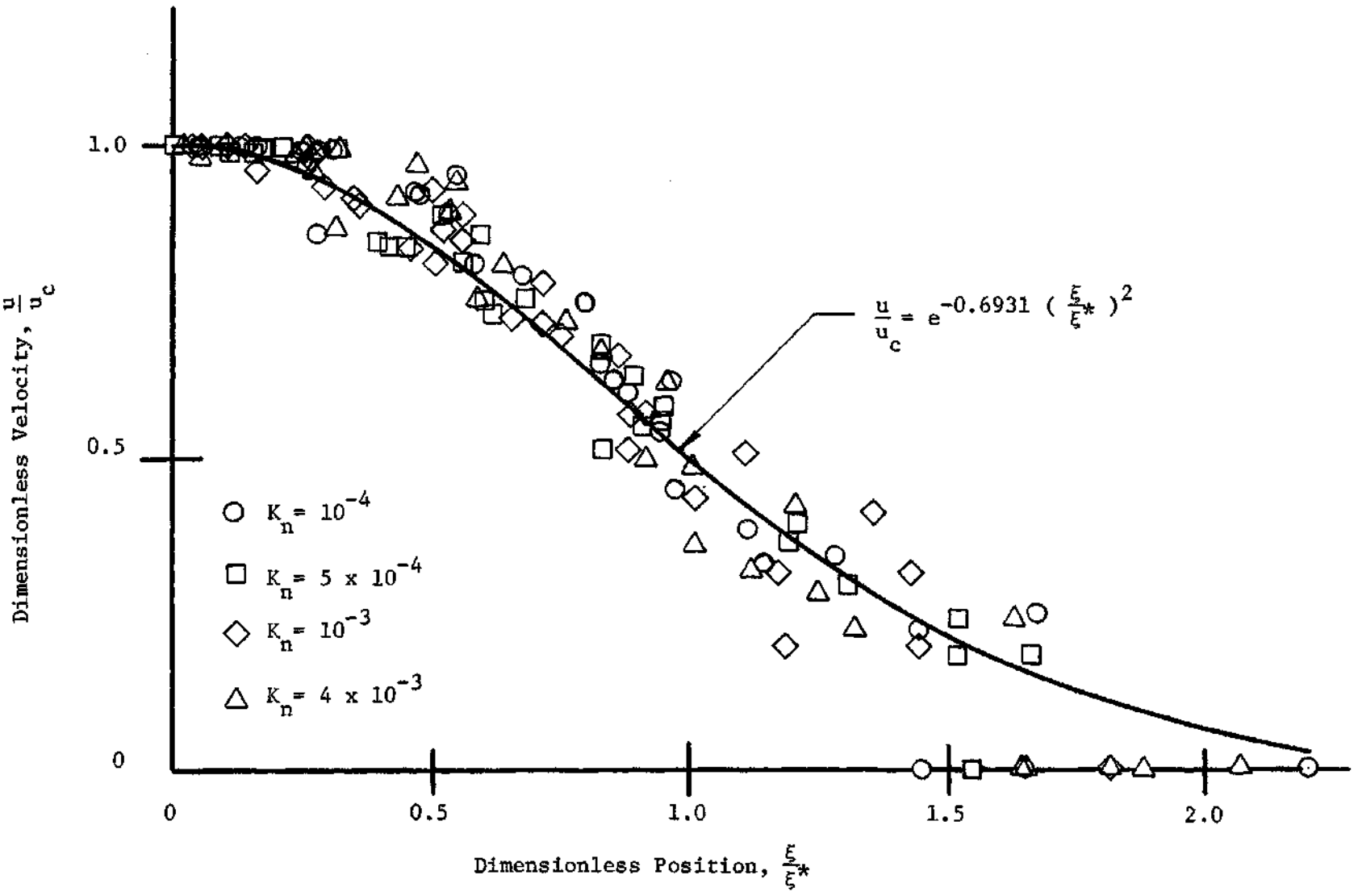

Figure 28. Dimensionless Velocity Profiles, Developed Region

suggested for use by Olson in previous studies, the curve appears to be a reasonable approximation and was utilized in the unattached jet calculations.

The jet centerline impact pressure measurements were converted to velocity values and normalized with respect to the maximum jet velocity calculated from experimental data. The centerline velocities for Mach numbers 0.5, 0.8, and 1.94 are plotted on semilog graphs in Appendix C and were found to approximately define a straight line in the fully developed region. The jet core length was considered to be defined by the intersection of the straight line that best fit the data of the developed region and the horizontal straight line through the velocities within the core region. The jets of Mach number 2.71 exhibited very widely fluctuating velocities along the centerline which indicated that a rather complicated shock pattern existed for this value of Mach number. Core length and centerline velocities could not be determined for this case and the unattached jet descriptions of Mach number 2.71 are incomplete. For the jets of Mach number 1.94 and less the relationship between centerline velocity and distance along the jet centerline may be represented as:

$$\begin{aligned} \frac{u_p}{u_o} &= 1 && x < x_c \\ \frac{x}{x_c} &= e^{m\left(1 - \frac{u_p}{u_o}\right)} && x_c < x \end{aligned} \tag{33}$$

where values of $\frac{x_c}{w}$ and m are compiled in Tables 27 and 28 in Appendix C for the applicable jets. Values of $\frac{x_c}{w}$ and m obtained from data presented in Reference (8) and the values from this investigation are

compared in Figure 29. The core length curves defined by this data exhibit the same general shape as the corresponding curves defined by the attachment distance data in Figure 24. This result is qualitatively explained in a similar manner as the attachment distance data was explained because both core length and attachment distance are determined by the existence of the apparent viscosity and the resulting jet entrainment properties. The data for Mach number 1.94 appear to agree very well for the lower Knudsen number. The subsonic jet values of m appear to agree fairly well, but the jet core lengths were somewhat larger in Reference (8). This result may have been caused by nozzle geometry differences or a somewhat thicker boundary layer to nozzle width ratio in the subsonic nozzles of this investigation. The increase in boundary layer to nozzle width ratio would be a result of the lower Reynolds number jets used in this study.

A qualitative indication of the velocity profiles at the nozzle exit may be found by examining the impact pressure profiles at that position. These pressure values have been included with the unattached jet data in Appendix C. The size of the nozzle and the rarefied flow made nozzle exit impact pressure measurements very difficult and inaccurate. Although the data was taken at relatively widely spaced intervals across one-half of the nozzle in each case, the magnitudes of the measured impact pressure appears to decrease slightly near the lip of the nozzle which indicates the presence of a boundary layer. In general, however, the impact pressure profiles appear to be very "full," and the nozzle exit velocity profile was assumed to be uniform in the calculations.

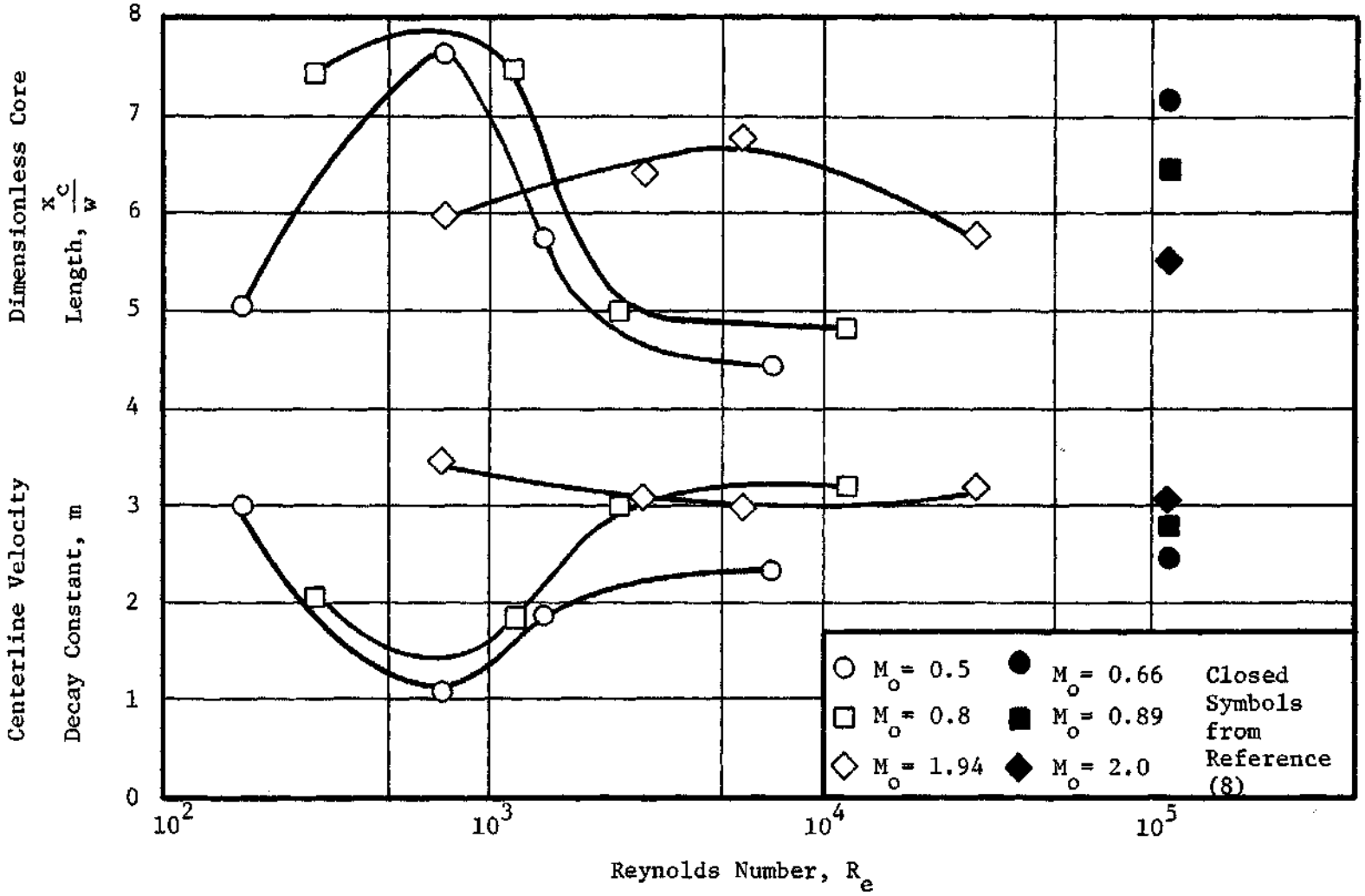

Figure 29. Dimensionless Core Length Variation with Reynolds Number, Centerline Decay Constant Variation with Reynolds Number

Comparison to Olson's Analysis

The comparison to Olson's analysis was conducted by determining the two empirical coefficients that arise in the derivation found in Reference (10) from the empirical results of this investigation. The value of K_1 is defined as the ratio of the distance along the attachment wall from the nozzle exit plane to the position where the pressure coefficient in Figures 19 through 22 is zero to the attachment distance along the wall. This coefficient is represented by Olson as a constant for a fixed geometry device, and it is easily determined from the wall static pressure curves and the attachment distance data. The values of K_1 are presented in Figure 30 as a function of Reynolds number. The data is scattered around the value 0.88 which was used in all the calculations of K_2. The value of K_1 recommended by Olson for devices with setback of 1.5 nozzle widths is approximately 0.75.

The value of K_2 is defined in Chapter II as the fraction of the maximum attachment bubble pressure force that is effective in recirculating fluid back into the attachment bubble. The value of this coefficient should be less than one. No convenient method is suggested by Olson for determining K_2. For reasons of comparison the values of K_2 corresponding to the empirically determined attachment distances were calculated as illustrated in Appendix D. Figure 31 is a plot of the results as a function of jet Reynolds number. Although the curves appear to have approximately similar shapes, all the values of K_2 are greater than one which is physically impossible. The values of K_2 suggested for use in Reference (10) are included in Figure 31 for comparison purposes. The rather large values of K_2 are in part a

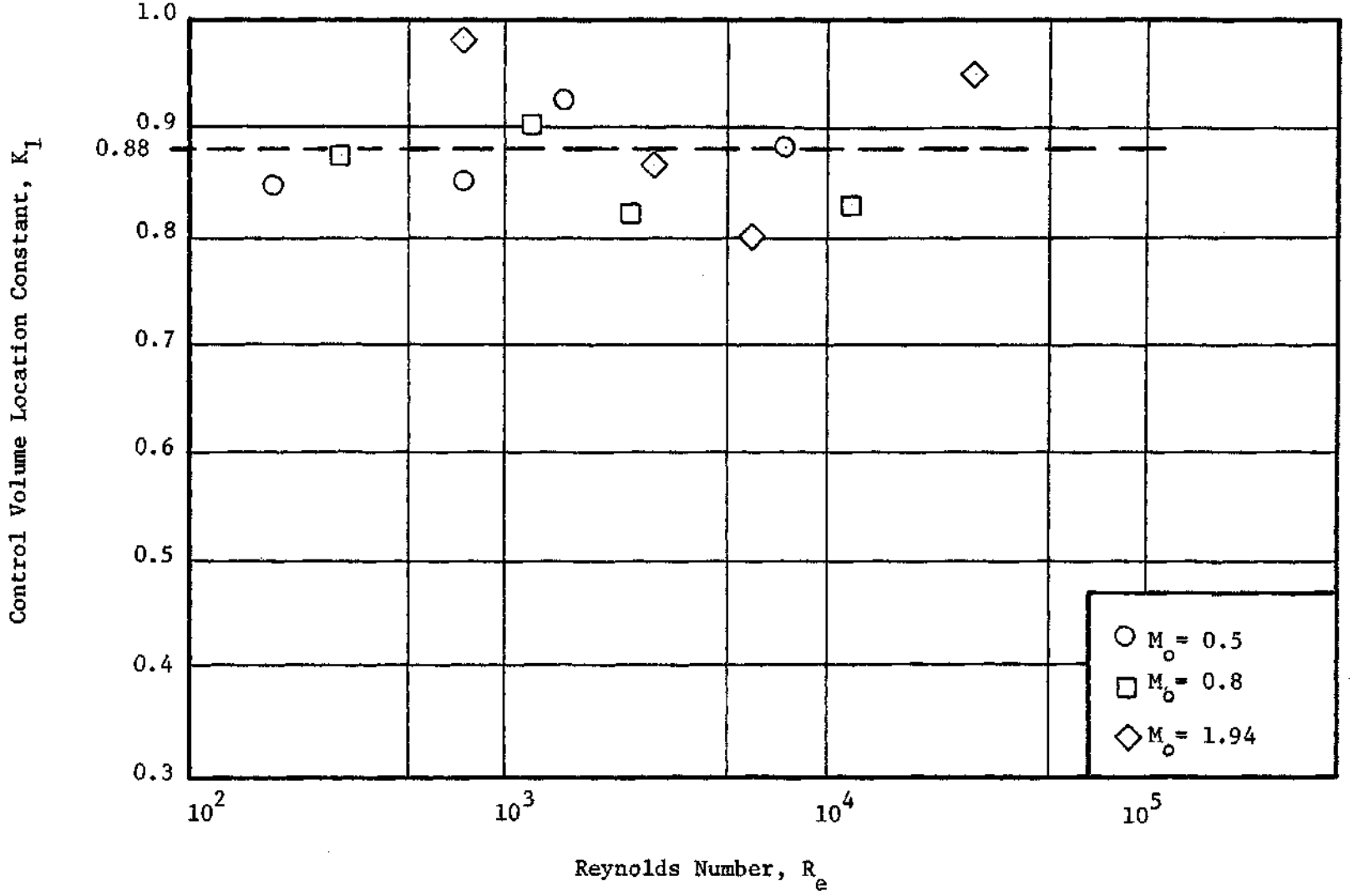

Figure 30. Control Volume Location Constant (K_1)

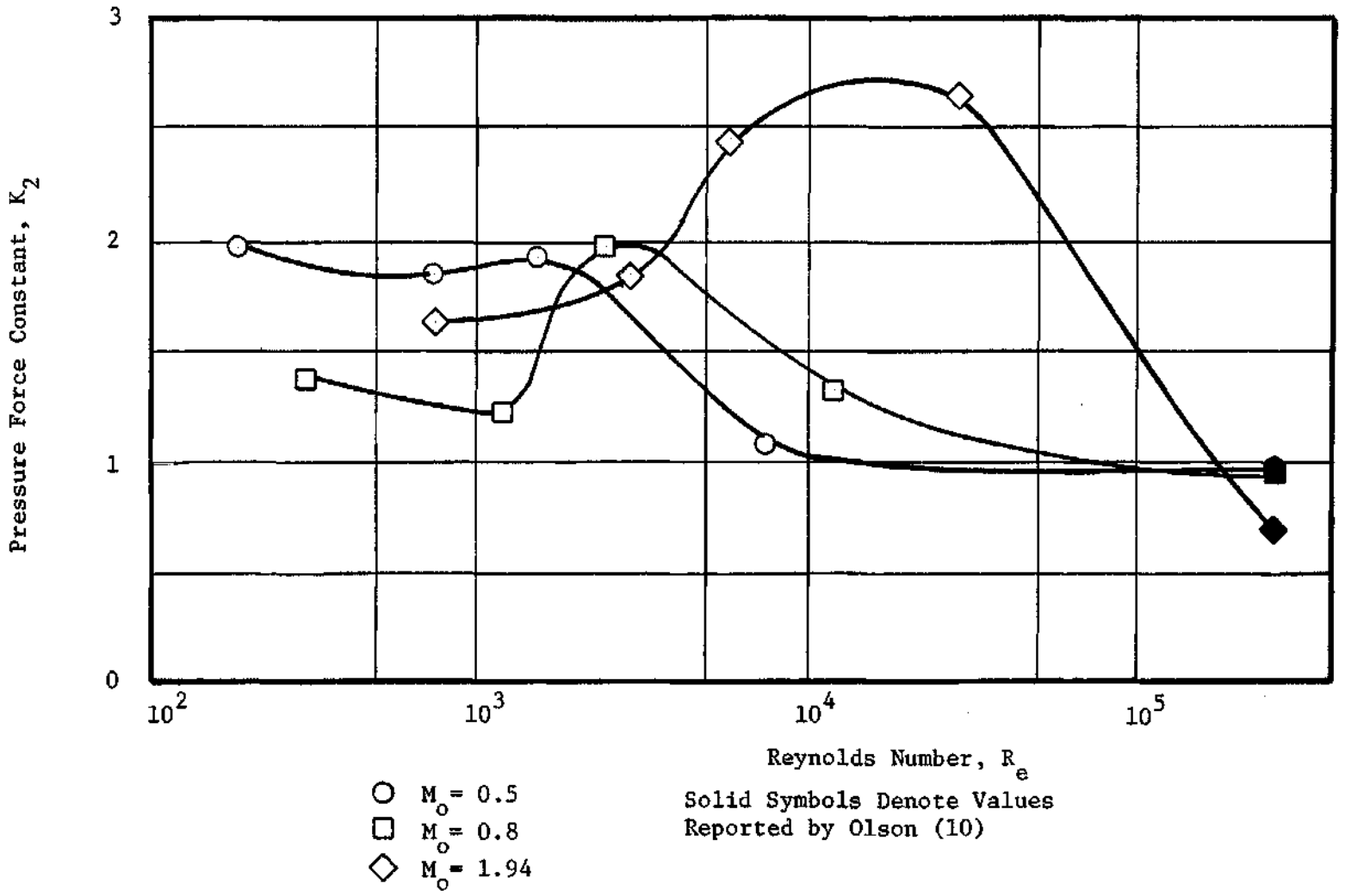

Figure 31. Pressure Force Constant (K_2)

result of inaccuracies in the analytical unattached jet model. Figures 27 and 28 exhibit very large spreads of data around the assumed velocity profile curves for small velocity ratios. These variations may be responsible for relatively large inaccuracies in calculated values of δ and J_1 which are important quantities in the calculation of K_2. In addition to these possible analytical inaccuracies, the calculation of K_2 from empirical data will reflect the accumulation of any experimental errors in the result.

The large variation in values of K_2 from the values suggested in Reference (10) indicates that use of Olson's model may predict erroneous attachment locations for jet Knudsen numbers larger than 10^{-4}. A more accurate analytical unattached jet model might result in improvements in Olson's method of attachment point location.

Correlation Between x_c and L_R

An examination of Figures 24 and 29 suggests that a simple empirical correlation between jet core length and attachment distance is possible. The advantage of this kind of correlation would be that jet core lengths are much easier to measure or estimate than jet attachment distances. The following assumptions are made:

1. Jet core lengths are inversely proportional to a characteristic jet shear stress.
2. The characteristic jet shear stress is proportional to $(\mu + A)$ and therefore inversely proportional to a characteristic apparent Reynolds number, R_{e_a}.
3. Jet attachment distance for a given geometry and Mach

number is a linear function of R_{e_a}.

From assumptions 1 and 2:

$$\frac{x_c}{w} \propto R_{e_a} \tag{34}$$

By assumption 3 and equation (34):

$$\frac{L_R}{w} = F_1 \frac{x_c}{w} + F_2 \tag{35}$$

Where F_1 and F_2 are not functions of R_{e_a}. Since solutions for turbulent jet attachment distances and core lengths are available from previous investigations and experimental data, we can evaluate F_2 in the turbulent flow region denoted by the subscript τ.

$$F_2 = \left(\frac{L_R}{w}\right)_\tau - F_1 \left(\frac{x_c}{w}\right)_\tau \tag{36}$$

Combination of equations (35) and (36) yields:

$$\frac{L_R}{w} - \left(\frac{L_R}{w}\right)_\tau = F_1 \left[\frac{x_c}{w} - \left(\frac{x_c}{w}\right)_\tau\right] \tag{37}$$

where F_1 may be a function of Mach number, Reynolds number, and wall and nozzle geometry. Values of $\frac{L_R}{w}$ calculated from equation (37) using large Reynolds number estimates of $\left(\frac{L_R}{w}\right)_\tau$ and $\left(\frac{x_c}{w}\right)_\tau$ from Figures 24 and 29 and $F_1 = 1.0$ are compared with experimental data from Figure 24 in Figure 32. The correlation yields reasonably good results which indicates that F_1 is only a weak function or is independent of Mach and Reynolds numbers. Variation of F_1 with geometry is not evaluated because only one geometry was used in this investigation.

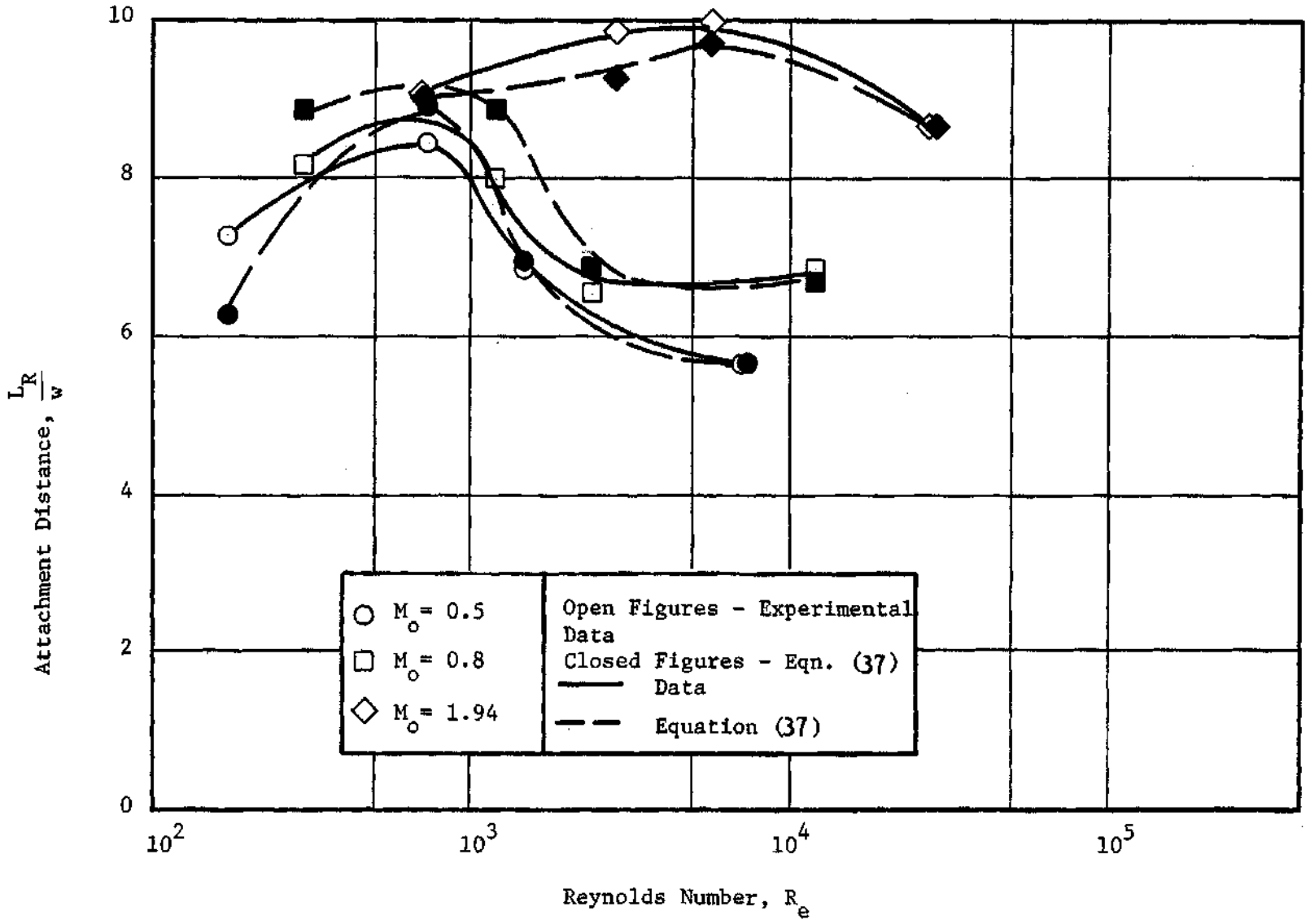

Figure 32. Correlated Attachment Distance

Simplified Attachment Model

The simplified attachment model was found to produce reasonably good estimates of attachment distance for the flow range and geometry of this investigation and other investigations as well. The values of $g(M_o)$ were determined for each flow condition of this investigation except the four attaching jets with $M_o = 2.71$ for which the unattached jet descriptions were not completed. A smooth curve was drawn through the data, and the resulting $g(M_o)$ curve is shown in Figure 33. This curve serves not only as a leakage flow parameter, but it also serves as a correction factor for the various inaccuracies in the model due to the simplifying assumptions in its derivation and the neglect of shock effects in the supersonic jets.

A comparison of the model employing the values of $g(M_o)$ and the jet centerline velocity curves in Appendix C with the data of this investigation is presented in Figure 34. As would be expected, the model shows good agreement with the data.

Figure 35 is a comparison of the simplified model with the theory and data from Reference (10) for several wall geometries. Two variations of the simplified model are compared to the data. One variation employed the small Knudsen number jet centerline descriptions of the unattached jets from this investigation and the values of $g(M_o)$ in Figure 33. The comparison shows that reasonably good agreement with both data and theory from Reference (10) was achieved for the geometries relatively near to that of this study. The model greatly overestimates the attachment distances for the smallest values of wall setback and wall angle. For this case the attachment distances are

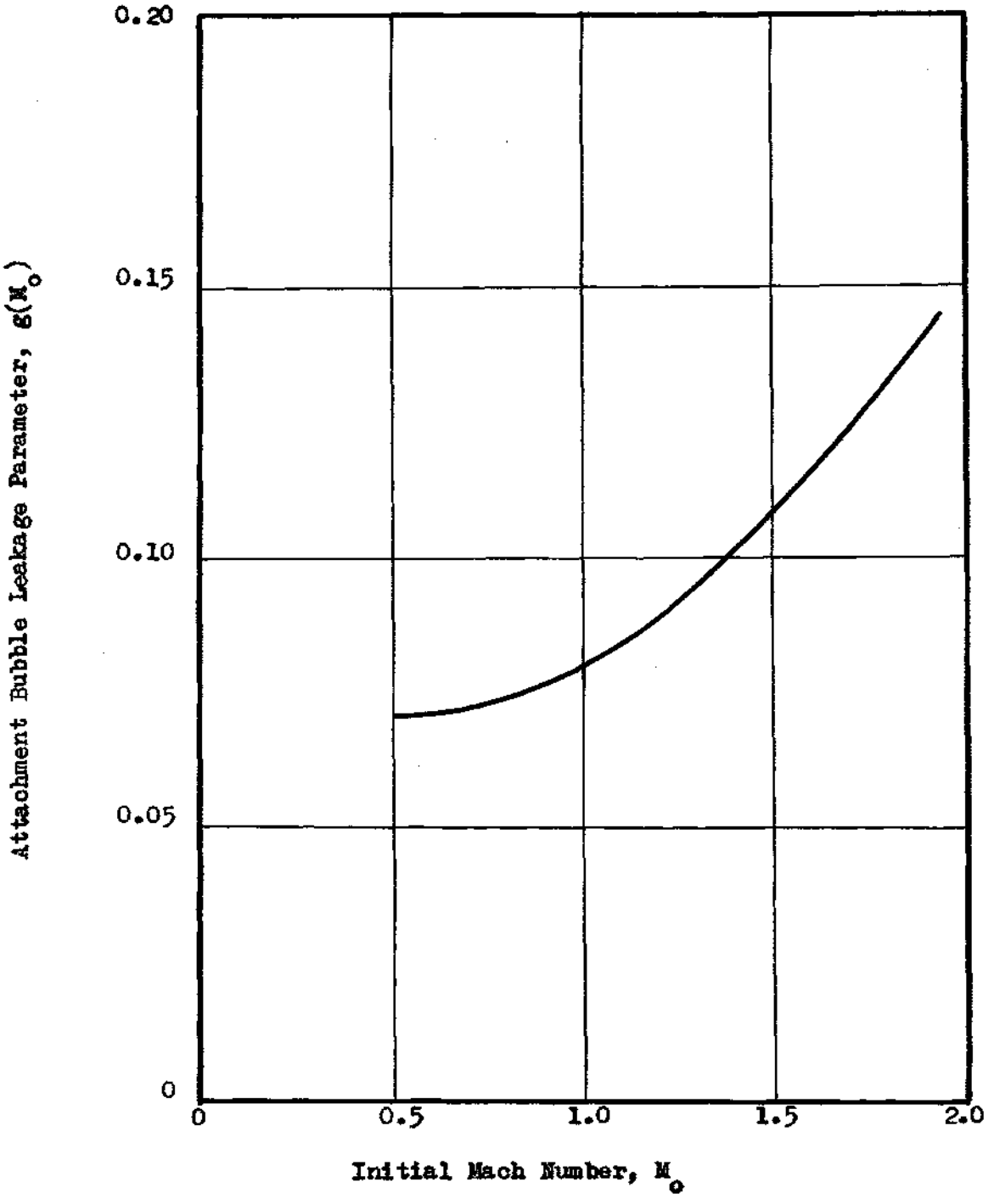

Figure 33. Attachment Bubble Leakage Parameter

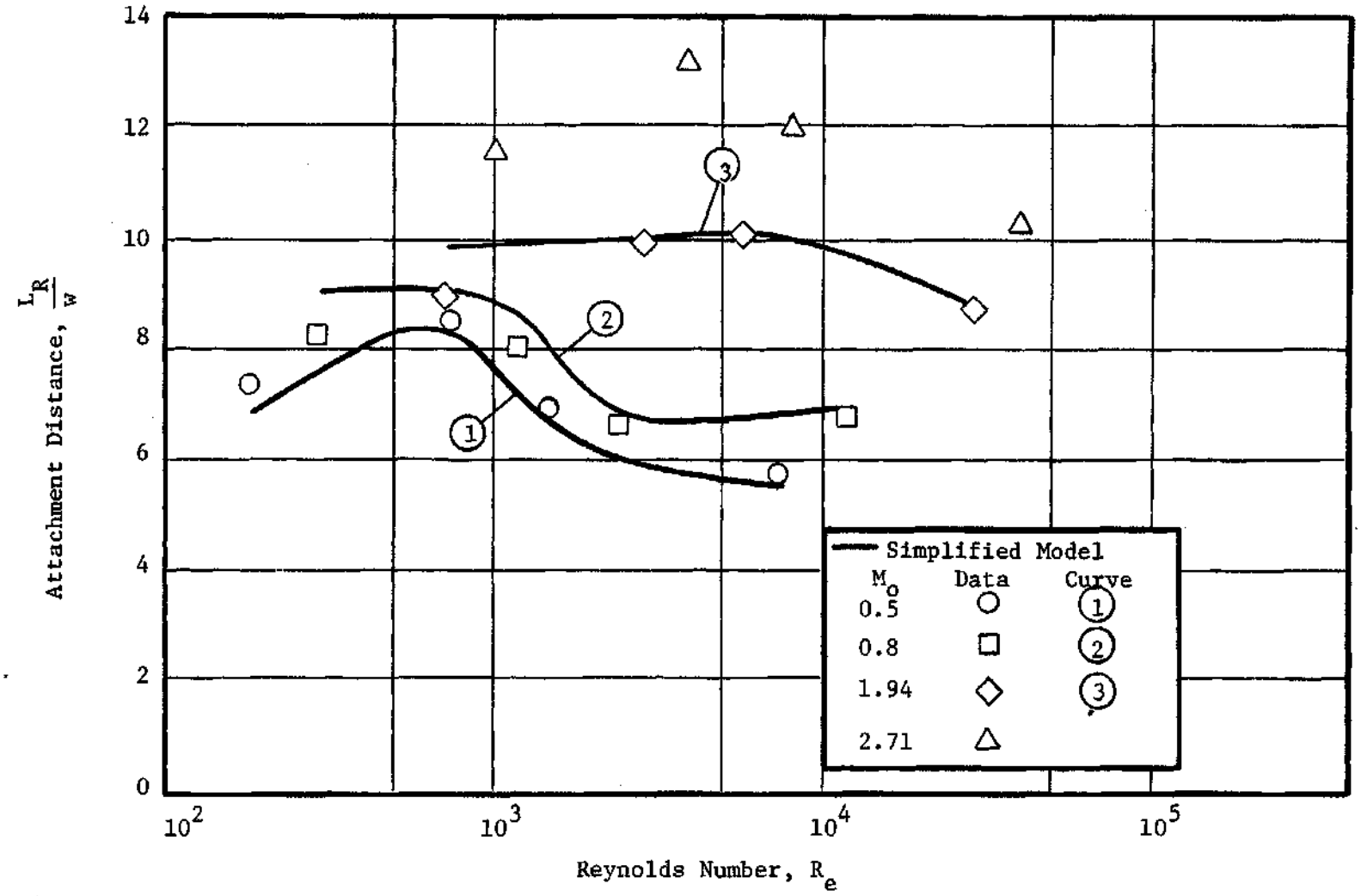

Figure 34. Simplified Model and Data from This Investigation

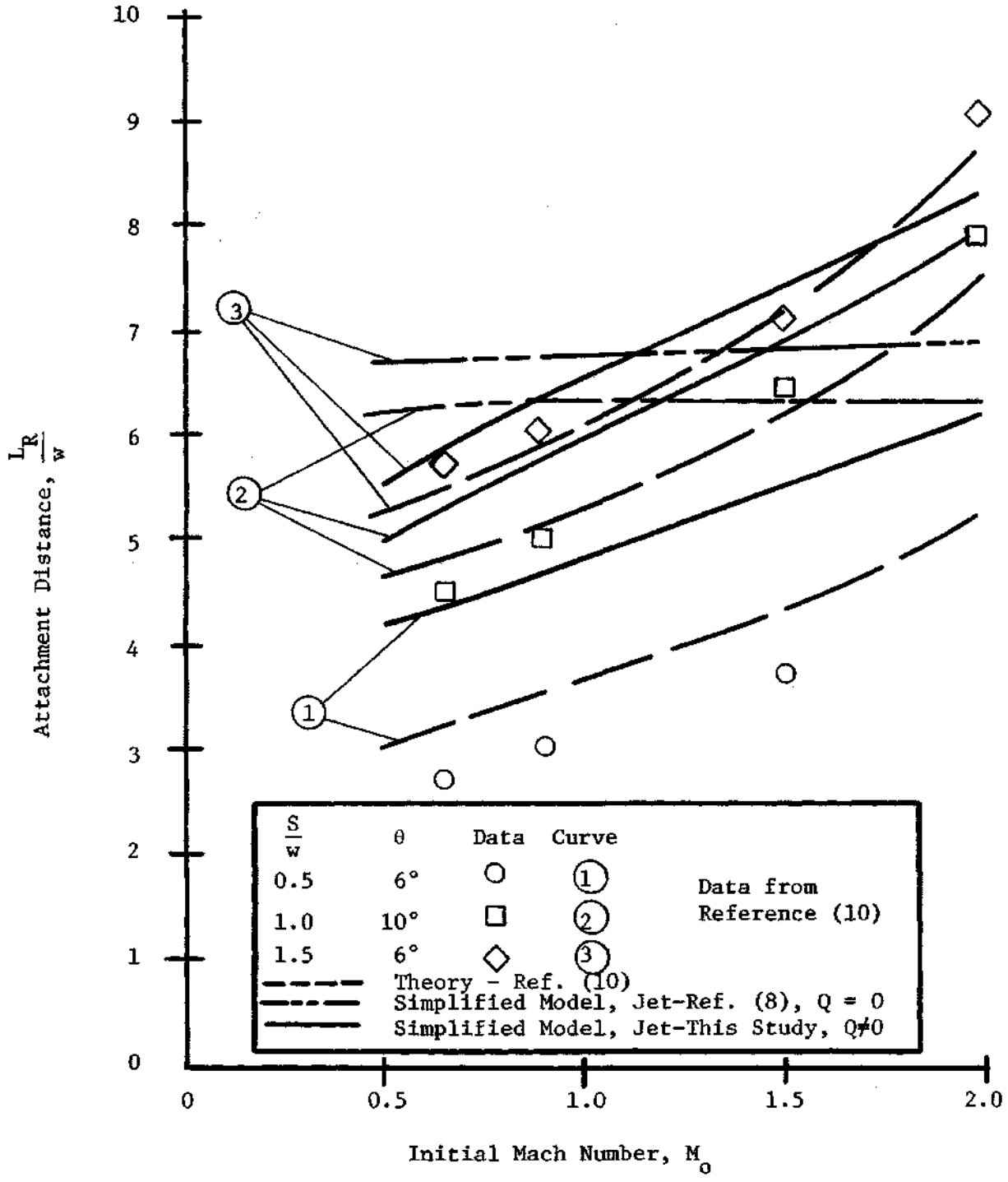

Figure 35. Simplified Model and Experimental Data, Several Geometries, Large R_e

small and the jet attaches before it can become fully developed. The second variation of the model employs the free jet centerline velocity curves from Reference (8) and a value of Q = 0. The two curves cross through the middle of the data of Reference (10) but do not exhibit the increase of attachment distance with Mach number found in the data and in the first variation of the model. Therefore, for the best results in using the model for large Reynolds number jet attachment it is suggested that the small Knudsen number centerline velocities and the values of $g(M_o)$ of this study be employed and the wall geometry should be relatively close to that of this investigation.

A comparison of the model with the theory and data from Reference (14) is presented in Figure 36 for low Reynolds number laminar incompressible jets. The laminar incompressible jet description by Schlichting from Reference (18) with a virtual jet origin of $\frac{R_e}{64}$ upstream of the nozzle exit was employed both in the simplified model and in Reference (14). The value of Q was assumed to be zero. In addition, the value of β in the simplified model was further simplified and assumed to be approximately equal to θ since the geometry included no wall setback and jet radii of curvature were assumed to be large. The model exhibits agreement with the data to about the same degree of accuracy as the theory of Reference (14), although large descrepancies and even negative attachment distances can result for small wall angles.

Use of the turbulent incompressible jet description from Reference (18) reduces the model to that of Bourque and Newman in Reference (3).

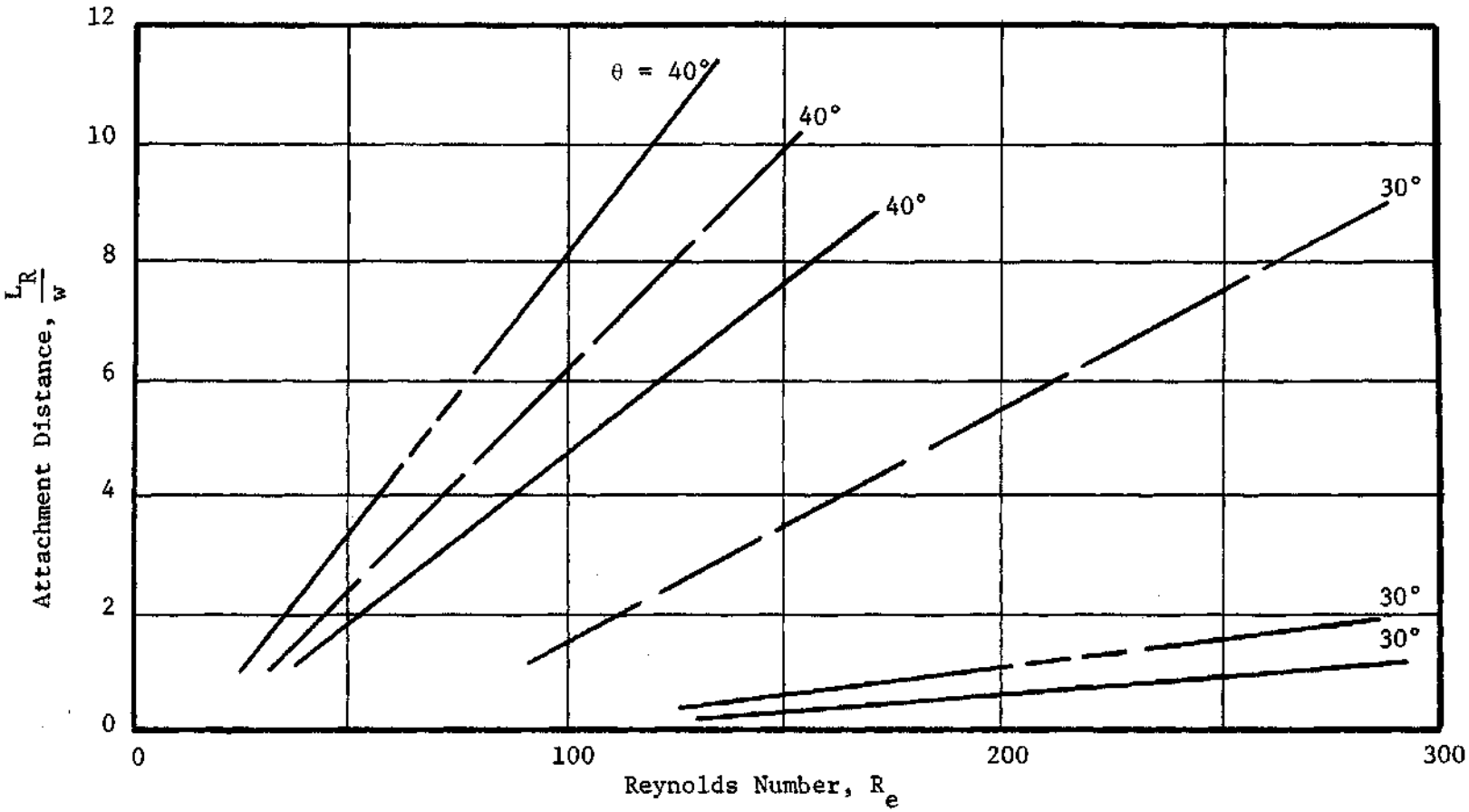

Average Data, Reference (14)

Theory, Reference (14)

Simplified Model, Jet - Reference (14), Q = 0

Figure 36. Simplified Model, Laminar Incompressible Jet, $\frac{S}{w} = 0$

It is concluded that the simplified jet attachment model is reasonably accurate for a wide range of flow conditions and geometries if the proper values of Q and the appropriate jet descriptions are employed. The model yields good results in compressible flow for the flow conditions of this investigation and those of Reference (14) with the jet descriptions and $g(M_o)$ of this study and for wall geometries relatively close to those of this investigation. It yields good results for laminar incompressible flow with Schlichting's laminar jet description and Q = 0 for large wall angles and no wall offset. For turbulent incompressible flow the model reduces to that of Bourque and Newman in Reference (3) where good agreement between theory and experiment are achieved for a wide variety of flow conditions and wall geometries.

CHAPTER VI

CONCLUSIONS AND SUGGESTIONS FOR FURTHER RESEARCH

Conclusions

The static pressure curves along the adjacent wall show that compressible jets will attach to the wall for the geometry and flow range of this investigation. The static pressure curve for each flow condition exhibited a similar shape to wall pressure curves of previous investigations of large Reynolds number attaching jets. The maximum wall static pressure rise near the attachment point was a smaller fraction of pressure drop across the nozzle for large Mach number jets than for small Mach number jets. This reflects the increase in jet radius of curvature with initial jet Mach number and therefore larger attachment distances and more shallow angles of contact between the jet and the wall for larger Mach numbers.

The attachment distance along the wall was also shown to increase with jet Mach number for a given Reynolds number by direct measurement of attachment distance with flexible fibers on the adjacent wall. Jet attachment distance along the wall for fixed initial jet Mach number was shown to be approximately constant for very large Reynolds numbers, but it increases to a maximum value for smaller Reynolds numbers and begins to decrease for even smaller Reynolds numbers. This result has not been previously observed for compressible jets. It is believed to be a result of laminar to turbulent jet

transition as explained in Chapter V. The value of Reynolds number for which the peak occurs was larger for the supersonic jets than subsonic jets.

Measurement of flow field properties within the attaching jets is not feasible by positioning a probe in the flow field. The presence of probes within the attaching jets was found to alter the flow and therefore invalidate any measurements.

The unattached jet velocity profiles in the mixing regions were found to be scattered around the curve:

$$\frac{u}{u_c} = e^{-0.6931\left(\frac{\xi}{\xi^*}\right)^2}$$

which was suggested in References (8) and (10). Although the curve was a good approximation of the collective data, the amount of scatter of the data increased with increase of ξ/ξ^*. The unattached jet centerline velocities were found to be described by the equations:

$$\frac{u_c}{u_o} = 1 \qquad , \quad x < x_c$$

$$\frac{x}{x_c} = e^{m\left(1 - \frac{u_o}{u_a}\right)} \quad , \quad x_c < x$$

where values of x_c and m were tabulated in Appendix C. Jet core length was found to correlate reasonably well with attachment distance in this investigation by the simple relation:

$$\frac{L_R}{w} - \left(\frac{L_R}{w}\right)_\tau = \frac{x_c}{w} - \left(\frac{x_c}{w}\right)_\tau$$

where τ denotes values for very large Reynolds numbers.

Values of Olson's two empirical constants that were calculated from the results mentioned in the previous paragraph did not correlate well with values presented in Reference (10). One of the constants, K_2, was too large to have any physical significance. Therefore, the method of calculating jet attachment distance as presented in Reference (10) requires modification for the flow range of this investigation or errors may result.

The simplified jet attachment model utilizing the unattached jet descriptions of the investigation and the values of $g(M_o)$ in Chapter V was found to correlate reasonably well with the data from Reference (10) and this investigation for wall geometries near that of the experimental model. Using a laminar incompressible jet profile the simplified model was found to agree well with the theory from Reference (14) for laminar incompressible jet attachment to walls with no offset and large wall angles. The model reduces to the theory of Bourque and Newman (3) for turbulent incompressible attaching jets where good agreement between theory and experiment has been achieved. The primary disadvantage of the model is that experimental values of jet centerline velocity and $g(M_o)$ must be available for its use in the compressible flow ranges. Reasonably good results are achieved with the jet descriptions and approximately the wall geometries of this investigation, however. The primary advantages of the model are the relatively easy computation of attachment distances and the applicability of a single model to a wide variety of flow conditions and wall geometries.

Suggestions for Further Research

Further experiments that could result in a better description and understanding of the Coanda Effect are recommended in the paragraphs that follow.

Studies of jet attachment at larger Knudsen numbers than those encountered in this investigation could be of value. These studies could establish a limit on the flow conditions for which the Coanda Effect exists and define jet attachment distance trends for further decreases in Reynolds number. Special equipment would be needed for establishing the flow and sensing attachment point locations and pressure values.

Experiments at higher Knudsen numbers with variations of model geometry are needed to extend the results of this investigation to other geometries. Variation of the nozzle aspect ratio would permit the evaluation of the role of three-dimensional flow effects near the sidewalls on jet attachment. This type of evaluation would also help clarify the concept of jet attachment distance variation with apparent Reynolds number that was presented in Chapter V.

Further experiments are suggested to determine the role of oblique shock waves on jet attachment. Shock wave interaction with jet boundaries at various Knudsen numbers and interaction with the surrounding device geometry probably plays a major role in wall attachment of supersonic jets. This type of investigation would require a new method of flow visualization for study of rarefied flows. A device for this purpose could also be used to examine the jet attachment flow fields for a variety of geometries and flow conditions

in subsonic flow.

The gap between accurate theoretical and experimental jet attachment results is clear from the results of this investigation. The semi-empirical analysis of attaching jets available from the literature require cumbersome calculations, are valid for only limited ranges of flow and wall geometries, and are highly dependent on free jet descriptions. The further development of a simple theoretical jet attachment model to incorporate a wide range of flow conditions and adjacent wall geometries and provide good agreement with presently available experimental data would be a valuable contribution to practical fluid research.

APPENDIX A

EXAMINATION OF MODEL SIMILITUDE

For steady state adiabatic compressible flow, model and prototype similitude is analyzed in the following paragraphs assuming the Mach numbers and Reynolds numbers are the same for the two flow fields.

Applicable results from the kinetic theory of gases are:

$$e\lambda = \text{constant} \tag{38}$$

$$\mu = \text{constant}\ \sqrt{T} \tag{39}$$

$$K_n = 1.26\ \sqrt{\gamma}\ \frac{M}{R_e} \tag{40}$$

Applicable perfect gas equations are:

$$\frac{P}{\rho} = RT \tag{41}$$

$$a = \sqrt{\gamma RT} \tag{42}$$

In steady state flow the total temperature is constant throughout the flow assuming heat transfer effects can be neglected due to the short time any element of the flow is within the experimental apparatus. From energy considerations, the temperature is determined

only by the velocity of flow. The speed of sound is determined by the temperature of the gas. Therefore, Mach number similitude is assured if the velocity of flow within the model and a small amplifier is the same at geometrically similar stations, if the two flows have equal total temperatures, and if the gas is the same gas in each case.

Equation (40) indicates that Reynolds number similitude is assured if Knudsen and Mach number similitude are assured. The definition of the Knudsen number is:

$$K_n = \frac{\lambda}{w} \tag{43}$$

Combine equations (38), (41), and (43) to get

$$K_n = \frac{RT}{Pw}(\text{constant}) \tag{44}$$

For Mach number similitude as previously discussed, RT is the same at geometrically similar flow stations. Equation (44) indicates that pressure must then be scaled inversely proportional to amplifier dimensions to achieve Knudsen number similitude.

To show that the flow velocities at similar flow stations are equal, the Navier Stokes Equations can be examined. The unprimed variables represent flow in a fluidic device, and the primed variables represent the modeled flow. The variable relations assuming equal temperatures and the scale factor D are:

$$\left.\begin{aligned}
&\text{dimension:}\quad x' = Dx,\ y' = Dy,\ z' = Dz \\
&\text{velocity:}\quad \underline{w}' = \underline{w} \\
&\text{pressure:}\quad p' = D^{-1}p \\
&\text{density:}\quad \rho' = D^{-1}\rho \\
&\text{viscosity:}\quad \mu' = \mu \\
&\text{time:}\quad t' = Dt
\end{aligned}\right\} \qquad (45)$$

For the unprimed case the Navier Stokes Equations neglecting body forces may be written in the form of:

$$\rho \frac{du}{dt} = -\frac{\partial P}{\partial x} + \frac{\partial}{\partial z}\left[(\mu)\left(2\frac{\partial u}{\partial x} - \frac{2}{3}\,\mathrm{div}\,\underline{w}\right)\right] + \frac{\partial}{\partial y}\left[(\mu)\left(\frac{\partial u}{\partial y} + \frac{\partial v}{\partial x}\right)\right] + \frac{\partial}{\partial x}\left[(\mu)\left(\frac{\partial w}{\partial x} + \frac{\partial u}{\partial z}\right)\right] \qquad (46)$$

where u, v, and w are actual x, y, and z components of $\underline{w}$. If equation (46) is written in terms of the primed variables and the relations (46) are substituted the result is:

$$D^{-1}\rho \frac{du}{d(Dt)} = -\frac{\partial (D^{-1}P)}{\partial (Dx)} + \frac{\partial}{\partial (Dx)}\left[(\mu)\left(2\frac{\partial u}{\partial (Dx)} - \frac{2}{3}\,\mathrm{div}\,\underline{w}'\right)\right] + \frac{\partial}{\partial (Dy)}\left[(\mu)\left(\frac{\partial u}{\partial (Dy)} + \frac{\partial v}{\partial (Dx)}\right)\right] + \frac{\partial}{\partial (Dz)}\left[(\mu)\left(\frac{\partial w}{\partial (Dx)} + \frac{\partial u}{\partial (Dz)}\right)\right] \qquad (47)$$

Equation (47) is the same as equation (46) when multiplied by D^2.

Therefore model similitude is established under the following conditions:

1. The same gas is used.
2. The same total temperature is maintained.
3. Similar amplifier geometry is used.
4. The same Mach number jet is supplied.
5. Pressure is scaled inversly with amplifier dimensions.

APPENDIX B

COMPUTER PROGRAM FOR f_1 AND f_2

Olson's analytical method of attachment point location is at best a difficult trial and error procedure. Further complications are introduced when equations (16) and (17) in Chapter II are examined and found to be extremely difficult to integrate for values of f_1 and f_2. In order to reduce the number of computations, a computer program was devised to integrate the equations. The use of the computer results is illustrated in Appendix D in the calculation of K_2.

The following is a Fortran IV Computer program devised to obtain tabulated values of f_1 and f_2 from the Burroughs B 5500 Digital Computer at the Rich Electronic Computer Center. The program plan is to numerically integrate the expressions of equations (16) and (17) for air by the trapezoidal rule for discrete values of M_o and U. The computer readout headings are included at the end of the program with the variable to be printed in parentheses. The following computer symbols were used in place of the symbols in equations (16) and (17).

EOES = $\frac{\xi}{\xi^*}$

F1 = f_1

F2 = f_2

MO = M_o

U = U

UOUC = $\frac{u}{u_c}$

Fortran IV Program to evaluate f_1 and f_2

```
    1 I=0
    2 REAL MO
    3 MO=0.5
    4 GO TO 11
    5 MO=0.8
    6 GO TO 11
    7 MO=1.94
    8 GO TO 11
    9 MO=2.71
   10 GO TO 11
   11 DO 29 U=0.2,1.0,0.1
   12 PRINT 13,MO,U
   13 FORMAT   (1H6, 10X,5HMO = ,F4.2,5X,4HU = ,F3.1,// 11X,4HE/E*,6X,4H
  141U/UC,9X,2HF1,12X,2HF2)
   15 A=0.0
   16 B=0.0
   17 DO 29 EOES=0.005,4.005,0.01
```

```
18 UOUC=EXP(-0.6931*(EOES**2.))
19 DEN=1.+0.2*(MO**2.)*(1.-(UOUC)**2.)
20 DF2=U*UOUC/DEN
21 DF1-U*UOUC*DF2
22 F2=A+DF2*0.01
23 A=F2
24 F1=B+DF1*0.01
25 B=F1
26 C=EOES+0.005
27 PRINT 28,C,UOUC,B,A
28 FORMAT ( 10X,F5.3,5X,F7.5,5X,F9.6,5X,F9.6)
29 CONTINUE
30 I1=I+1
31 I+I1
32 IF (I1-3)33,33,34
33 GO TO (5,7,9),I1
34 STOP
   END
```

Each table of the computer results will have the following headings:

MO=(M_o) U=(U)

E/E* U/UC F1 F2

(ξ/ξ^*) (U/U_c) (f_1) (f_2)

A table is typed for one value of Mach number and one value of U for the Mach numbers of this study and values of U between 1.0 and 0.2 in steps of 0.1. Values in the tables are computed for values of ξ/ξ^* between 0.01 and 4.01 in steps of 0.01.

APPENDIX C

DATA

Desired Flow Conditions

Adjustment of the nozzle supply pressure and the model ambient pressure to within reasonably close agreement with the theoretical values for each initial jet Mach number and Knudsen number was essential in minimizing errors in the comparison of the results. Maintaining the appropriate stagnation temperature of the air within acceptable limits near 77°F was shown to be easily accomplished as described in Chapter IV. Adjustment of the desired pressures was more difficult to accomplish, and the trial and error procedure of manual control valve adjustment presented a time consuming task. The desired pressure value adjustment as determined from equation (4) of Chapter I for air are presented in Table 1. The actual pressure settings that were achieved for the experiments are presented in the sections that follow.

Table 1. Desired Flow Pressure Settings*

Mach Number \ Knudsen Number	10^{-4}	5×10^{-4}	10^{-3}	3.92×10^{-3}
0.5	110	22.0	11.0	2.81
	92.6	18.5	9.26	2.36
0.8	131	26.2	13.1	3.34
	86.2	17.2	8.62	2.20
1.94	397	79.4	39.7	10.1
	55.6	11.1	5.56	1.42
2.71	926	185	92.6	23.6
	39.2	7.84	3.92	1.00

*Upper values denote nozzle supply pressure (mm of Mercury).
Lower values denote model ambient pressure (mm of Mercury).

Data From Jet Attachment Experiments

The actual model pressure values were adjusted to within reasonably close agreement with desired values as illustrated in Table 2. Actual jet attachment distance was measured along the attachment wall from the nozzle exit plane using the fiber fringe that was glued to the wall to indicate the attachment point location. The results are presented in Table 3 as a function of jet nozzle width. Static pressure along the attachment wall was measured using the wall probe in Figure 14. The results are tabulated in Tables 4 through 7 in the form of a pressure coefficient $P_w-P_e/P_{t_o}-P_e$ for randomly selected locations along the attachment wall. This data is plotted in Figures 19 through 22. Location of the zero value of the pressure coefficient in the pressure rise portion of the curves of Figures 19 through 22 provided values of L'/w for each flow condition. Values of L'/w were divided by the appropriate values of L_R/w from Table 3 to obtain the control volume -ocation coefficient of Olson's analysis (K_1), and the results are presented in Table 8. Values of Olson's pressure force coefficient (K_2) were determined using the attachment data and the unattached jet data from the next section in the manner illustrated in Appendix D. Values of K_2 are presented in Table 9.

Table 2. Actual Flow Pressure Settings, Jet Attachment*

Mach Number \ Knudsen Number	10^{-4}	5×10^{-4}	10^{-3}	4×10^{-3}
0.5	103	22.2	11.0	3.0
	83.9	18.3	9.4	2.5
0.8	133	25.9	13.8	3.3
	85.8	17.5	8.9	2.1
1.94	393	78.0	42.9	10.2
	56.7	10.9	5.9	1.4
2.71	930	189	89.7	28.1
	39.7	7.8	3.9	1.2

*Upper values denote nozzle supply pressure (mm of Mercury).
Lower values denote model ambient pressure (mm of Mercury).

Table 3. Jet Attachment Distance $\frac{L_R}{w}$

Mach Number \ Knudsen Number	10^{-4}	5×10^{-4}	10^{-3}	4×10^{-3}
0.5	5.75	6.90	8.45	7.3 (estimated)
0.8	6.85	6.55	8.0	8.2 (estimated)
1.94	8.70	10.05	9.9	8.95
2.71	10.25	12.00	13.2	11.55

Table 4. Attachment Wall Static Pressure Coefficient, M_o=0.5

Knudsen Number K_n	Distance Along Wall $\frac{L}{w}$	Pressure Coefficient $\frac{P_w-P_e}{P_{t_o}-P_e} \times 10^2$
10^{-4}	2.25	-14.6
	4.50	- 9.65
	4.95	- 3.94
	5.45	5.92
	6.20	12.6
	6.70	16.2
	7.40	12.4
	8.50	5.52
	9.70	.59
5×10^{-4}	3.25	-10.7
	4.70	-14.6
	6.05	- 9.70
	7.80	15.5
	9.40	4.86
	10.85	- 1.94
	12.80	- 4.86
	15.10	- 4.86
10^{-3}	4.25	- 7.31
	6.30	- 2.44
	8.10	2.44
	9.30	7.31
	10.40	12.2
	11.65	7.31
	12.50	4.88
	14.75	2.44
	17.25	0
4×10^{-3}	3.15	- 9.15
	4.65	- 5.00
	5.85	- 1.67
	7.45	4.17
	8.05	6.76
	9.00	5.00
	10.65	0
	12.15	0

Table 5. Attachment Wall Static Pressure Coefficient, M_o=0.8

Knudsen Number K_n	Distance Along Wall $\frac{L}{w}$	Pressure Coefficient $\frac{P_w-P_e}{P_{t_o}-P_e} \times 10^2$
10^{-4}	4.55	-13.4
	5.35	- 6.75
	7.00	12.7
	7.65	13.4
	8.00	12.3
	9.10	5.93
	10.80	- 2.84
	16.95	- 2.03
5×10^{-4}	3.45	-15.0
	4.75	- 8.60
	6.05	7.70
	7.40	13.6
	8.65	6.36
	10.05	- 1.36
	12.95	- 4.54
	15.10	- 4.54
10^{-3}	3.50	- 7.26
	4.50	- 7.25
	6.50	- 4.84
	7.90	6.45
	9.50	11.3
	11.75	0.81
	14.25	- 1.61
	16.50	- 0.81
4×10^{-3}	3.30	- 7.41
	4.70	- 5.16
	5.90	- 2.90
	7.30	0
	8.70	3.54
	10.15	4.83
	11.35	2.90
	12.90	0.64
	15.05	- 0.32

Table 6. Attachment Wall Static Pressure Coefficient, M_o=1.94

Knudsen Number K_n	Distance Along Wall $\frac{L}{w}$	Pressure Coefficient $\frac{P_w-P_e}{P_{t_o}-P_e} \times 10^2$
10^{-4}	3.05	- 4.20
	5.25	- 4.91
	7.70	- 1.28
	9.40	2.45
	10.65	6.34
	11.55	5.40
	12.10	3.46
	13.05	- 1.27
	14.20	- 0.50
	15.55	- 1.12
	16.80	- 0.86
	18.70	- 1.64
5×10^{-4}	4.25	- 4.03
	5.55	- 3.18
	7.05	- 1.59
	8.60	0.91
	10.05	3.18
	11.55	3.98
	13.10	0.97
	14.80	- 1.36
	16.55	- 1.71
	18.20	- 2.05
	20.35	- 1.93
10^{-3}	5.15	- 3.00
	7.50	- 1.95
	9.60	2.68
	10.50	4.44
	11.50	4.03
	12.90	1.45
	15.40	- 1.14
	18.20	- 1.34

Table Continued

4×10^{-3}	4.25	- 2.16
	5.60	- 2.16
	7.05	- 1.73
	8.65	- 0.43
	9.95	2.16
	11.55	3.46
	13.05	1.30
	14.95	- 0.43
	17.75	- 0.43

Table 7. Attachment Wall Static Pressure Coefficient, M_o=2.71

Knudsen Number K_n	Distance Along Wall $\frac{L}{w}$	Pressure Coefficient $\frac{P_w-P_e}{P_{t_o}-P_e} \times 10^2$
10^{-4}	5.05	- 2.10
	6.40	- 1.07
	7.20	- 0.40
	8.50	0.75
	9.75	1.56
	11.10	2.35
	12.80	1.03
	16.05	0.71
	19.75	0.21
5×10^{-4}	5.15	- 1.50
	7.10	- 1.18
	8.80	0.09
	10.45	0.70
	12.10	0.87
	15.50	1.20
	16.95	0.93
	18.05	0.48
	20.10	- 0.02
10^{-3}	4.55	- 1.11
	7.50	- 0.76
	10.50	- 0.18
	13.40	0.94
	15.45	1.02
	16.60	1.16
	18.00	1.02
	19.60	0.18
4×10^{-3}	5.10	- 0.99
	7.25	- 0.99
	8.90	- 0.57
	10.65	0.43
	11.95	0.99
	13.00	1.56
	14.75	0.71
	16.85	0.14
	19.10	0.14

Table 8. Control Volume Location Coefficient (K_1)

Mach Number \ Knudsen Number	10^{-4}	5×10^{-4}	10^{-3}	4×10^{-3}
0.5	0.886	0.927	0.852	0.850
0.8	0.832	0.824	0.911	0.878
1.94	0.954	0.805	0.869	0.984

Table 9. Pressure Force Coefficient at Attachment (K_2)

Mach Number \ Knudsen Number	10^{-4}	5×10^{-4}	10^{-3}	4×10^{-3}
0.5	1.08	1.93	1.85	1.98
0.8	1.32	1.98	1.22	1.38
1.94	2.64	2.46	1.85	1.63

Unattached Jet Experimental Data

The actual model pressure settings and the impact pressure measurements obtained for the unattached jet experiments are presented in the following tables. Pressure values expressed in millimeters of mercury represent absolute pressures, and values expressed in millimeters of oil are differential pressures representing the difference between the measured impact pressure and the model ambient pressure. Specific gravity of the manometer oil was 1.04, and measurements were taken from manometers inclined at 30° to the horizontal. The effective specific gravity of the oil that should be used in any conversion of the differential pressures is then 0.52.

Figures 37 through 48 represent the centerline velocity data and the assumed straight line variations of the centerline velocities utilized in the calculations of values of K_2.

Table 10. Actual Flow Pressure Settings, Unattached Jet*

Knudsen Number / Mach Number	10^{-4}	5×10^{-4}	10^{-3}	4×10^{-3}
0.5	109.0	21.9	11.56	3.1
	90.8	18.3	9.5	2.6
0.8	128.7	26.2	13.2	3.3
	85.6	17.3	8.6	2.2
1.94	389.0	76.6	41.2	10.1
	54.7	10.8	5.7	1.4
2.71	916.0	185.2	92.4	24.0
	38.3	8.0	4.0	1.0

*Upper values denote nozzle supply pressure (mm of Mercury).
Lower values denote model ambient pressure (mm of Mercury).

Table 11. Unattached Jet Impact Pressure Measurements, M_o=0.5, K_n=10^{-4}

Position			Developed Region Width	Impact Pressure Measurement
$\frac{x}{w}$	$\frac{y}{w}$	$\frac{\xi}{w}$	$\frac{\xi^*}{w}$	P_t (mm Mercury)
3.45	- 0.85	0.77	0.51	91.7
	- 0.5	0.42		95.1
	- 0.3	0.22		99.9
	- 0.1	0.02		103.5
	0.1			104.3
	0.3			104.1
	0.7	0.28		99.6
	1.1	0.68		91.6
10.45	- 1.4	2.02	0.92	89.7
	- 0.9	1.52		90.1
	- 0.4	1.02		91.5
	0	0.62		94.4
	0.5	0.12		96.3
	1.05	0.43		95.7
	1.5	0.88		92.8
	1.95	1.33		89.8
2.85	0			107.1
4.75				105.0
6.55				101.8
8.35				99.4
10.45				97.0
12.35				95.2
14.25				93.5
0	0.45			107.3
	0.40			107.2
	0.35			107.0
	0.20			106.8
	0			106.8

Table 12. Unattached Jet Impact Pressure Measurements, M_o=0.5, K_n=5x10^{-4}

Position			Developed Region Width	Differential Impact Pressure
$\frac{x}{w}$	$\frac{y}{w}$	$\frac{\xi}{w}$	$\frac{\xi^*}{w}$	P_t-P_e (mm oil)
3.0	- 0.75	0.61	0.38	0
	- 0.50	0.36		27
	- 0.35	0.21		88
	- 0.20	0.06		90
	0			91
	0.25			90
	0.35	0.09		87
	0.45	0.19		81
	0.70	0.44		7
	0.85	0.59		0
11.6	2.9	2.43	1.47	0
	2.25	1.78		5
	1.65	1.18		15
	0	0.47		34
	- 0.35	0.82		21
	- 0.75	1.22		9
	- 1.8	2.27		1
3.35	0			89
5.3				89
7.15				66
8.5				52
10.45				36
11.55				31
13.35				24
0	- 0.45			88
	- 0.40			89
	- 0.30			92
	0			89

Table 13. Unattached Jet Impact Pressure Measurements, M_o=0.5, K_n=10^{-3}

Position			Developed Region Width	Differential Impact Pressure
$\frac{x}{w}$	$\frac{y}{w}$	$\frac{\xi}{w}$	$\frac{\xi^*}{w}$	P_t-P_e (mm oil)
2.8	- 0.90	0.85	0.36	0
	- 0.55	0.50		2
	- 0.40	0.35		11
	- 0.25	0.20		42
	0			51
	0.25			53
	0.50	0.05		53
	0.65	0.20		28
	1.0	0.55		0
9.95	- 0.90	1.40	0.77	0
	- 0.40	0.90		4
	0	0.50		16
	0.40	0.10		33
	0.85	0.35		30
	1.35	0.85		10
	1.60	1.10		4
3.95	0			53
5.50				52
8.35				46
10.85				23
13.30				14
0	- 0.45			36
	- 0.35			51
	0			53

Table 14. Unattached Jet Impact Pressure Measurements, M_o=0.5, K_n=4x10^{-3}

Position			Developed Region Width	Differential Impact Pressure
$\frac{x}{w}$	$\frac{y}{w}$	$\frac{\xi}{w}$	$\frac{\xi^*}{w}$	P_t-P_e (mm oil)
2.3	- 0.90	0.87	0.40	0
	- 0.40	0.37		2
	- 0.15	0.12		10
	0			11
	0.35	0		11
	0.45	0.10		10
	0.75	0.40		2
	1.10	0.75		0
6.95	- 0.70	0.94	0.50	0
	0	0.24		7.5
	0.40	0.16		8
	0.65	0.41		3.5
	0.90	0.66		0.5
	1.15	0.91		0
1.30	0			11
2.60				11
4.40				11
6.45				9
8.30				7.5
10.45				5.5
14.0				4.5
0	- 0.45			6
	- 0.35			10
	- 0.25			11.5
	0			11.5

Table 15. Unattached Jet Impact Pressure Measurements, M_o=0.8, K_n=10^{-4}

Position		Developed Region Width		Impact Pressure Measurement
$\frac{x}{w}$	$\frac{y}{w}$	$\frac{\xi}{w}$	$\frac{\xi^*}{w}$	P_t (mm Mercury)
3.45	- 1.20	1.27	0.67	86.4
	- 0.70	0.77		92.6
	- 0.40	0.47		105.6
	- 0.15	0.22		117.2
	0.10			126.7
	0.35	0.02		124.8
	0.65	0.32		114.8
	1.10	0.77		89.9
11.20	- 1.45	2.22	1.33	86.8
	- 0.95	1.72		87.6
	- 0.40	1.17		91.7
	0	0.77		97.4
	0.55	0.22		104.7
	1.15	0.38		103.5
	1.85	1.08		93.0
2.65	0			128.1
4.25				126.0
6.05				119.2
8.25				114.0
10.20				109.3
12.00				105.2
14.00				102.4
0	- 0.45			120.2
	- 0.35			128.6
	- 0.15			128.7
	0			128.8

Table 16. Unattached Jet Impact Pressure Measurements, M_o=0.8, K_n=5x10^{-4}

Position			Developed Region Width	Differential Impact Pressure
$\frac{x}{w}$	$\frac{y}{w}$	$\frac{\xi}{w}$	$\frac{\xi^*}{w}$	P_t-P_e (mm oil)
3.05	- 0.80	0.70	0.33	0
	- 0.55	0.45		16
	- 0.35	0.25		65
	- 0.20	0.10		199
	- 0.10	0		213
	0			219
	0.25			224
	0.35			219
	0.50	0.14		177
	0.80	0.44		28
	1.05	0.69		0
12.45	2.95	2.28	1.50	3
	1.70	1.03		52
	0.80	0.13		93
	0	0.67		63
	- 0.75	1.42		20
	- 1.85	2.52		3
3.50	0			226
4.85				205
6.10				181
7.65				152
9.75				122
11.85				102
14.00				84
0	- 0.45			190
	- 0.35			228
	- 0.30			228
	0			230

Page missing from thesis

Table 18. Unattached Jet Impact Pressure Measurements, M_o=0.8, K_n=4x10^{-3}

Position			Developed Region Width	Differential Impact Pressure
$\frac{x}{w}$	$\frac{y}{w}$	$\frac{\xi}{w}$	$\frac{\xi^*}{w}$	P_t-P_e (mm oil)
2.20	- 0.90	0.90	0.50	1
	- 0.55	0.55		2
	- 0.45	0.45		8
	- 0.20	0.20		23
	0	0		27
	0.30			27
	0.55	0.23		17
	0.75	0.43		6
	1.05	0.73		0
7.25	- 0.95	1.20	0.58	0
	- 0.40	0.65		2
	0	0.25		19
	0.10	0.15		23
	0.50	0.25		19
	0.80	0.55		8
	1.20	0.95		0
2.65	0			27
3.40				27
4.90				25
8.00				23
10.25				20
13.05				14
16.30				8
0	0.45			16
	0.40			24
	0.30			28
	0			28

Table 19. Unattached Jet Impact Pressure Measurements, M_o=1.94, K_n=10^{-4}

Position			Developed Region Width	Impact Pressure Measurement
$\frac{x}{w}$	$\frac{y}{w}$	$\frac{\xi}{w}$	$\frac{\xi^*}{w}$	P_t (mm Mercury)
2.75	- 0.75	0.59	0.40	57.7
	- 0.35	0.19		234
	- 0.15			335
	0.45	0.03		326
	0.90	0.48		59
11.50	- 1.50	2.00	1.76	60
	- 0.90	1.40		92
	- 0.35	0.85		130
	0	0.50		145
	0.40	0.10		145
	1.05	0.55		146
	1.45	0.95		137
	2.15	1.65		72
3.10	0			305
4.65				246
7.10				226
9.90				177
12.30				136
14.90				117
0	- 0.45			299
	- 0.40			326
	- 0.15			300
	0			294

Table 20. Unattached Jet Impact Pressure Measurements, M_o=1.94, K_n=5x10^{-4}

Position			Developed Region Width	Impact Pressure Measurement
$\frac{x}{w}$	$\frac{y}{w}$	$\frac{\xi}{w}$	$\frac{\xi^*}{w}$	P_t (mm Mercury)
3.30	- 0.70	0.56	0.43	11.4
	- 0.50	0.36		24.6
	- 0.15	0.01		48.9
	0.15			46.8
	0.40	0		47.9
	0.85	0.45		15.7
11.40	- 1.40	2.02	2.22	15.3
	- 0.75	1.37		19.9
	- 0.30	0.92		24.9
	0.25	0.37		35.6
	0.60	0.02		36.5
	0.85	0.23		36.1
	1.50	0.88		25.4
	1.95	1.33		21.3
3.05	0			48.3
4.05				50.4
5.45				60.5
8.20				45.9
9.75				35.0
12.40				32.8
15.15				24.7
0	0.45			60.7
	0.35			57.2
	0.10			56.7
	0			56.7

Table 21. Unattached Jet Impact Pressure Measurements, M_o=1.94, K_n=10^{-3}

Position			Developed Region Width	Impact Pressure Measurement
$\frac{x}{w}$	$\frac{y}{w}$	$\frac{\xi}{w}$	$\frac{\xi^*}{w}$	P_t (mm Mercury)
3.35	- 0.60	0.30	0.38	11.3
	- 0.45	0.15		23.4
	- 0.25			28.9
	0			25.3
	0.25			25.0
	0.45			28.9
	0.75	0.29		10.6
	1.05	0.59		6.4
11.40	- 1.40	1.93	2.27	9.2
	- 1.10	1.63		11.2
	- 0.65	1.18		13.4
	- 0.30	0.83		14.3
	0.15	0.38		16.2
	0.60	0.07		17.8
	1.20	0.67		15.4
	1.80	1.27		13.0
3.20	0			24.6
5.35				28.3
7.55				25.0
9.75				18.9
12.50				16.4
14.75				14.1
0	0.45			24.2
	0.35			30.9
	0.20			31.4
	0			31.4

Table 22. Unattached Jet Impact Pressure Measurements, M_o=1.94, K_n=4x10^{-3}

Position			Developed Region Width	Differential Impact Pressure
$\frac{x}{w}$	$\frac{y}{w}$	$\frac{\xi}{w}$	$\frac{\xi^*}{w}$	P_t-P_e (mm oil)
3.15	- 0.60	0.56	0.42	0
	- 0.40	0.36		33
	- 0.20	0.16		118
	0			168
	0.15			170
	0.40	0.16		104
	0.70	0.46		25
	0.90	0.66		5
12.65	- 1.50	2.23	1.35	0
	- 0.95	1.68		3
	- 0.50	1.23		11
	0	0.73		64
	0.35	0.38		66
	0.65	0.08		70
	1.05	0.32		76
	1.45	0.72		55
	1.75	1.02		28
	2.10	1.37		11
2.90	0			146
4.90				142
7.45				123
10.10				105
12.70				66
0	- 0.45			45
	- 0.40			144
	- 0.30			168
	0			160

Table 23. Unattached Jet Impact Pressure Measurements, M_o=2.71, K_n=10^{-4}

Position			Developed Region Width	Impact Pressure Measurement
$\frac{x}{w}$	$\frac{y}{w}$	$\frac{\xi}{w}$	$\frac{\xi^*}{w}$	P_t (mm Mercury)
11.70	- 1.80	2.16	1.50	41.9
	- 1.10	1.46		55.9
	- 0.60	0.42		166.9
	0	0.36		266.9
	0.75	0.39		246.9
	1.15	0.79		186.9
	1.65	1.29		81.9
14.35	0			346.9
12.40				276.9
10.10				346.9
7.35				261.9
4.55				521.9

Table 24. Unattached Jet Impact Pressure Measurements, M_o=2.71, K_n=5x10^{-4}

Position $\frac{x}{w}$	Position $\frac{y}{w}$	Position $\frac{\xi}{w}$	Developed Region Width $\frac{\xi^*}{w}$	Impact Pressure Measurement P_t (mm Mercury)
2.80	- 0.60	0.32	0.30	11.4
	- 0.50	0.22		28.4
	- 0.40	0.12		58.2
	- 0.25			82.0
	0			92.5
	0.30	0.02		82.0
	0.50	0.22		20.5
	0.70	0.42		10.7
10.60	- 1.60	1.85	1.18	9.0
	- 1.30	1.55		9.6
	- 0.85	1.10		16.0
	- 0.35	0.60		46.1
	0	0.25		70.1
	0.45	0.20		69.7
	0.95	0.70		41.1
	1.30	1.05		19.5
	1.65	1.40		10.6
2.65	0			77.2
4.60				68.9
6.75				76.9
9.05				74.8
11.30				84.0
14.50				68.8
0	0.48			24.0
	0.40			79.8
	0.25			82.8
	0			83.2

Table 25. Unattached Jet Impact Pressure Measurements, M_o=2.71, K_n=10^{-3}

Position			Developed Region Width	Impact Pressure Measurement
$\frac{x}{w}$	$\frac{y}{w}$	$\frac{\xi}{w}$	$\frac{\xi^*}{w}$	P_t (mm Mercury)
2.50	- 0.85	0.65	0.46	5.2
	- 0.40	0.20		29.3
	- 0.15			41.0
	0			45.5
	0.25	0.01		40.9
	0.50	0.26		20.8
	0.60	0.36		7.2
11.60	- 1.35	1.67	1.24	5.9
	- 1.00	1.32		6.3
	- 0.60	0.92		13.1
	- 0.30	0.62		31.2
	0	0.32		39.1
	0.25	0.07		43.1
	0.65	0.33		42.0
	1.00	0.68		26.0
	1.45	1.13		8.6
2.80	0			49.5
5.35				26.2
7.95				47.5
10.35				35.7
13.10				38.2
15.45				34.8
0	0.45			30.9
	0.40			39.7
	0.30			40.5
	0			42.5

Table 26. Unattached Jet Impact Pressure Measurements, M_o=2.71, K_n=4x10^{-3}

Position			Developed Region Width	Differential Impact Pressure
$\frac{x}{w}$	$\frac{y}{w}$	$\frac{\xi}{w}$	$\frac{\xi^*}{w}$	P_t-P_e (mm oil)
2.75	- 0.75	0.55	0.40	4
	- 0.55	0.35		23
	- 0.35	0.15		230
	- 0.20			317
	0			343
	0.20			272
	0.40	0.16		115
	0.60	0.36		41
	0.90	0.66		6
11.85	- 1.45	1.47	0.90	4
	- 0.95	0.97		9
	- 0.55	0.57		96
	0	0.02		227
	0.30	0.28		121
	0.55	0.53		74
	1.10	1.08		12
2.90	0			317
5.55				360
8.25				267
10.90				215
13.75				196
16.65				158
0	- 0.40			83
	- 0.35			93
	- 0.25			263
	0			268

Table 27. Dimensionless Unattached Jet Core Length $\left(\frac{x_e}{w}\right)$

Mach Number \ Knudsen Number	10^{-4}	5×10^{-4}	10^{-3}	4×10^{-3}
0.5	4.5	5.75	7.7	5.05
0.8	4.8	5.00	7.5	7.5
1.94	5.8	6.8	6.4	6.0

Table 28. Centerline Velocity Decay Constant (m)

Mach Number \ Knudsen Number	10^{-4}	5×10^{-4}	10^{-3}	4×10^{-3}
0.5	2.31	1.85	1.15	3.00
0.8	3.21	3.00	1.85	2.06
1.94	3.21	3.00	3.12	3.45

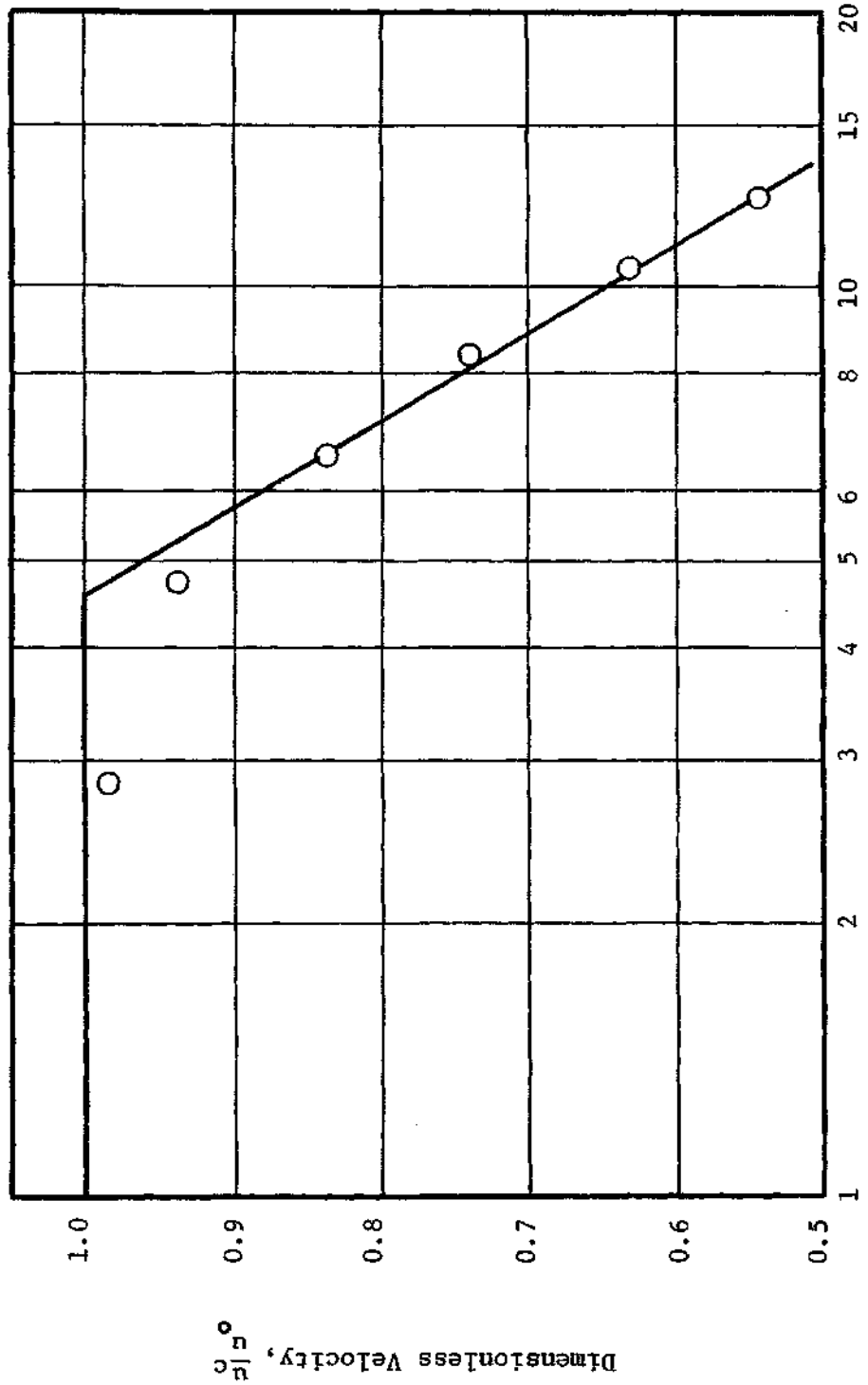

Figure 37. Unattached Jet Centerline Velocity, M_o=0.5, K_n=10^{-4}

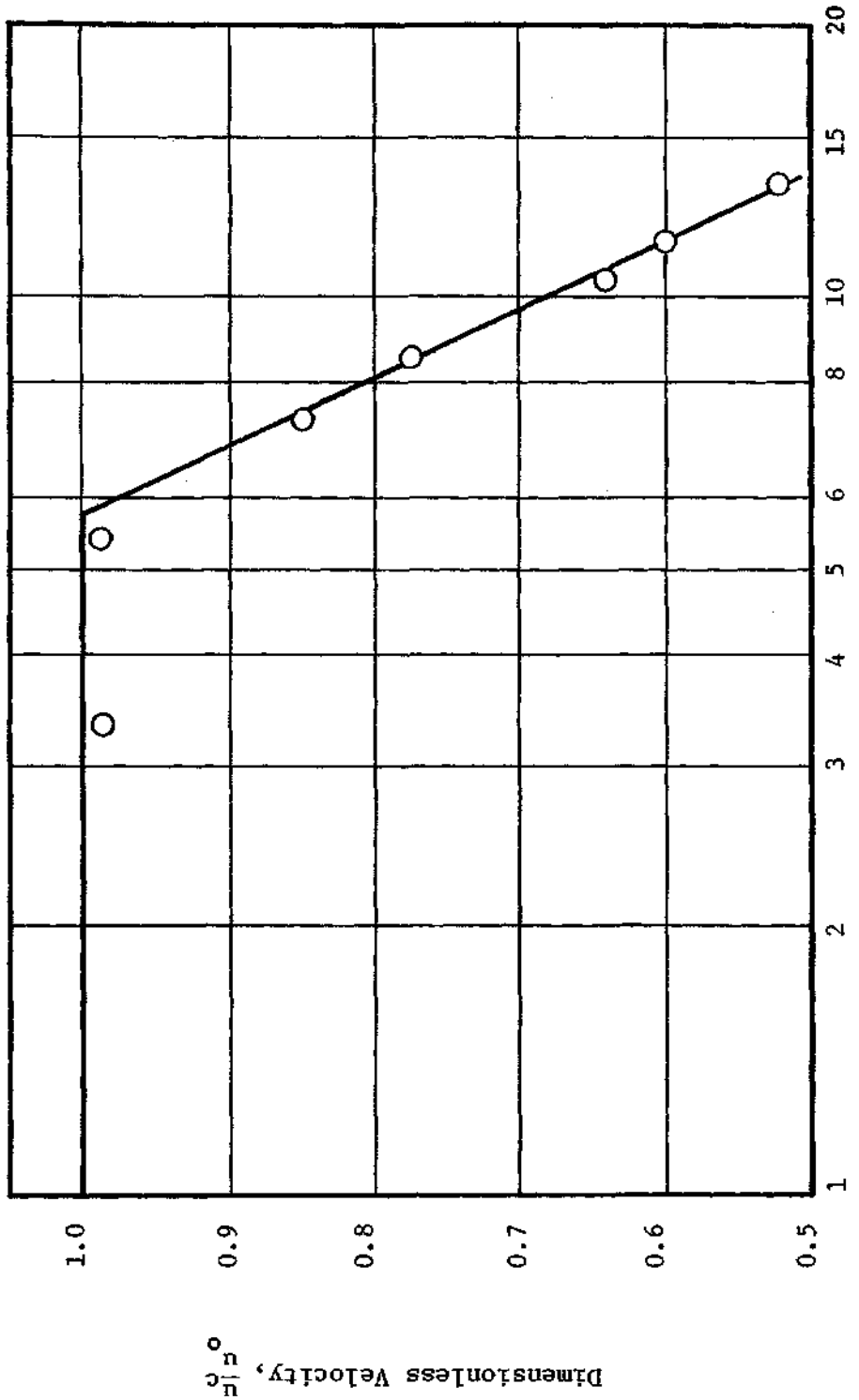

Figure 38. Unattached Jet Centerline Velocity, M_o=0.5, $K_n = 5 \times 10^{-4}$

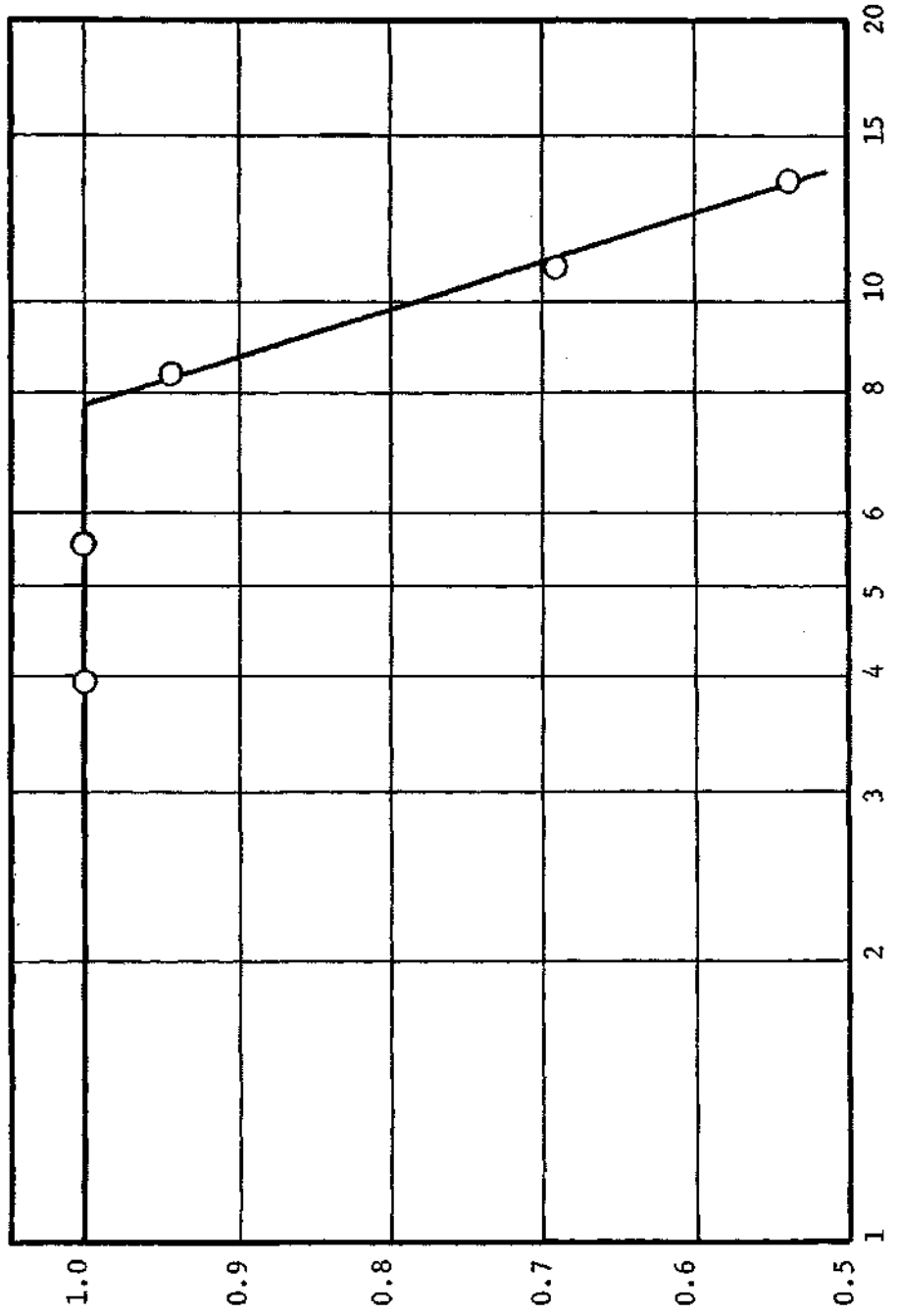

Figure 39. Unattached Jet Centerline Velocity, M_o=0.5, K_n=10^{-3}

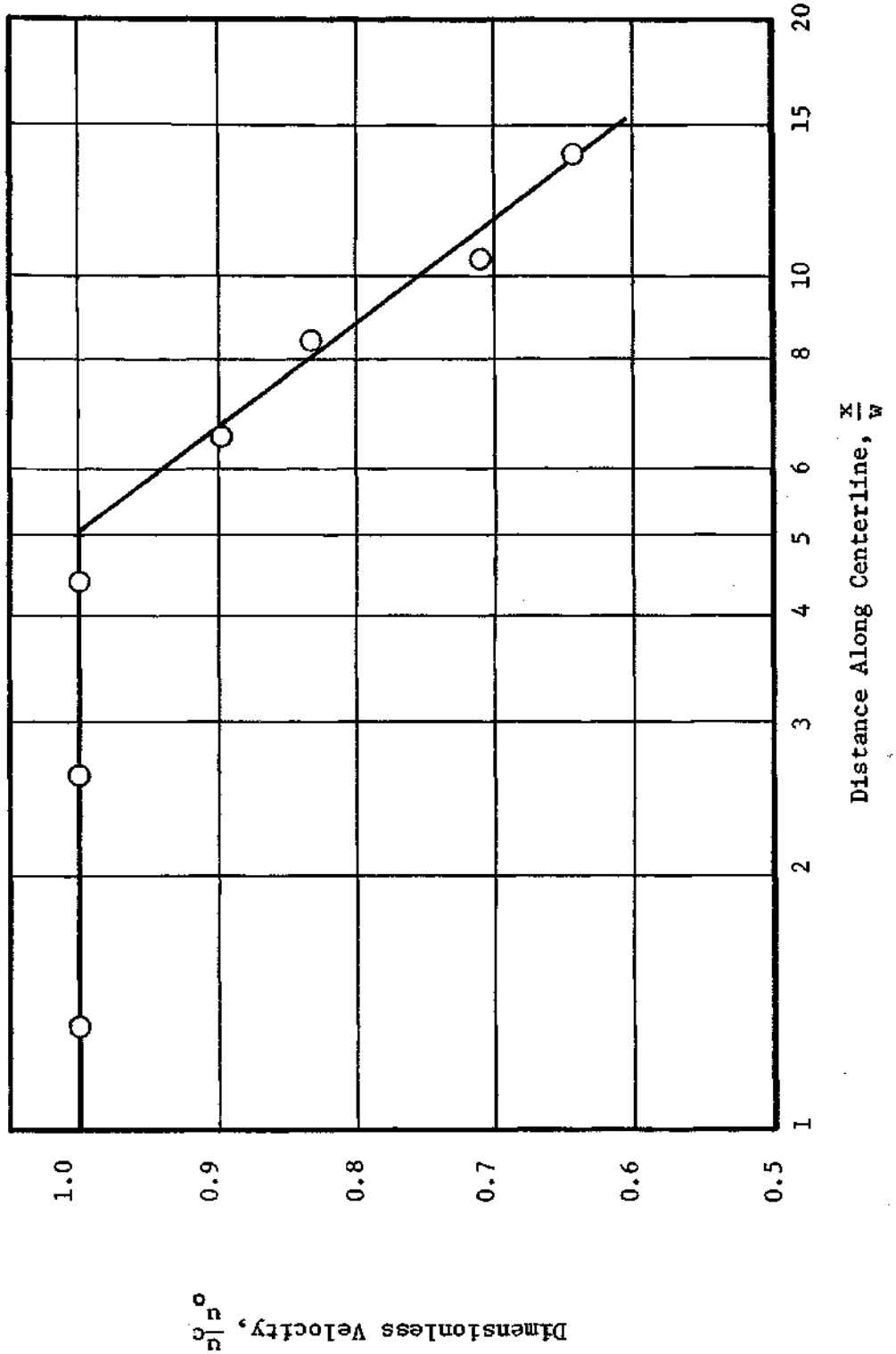

Figure 40. Unattached Jet Centerline Velocity, M_o=0.5, K_n=4x10^{-3}

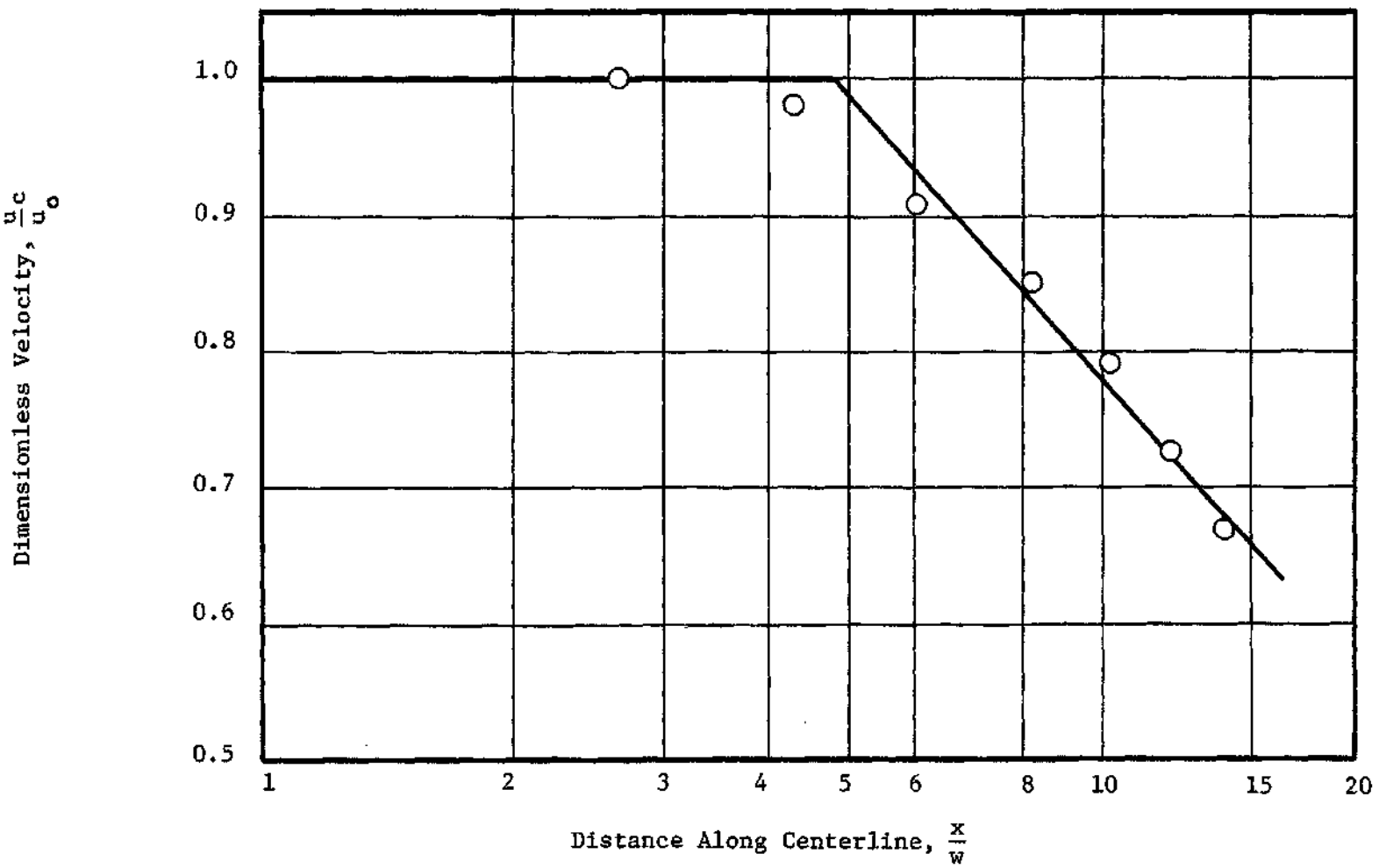

Figure 41. Unattached Jet Centerline Velocity, M_o=0.8, K_n=10^{-4}

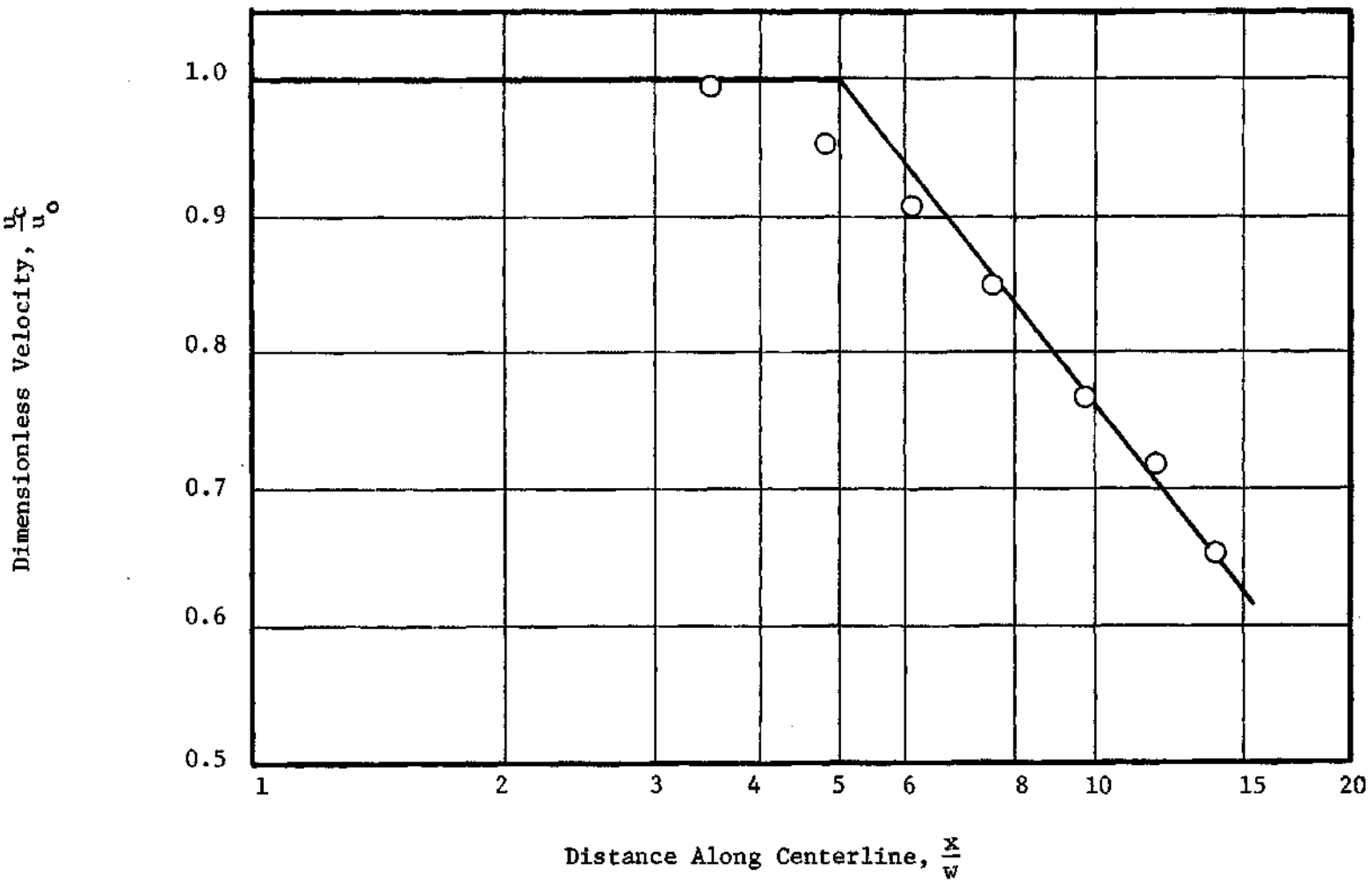

Figure 42. Unattached Jet Centerline Velocity, M_o=0.8, K_n=5x10^{-4}

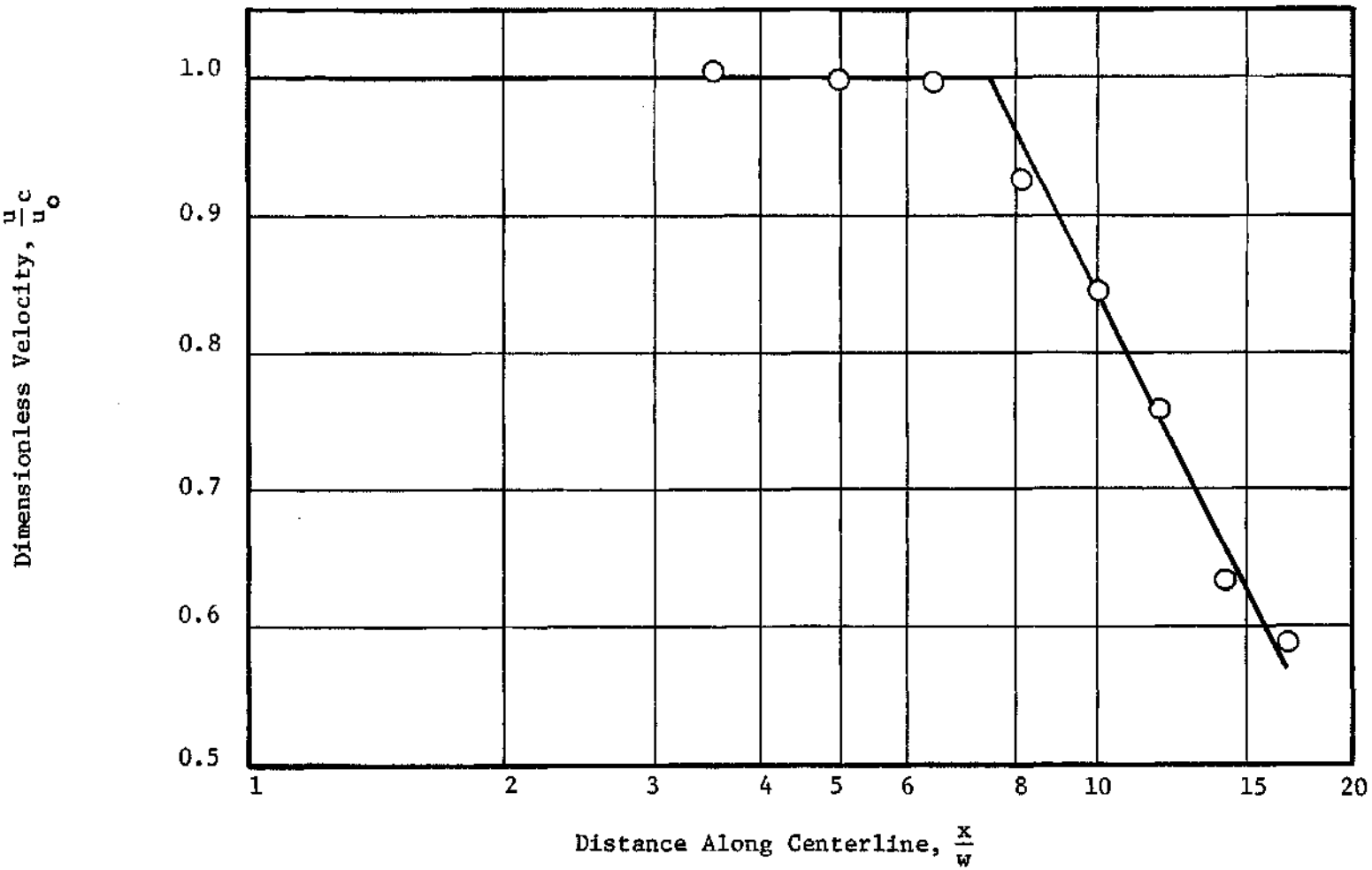

Figure 43. Unattached Jet Centerline Velocity, M_o=0.8, K_n=10^{-3}

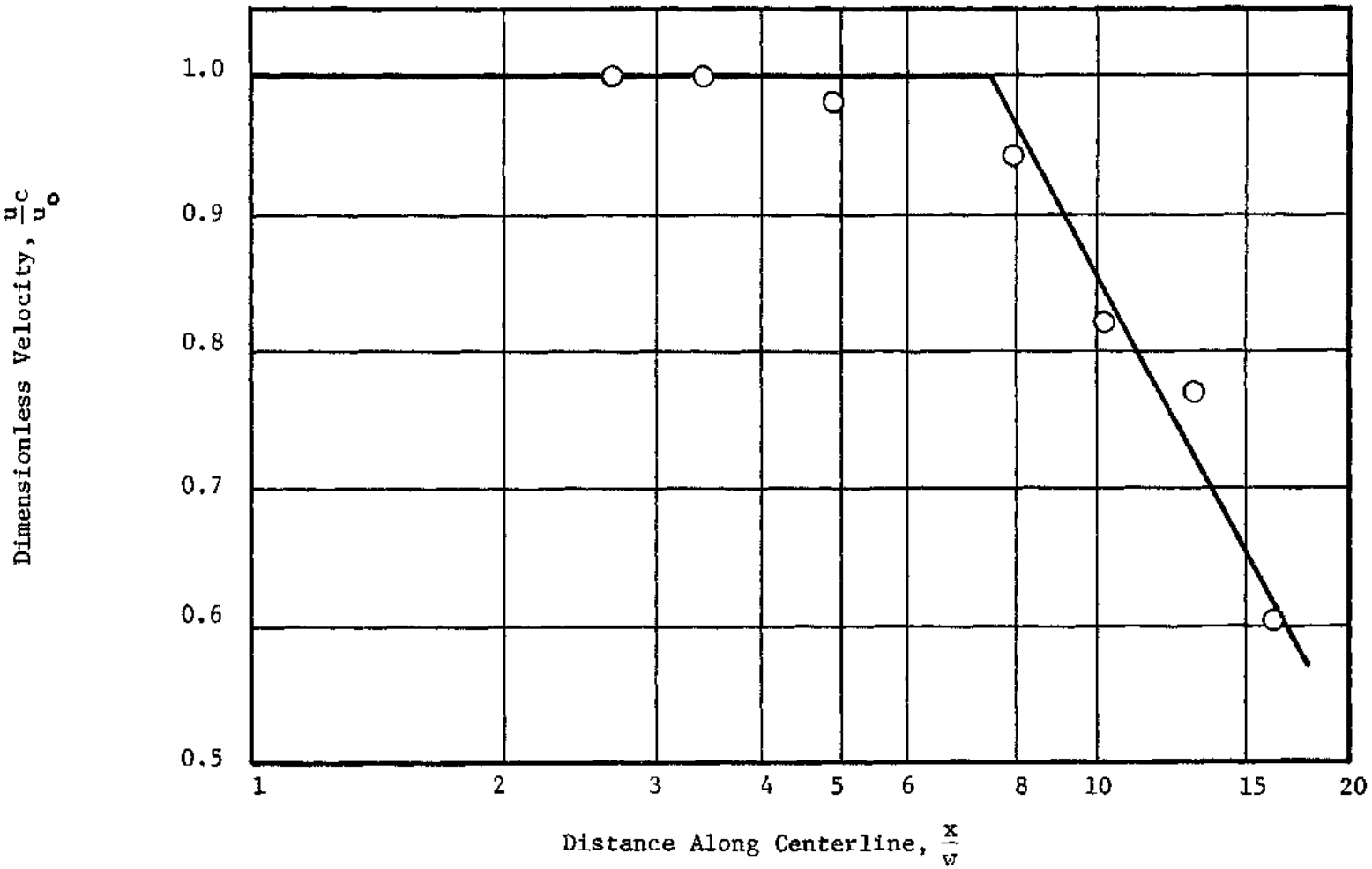

Figure 44. Unattached Jet Centerline Velocity, M_o=0.8, K_n=4×10^{-3}

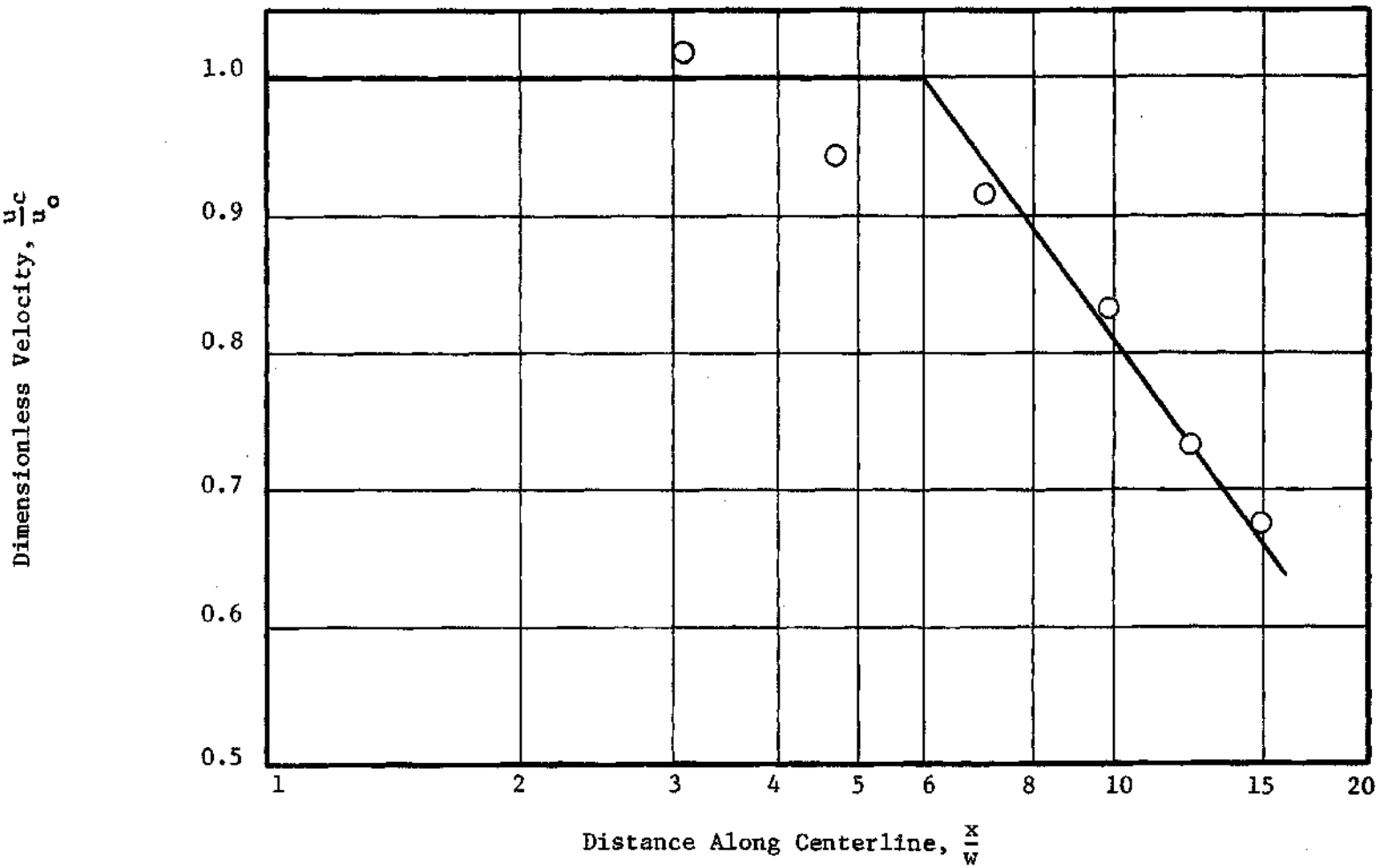

Figure 45. Unattached Jet Centerline Velocity, M_o=1.94, K_n=10^{-4}

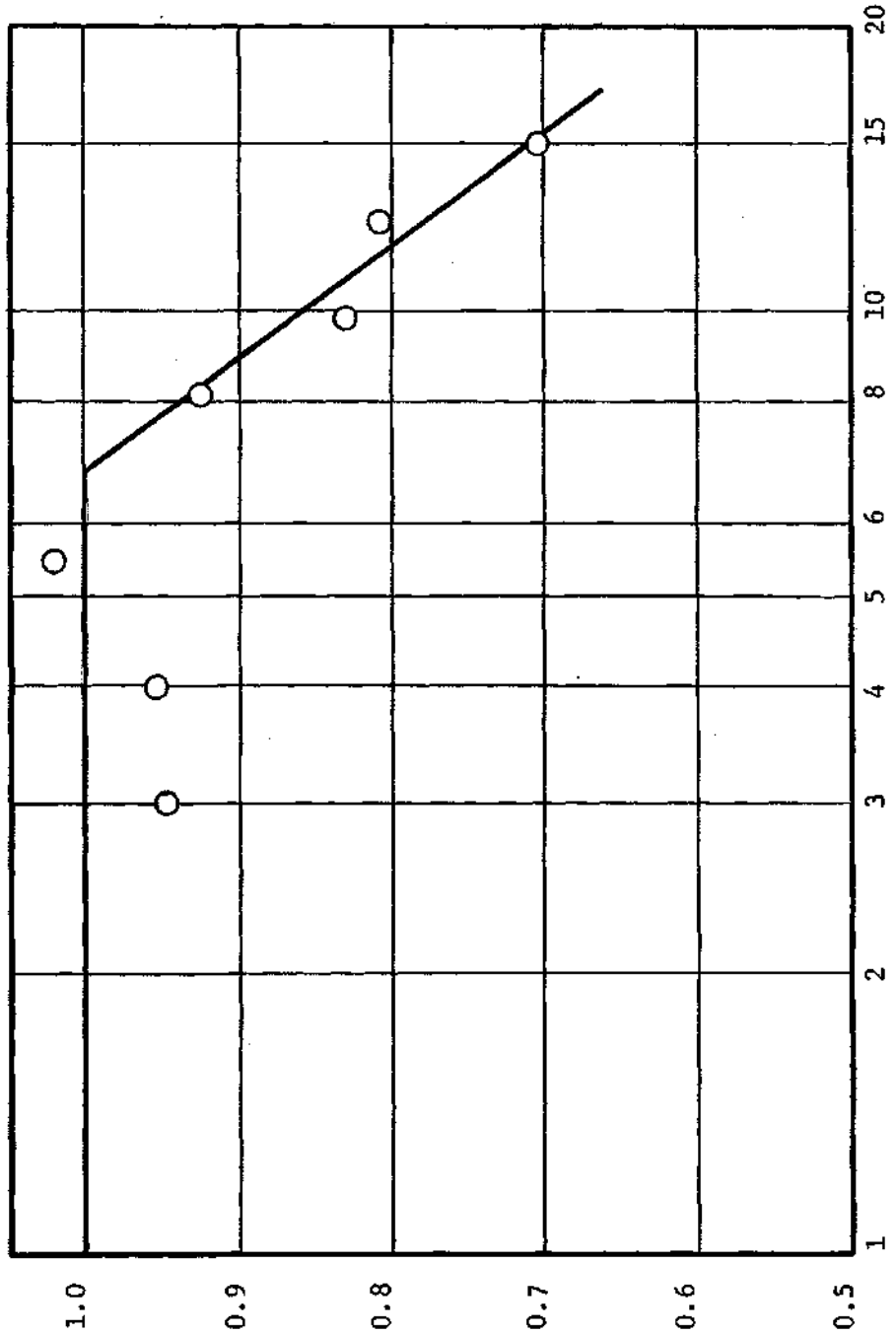

Figure 46. Unattached Jet Centerline Velocity, M_o=1.94, $K_n = 5 \times 10^{-4}$

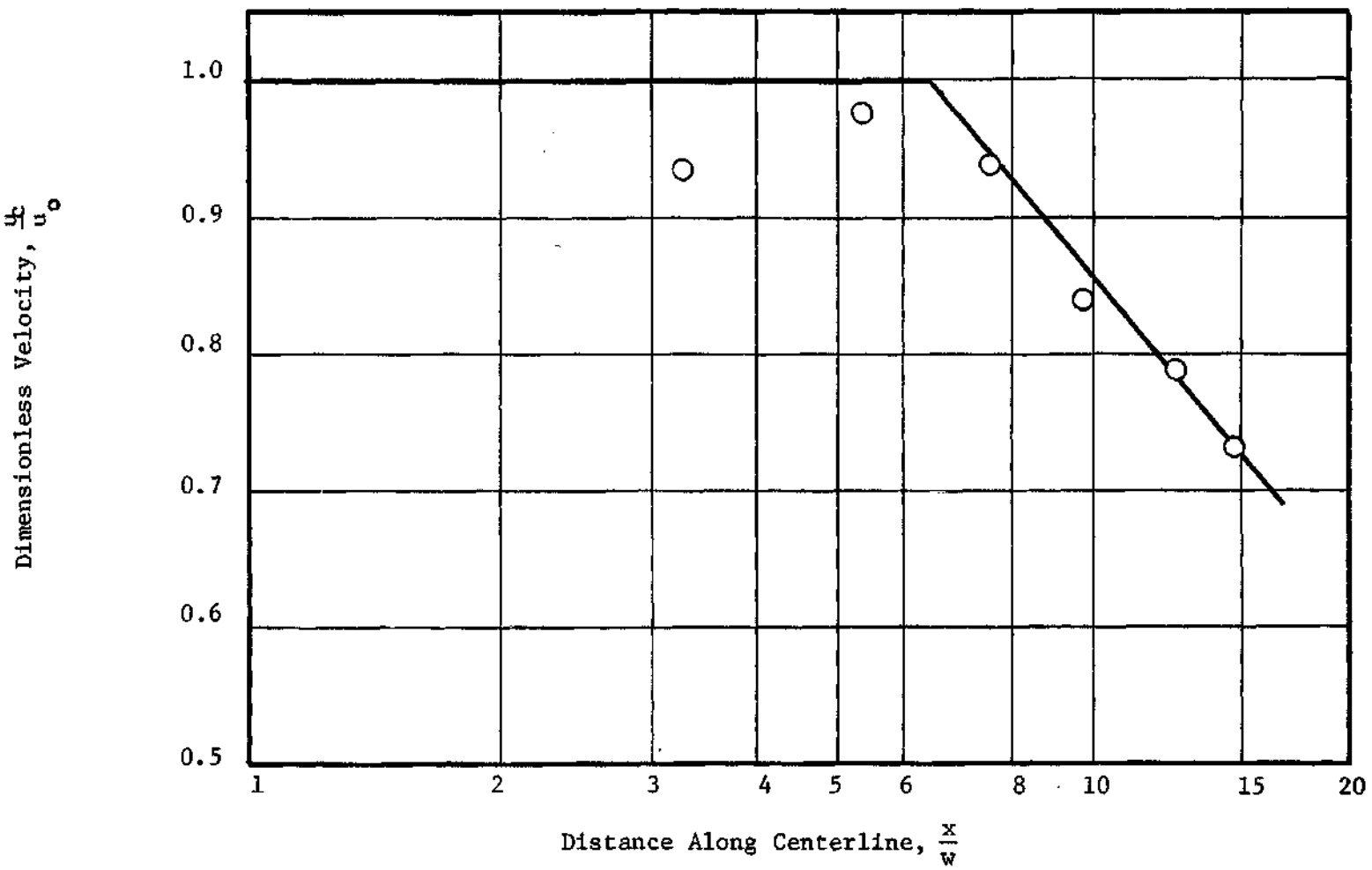

Figure 47. Unattached Jet Centerline Velocity, M_o=1.94, K_n=10^{-3}

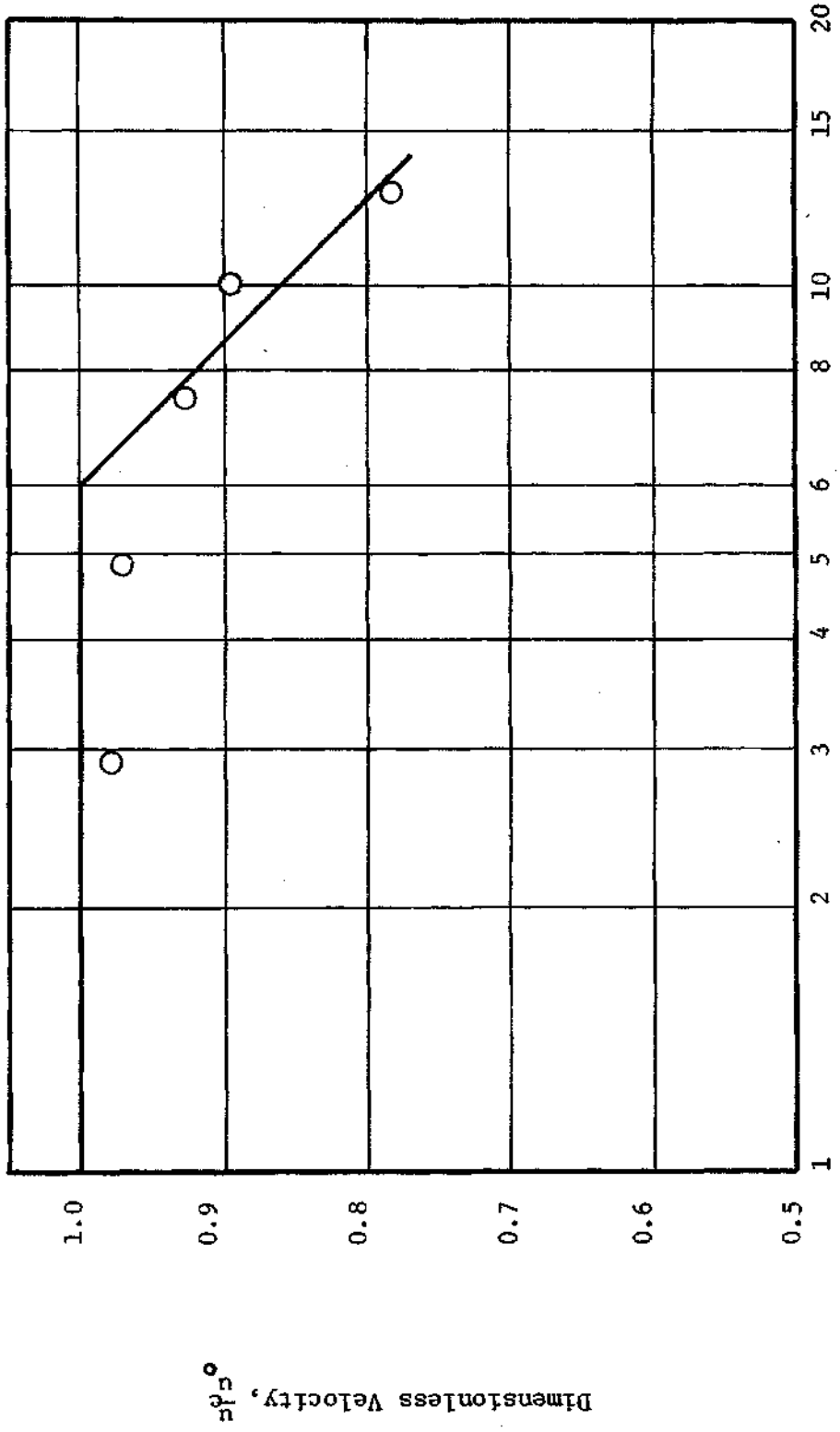

Figure 48. Unattached Jet Centerline Velocity, M_o=1.94, K_n=4x10^{-3}

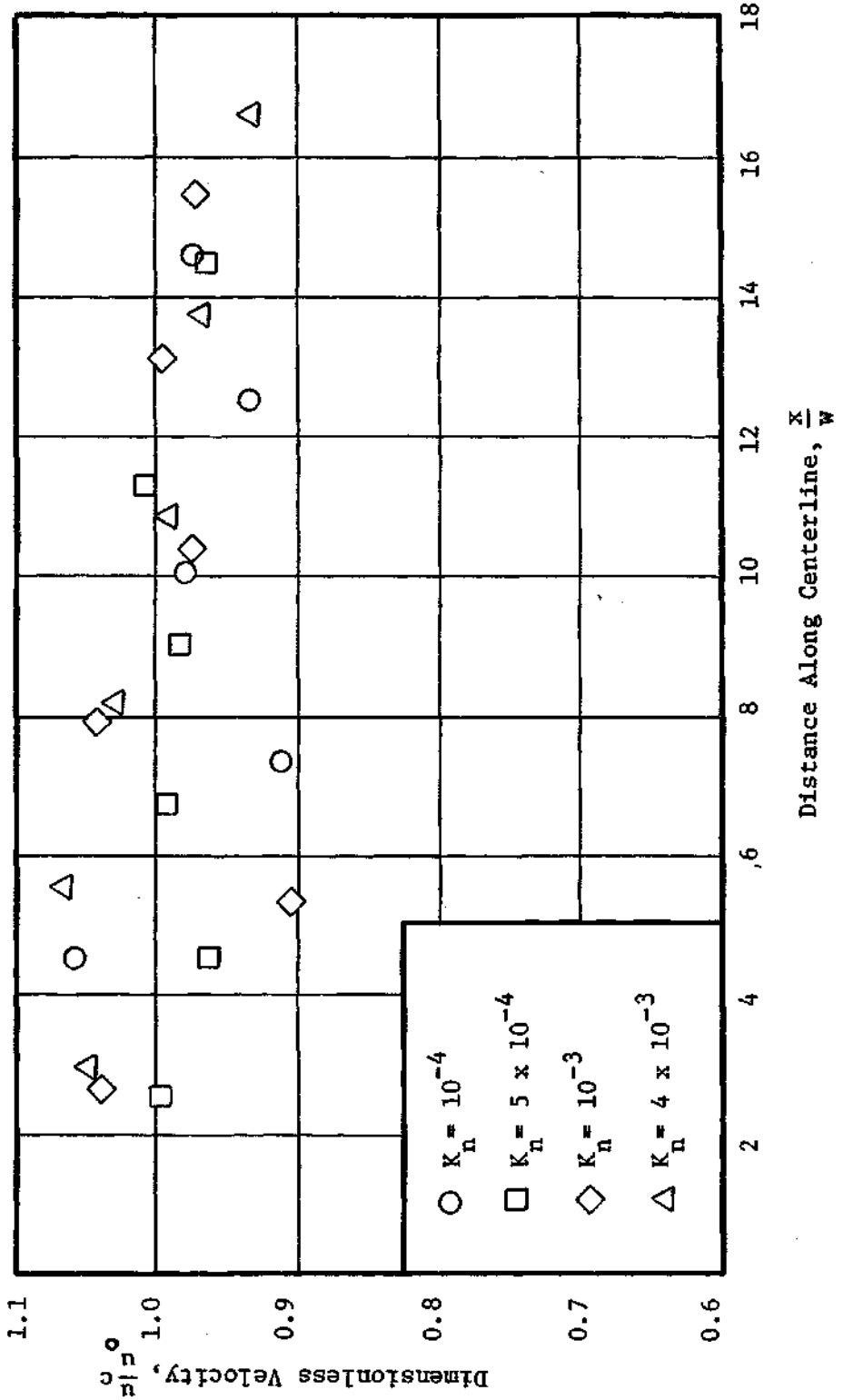

Figure 49. Unattached Jet Centerline Velocities, $M_o = 2.71$

APPENDIX D

SAMPLE CALCULATIONS

Calculation of Jet Velocities

Calculation of the velocity from the impact pressure at one location in a subsonic jet is illustrated with the following data:

measured impact pressure = 3.2 mm of mercury

P_e = 2.2 mm of mercury

The pressure ratio is:

$$\frac{P_e}{P_t} = \frac{2.2}{3.2}$$

$$= 0.688$$

From isentropic flow tables for the pressure ratio of 0.688 the following relationships are determined:

$$M = 0.75$$

$$\frac{T}{T_t} = 0.899$$

From the definition of speed of sound and Mach number:

$$a = \sqrt{\gamma RT} \quad , \quad M = \frac{u}{a}$$

For all experiments $T_t = 537°R$ where R denotes degrees Rankine. The speed of sound may be determined from the last two relations with $\gamma = 1.4$ and $R = 53.3 \frac{ft\text{-}lbf}{lbm\text{-}°R}$ for air and the gravitational constant equal to $32.2 \frac{ft\text{-}lbf}{lbf\text{-}sec^2}$.

$$a = \sqrt{1.4(53.3)(0.899)(537)(32.2)}$$

$$a = 1077 \text{ fps}$$

$$u = Ma$$

$$= 0.75\ (1077)$$

$$\boxed{u = 807 \text{ fps}}$$

Calculation of the velocity from the impact pressure at one location in a supersonic jet is illustrated with the following data:

$$\text{measured impact pressure} = 335 \text{ mm of mercury}$$

$$P_e = 54.7 \text{ mm of mercury}$$

The following pressure ratio is calculated:

$$\frac{\text{measured impact pressure}}{P_e} = 6.12$$

From isentropic flow tables and normal shock tables the following information is determined:

$$M = 2.10$$

$$\frac{T}{T_t} = 0.531$$

As in the previous paragraph, the speed of sound is calculated:

$$a = 828 \text{ fps}$$

$$u = Ma$$

$$= 2.10(828)$$

$$\boxed{u = 1740 \text{ fps}}$$

Calculation of K_2

The calculation procedure for determining the values of K_2 is illustrated for the case of M = 0.5 and Kn = 10^{-3}. For the geometry of the attachment model and the value $\frac{L_R}{w} = 8.45$ from Table 3, equations (7), (8), and (9) may be written:

$$\frac{\Delta}{w} = \frac{r}{w} - \sqrt{69.1 + \left(\frac{r}{w} - 3.47\right)^2}$$

$$\frac{x}{w} = \frac{r}{w}\ \alpha$$

$$\alpha = \tan^{-1} \frac{8.32}{\frac{r}{w} - 3.47}$$

The value of $\frac{\delta}{w}$ is easily plotted as a function of U in Figure 50 from the results of the computer program and conservation of momentum considerations for this flow condition. Utilizing the equations above, the graph of $\frac{\delta}{w}$, and the straight line centerline velocity graph for this flow condition, the following trial and error solution for $\frac{r}{w}$ was conducted with the condition that $\frac{\delta}{w}$ must equal $\frac{\Delta}{w}$ at the attachment point.

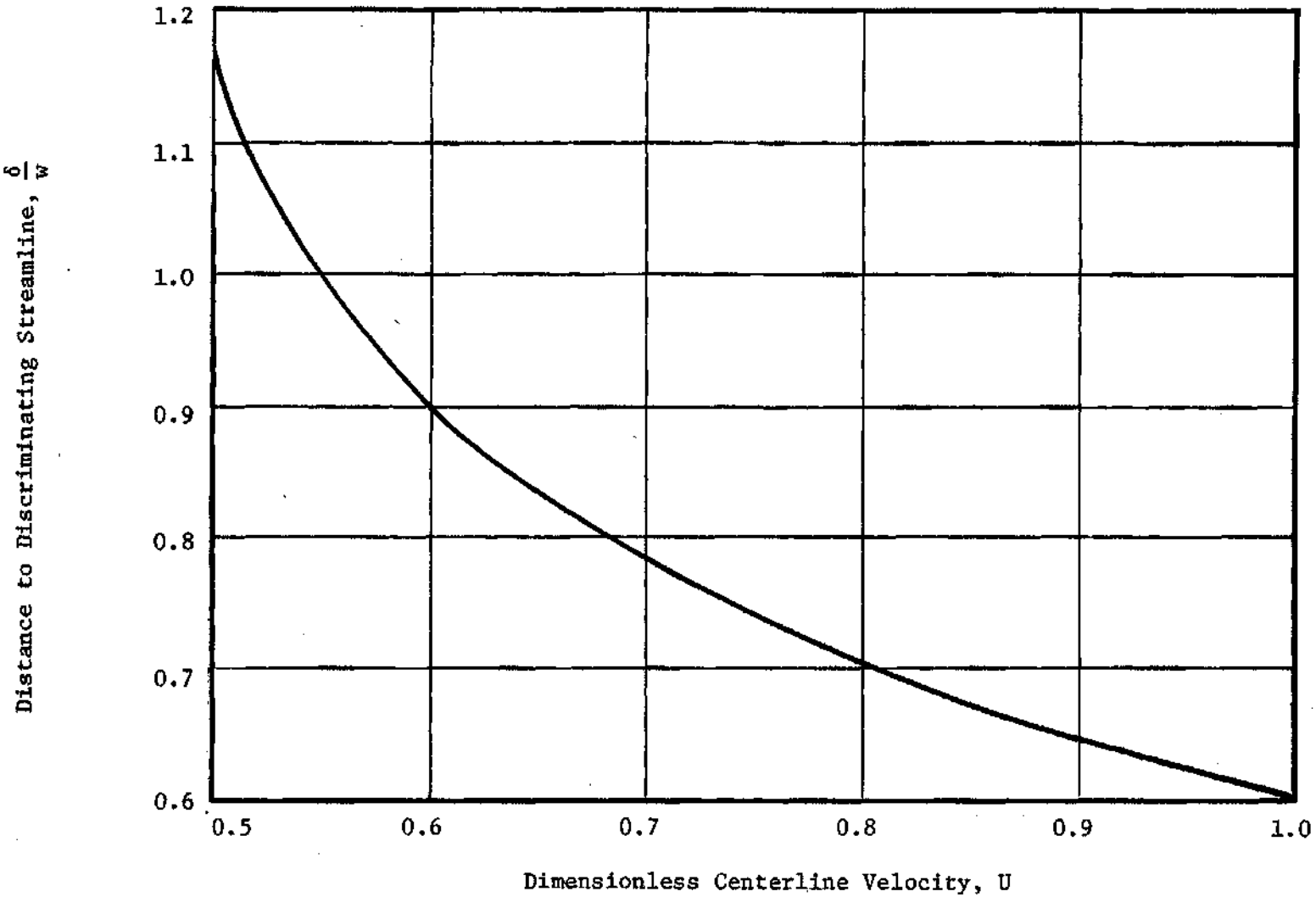

Figure 50. Distance To Discriminating Streamline, M_o=0.5

$\frac{r}{w}$	$\frac{\Delta}{w}$	α degrees	α radians	$\frac{x}{w}$	U	$\frac{\delta}{w}$
15.00	0.76	35.8°	0.624	9.37	0.835	0.680
14.50	0.69	37.0°	0.646	9.36	0.836	0.679
14.40	0.67	37.2°	0.650	9.36	0.836	0.679
14.45	0.68	37.2°	0.650	9.36	0.836	0.679

The stagnation pressure on the discriminatory streamline at the attachment point must be determined. The attachment point value of $\frac{\xi^*}{w}$ is determined by interpolation from the computer solution of Appendix B for the value of U = 0.836:

$$\frac{\xi^*}{w} = 0.983$$

and for $\frac{\delta}{w} = 0.679$ we may calculate

$$\frac{\delta}{\xi^*} = 0.850$$

The dimensionless velocity on the discriminating streamline is calculated from equation (14).

$$\frac{u}{u_c} = e^{-0.6931(0.850)^2}$$
$$= 0.606$$

Centerline velocity is calculated from isentropic nozzle relations for $M_o = 0.5$ and $T_t = 77°F$ and the value of U = 0.836

$$u_c = 473 \text{ fps}$$

Velocity along the discriminating streamline is, therefore:

$$u = 287 \text{ fps}$$

From isentropic flow relations the Mach number on the stagnation streamline is determined to be 0.26 for which the stagnation pressure on the discriminating streamline is determined as:

$$\frac{P_s}{P_o} = 1.05$$

The other important analytical properties to be used in equation (11) may be determined using the value of K_1 which was determined to be 0.880 for the model geometry of this investigation.

$$\frac{L'}{w} = K_1 \frac{L_R}{w}$$

$$\frac{L'}{w} = 7.44$$

The following values were calculated with the value of $\frac{L'}{w}$ above:

$$\frac{\Delta'}{w} = 1.09$$

$$\alpha' = 0.581 \text{ radians}$$

$$\frac{X'}{w} = 8.4$$

$$U' = 0.925$$

$$\frac{\delta'}{w} = 0.633$$

$$\frac{\xi^*}{w} = 0.796$$

$$\frac{\delta'}{\xi^{*'}} = 0.794$$

Interpolation within the results of the computer program of Appendix B using the values of U' and $\frac{\delta'}{\xi^{*'}}$ above the value of J_1 may be determined as:

$$J_1 = 0.91$$

Equations (6) and (11) are solved simultaneously by eliminating $\frac{P_i}{P_e}$ for the value of K_2.

$$\boxed{K_2 = 1.85}$$

Values of K_2 for 12 of the flow conditions of this study are presented in Figure 31.

APPENDIX E

EQUIPMENT CAPABILITIES

The equipment utilized in this investigation and sketched in Figure 12 is capable of producing a much wider range of flow conditions than utilized in the experiments. The limiting flow capabilities of the equipment are determined by the maximum and minimum pressures achievable in the wall attachment model and the volume flowrate capacity of the vacuum pump presented in Figure 51.

The maximum model pressure is approximately atmospheric pressure because the model was designed to utilize an internal vacuum to assist in holding the assembly together, and it could easily be blown apart under internal pressures greater than atmospheric. The minimum model pressure achieved in tests subsequent to the experiments was 0.10 mm of mercury. The primary reason that the pressure was not reduced further is believed to be that moisture condenses within the equipment when it is brought up to atmospheric pressure after an experiment is completed. The next time the model is evacuated the condensed moisture continues to boil away for very long periods of time and thereby prevents pressures much lower than 0.10 mm of mercury from being achieved. Leakage rates have been determined to be very low and could not be responsible for the limiting minimum pressure. Lower pressures could possibly be reached by installing valves at positions

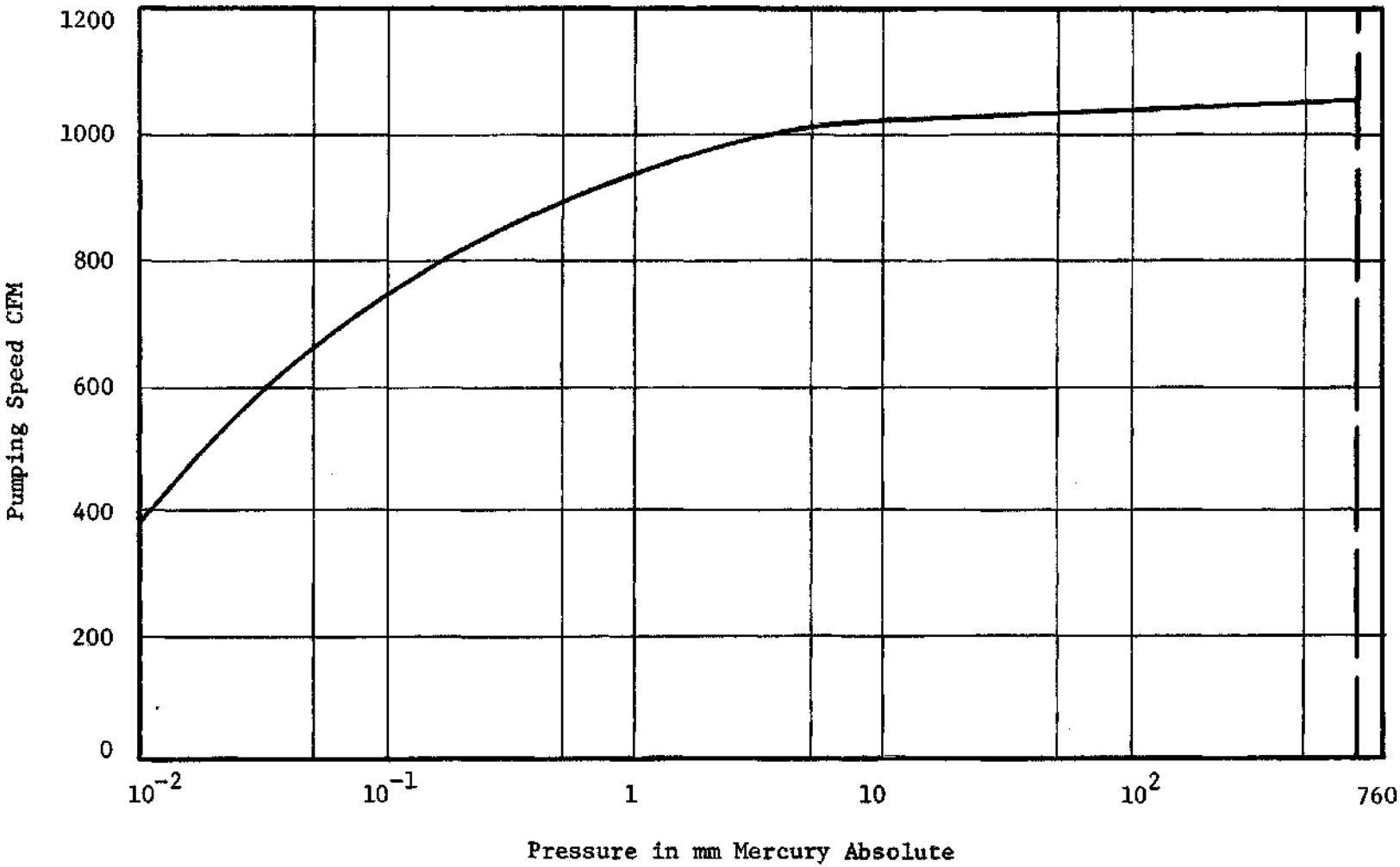

Figure 51. Beach-Russ Model 1000 RP Typical Pumping Speed Curve

where the equipment could be isolated from the vacuum pump, and the equipment could be continuously held under vacuum and thus prevent moisture condensation.

The envelope of equipment capabilities is presented in Figure 52 for the nozzle exit width and total air temperature of this investigation. The envelope of the jet attachment experiments is also presented in this figure as a dashed line for comparison purposes. Experiment limits were determined by the limits of previous investigations and the capabilities of available pressure sensing instrumentation.

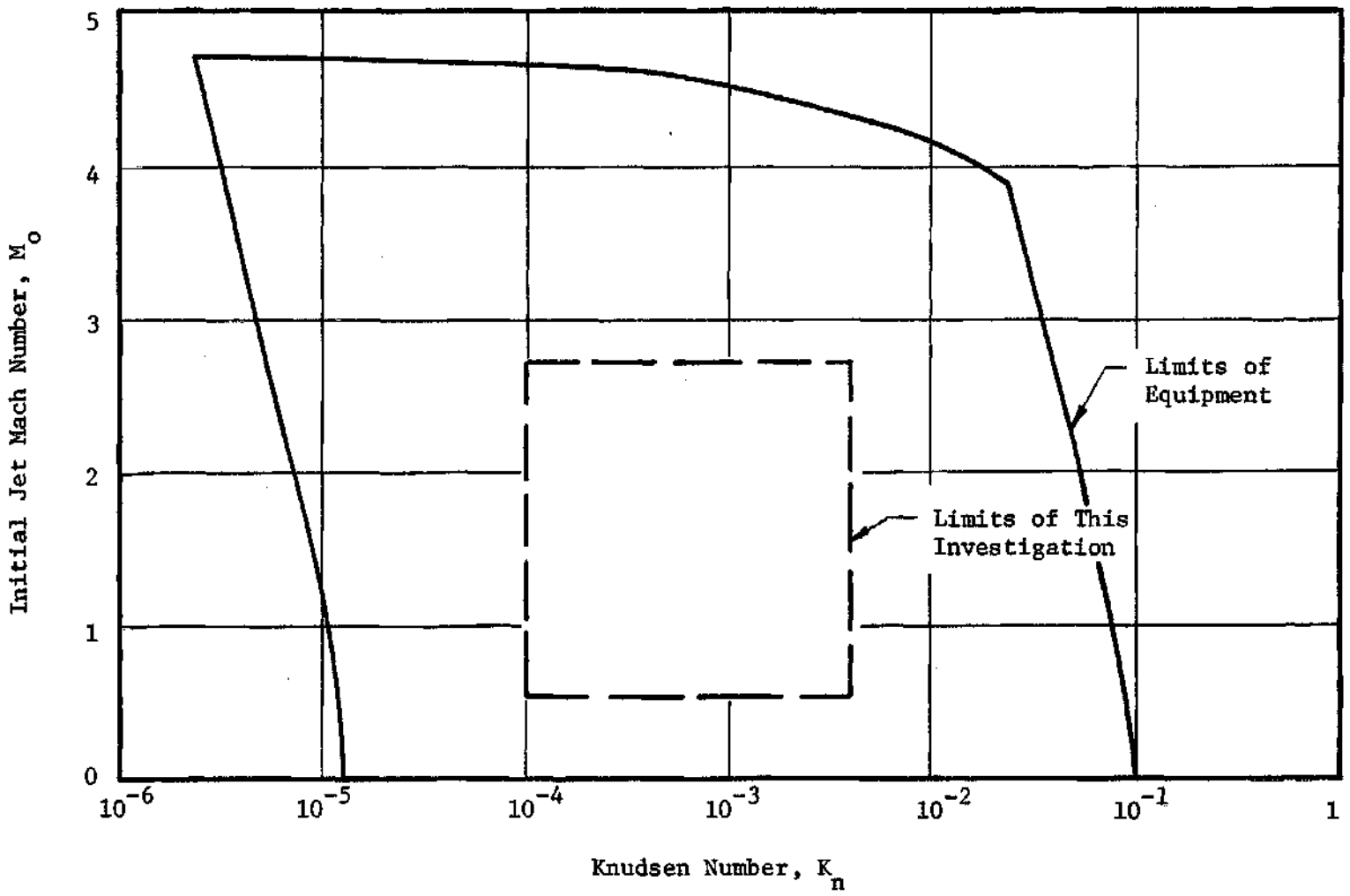

Figure 52. Envelope of Equipment Capabilities
(T_t=537°R, w=0.20inch)

APPENDIX F

EXPERIMENTAL ERRORS

The results of this investigation were subject to errors from three primary sources; limitations of measurement equipment, the calculations used to transform the data into interpretable results, and the influence of uncontrolled variables in the experiments. The most difficult type of error to analyze is that caused by uncontrolled variables which include the accumulation of contaminants in the manometers, the very small leaks associated with periodic disassembly of the model, the errors associated with visual data taking, and the slight drift of barometric pressure during the experiments which resulted in errors in the absolute pressure manometer readings. Accurate estimates of this type of error are not readily available, but wherever possible the errors were minimized by careful model assembly and data collection.

Estimates of the order of magnitude of errors caused by equipment limitations could be made from examinations of instrument resolution and previous studies of errors in measurement equipment. With the exception of the 1/32 inch probe used for nozzle exit impact pressure measurements, the impact pressure probes were designed to provide less than one percent error in measurements of the maximum impact pressure in any experiment. Reference (17) shows that the accuracy of the probe measurements decreases with reduction in

Reynolds number based on probe diameter. For this reason experimental errors are larger in the outer edges of the jets than in the middle of the jet. The maximum possible probe error in u/u_c at $\xi/\xi^* = 1.0$ in the core region is estimated to be 25% for the lowest value of R_e encountered in the experiments.

Mercury manometers open to the atmosphere were used for measurement of absolute pressures. The accuracy of the measurements was determined by the resolution of the barometer used to correct the data to be within 0.1 mm of mercury. Differential pressures between the probes and the model were measured with inclined and vertical oil filled manometers. Inclined manometer resolution was approximately 0.04 mm of mercury, and vertical manometer resolution utilizing a telescopic cathetometer was approximately 0.004 mm of mercury. The accuracy of the majority of static pressure measurements was dependent on the oil manometer resolutions while the impact pressure accuracy was dependent on the mercury manometer accuracy.

Jet velocities were calculated with pressure ratios obtained by measurement and isentropic flow relations. Mach numbers were determined to two decimal place accuracy. The nature of the isentropic flow relations is to reduce the error from inaccurate pressure ratios in calculating the Mach number and the temperature and thus to reduce the measurement error in calculated velocities. The effects of shock waves in supersonic jets was to introduce errors in calculations of velocity due to the assumption that static pressure was uniform within the unattached jets.

Probe position errors were estimated to be less than 0.01 inch in Chapter IV. Jet attachment locations on the adjacent wall were subject to the errors of probe position measurements and errors caused by some tangling of the fibers on the wall. To minimize this error, the fibers were replaced with new ones each time the model was disassembled. The attachment point location error is estimated to be less than 0.05 inch or 0.25 w.

LITERATURE CITED

1. Chang, P. K., "Survey on Coanda Flow," Proceedings of the Harry Diamond Laboratories Fluid Amplification Symposium, Vol. I, 1962.

2. Warren, R. W., "Wall Effects and Binary Devices," Proceedings of the Harry Diamond Laboratories Fluid Amplification Symposium, Vol. I, 1962.

3. Bourque, C. and Newman, B. G., "Reattachment of a Two-Dimensional Incompressible Jet to an Adjacent Flat Plate," The Aeronautical Quarterly, Vol. XI, August, 1960, pp. 201-232.

4. Bourque, C., "Reattachment of a Two-Dimensional Jet to an Adjacent Flat Plate," Advances in Fluidics, American Society of Mechanical Engineers, New York, 1967, p. 192.

5. Perry, C. C., "Two-Dimensional Jet Attachment," Advances In Fluidics, American Society of Mechanical Engineers, New York, 1967, p. 205.

6. McRee, D. I. and Moses, H. L., "The Effect of Aspect Ratio and Offset on Nozzle Flow and Jet Reattachment," Advances in Fluidics, American Society of Mechanical Engineers, New York, 1967, p. 142.

7. Mueller, T. J. and Olson, R. E., "Spreading Rates of Compressible Two-Dimensional Reattaching Jets," Proceedings of the Harry Diamond Laboratories Fluid Amplification Symposium, Vol. I, 1964.

8. Olson, R. E., "An Analytical and Experimental Study of Two-Dimensional Compressible Submerged Jets," Proceedings of the Harry Diamond Laboratories Fluid Amplification Symposium, Vol. I, 1962.

9. Olson, R. E., "Characteristics of Two-Dimensional Compressible Attached Jets," Proceedings of the Harry Diamond Laboratories Fluid Amplification Symposium, Vol. I, 1962.

10. Olson, R. E., "Reattachment of a Two-Dimensional Compressible Jet to an Adjacent Plate," Symposium on Fluid Jet Control Devices, American Society of Mechanical Engineers, 1962.

11. Olson, R. E. and Miller, D. P., "The Interaction of Oblique Shocks and Expansion Waves with a Jet Boundary Mixing Zone," Proceedings of the Harry Diamond Laboratories Fluid Amplification Symposium, Vol. I, 1964.

12. Olson, R. E. and Stoeffler, R. C., "Analytical Method for Predicting Power Jet Reattachment Characteristics in Wall-Attachment-Type Fluidic Devices," Advances in Fluidics, American Society of Mechanical Engineers, New York, 1967, p. 177.

13. Small, D. A., "Optimizing Fluidic Element Size for Speed and Power Consumption," ASME Technical Paper No. 67-WA/FE-39, 1967.

14. Comparin, R. A., Jenkins, W. C., and Moore, R. B., Jet Reattachment at Low Reynolds Numbers and Moderate Aspect Ratios, ASME Technical Paper No. 67-FE-25, 1967.

15. Dushman, S., Scientific Foundations of Vacuum Technique, John Wiley and Sons, New York, 2nd ed., 1962.

16. Huang, A. B., Lectures on Molecular Gasdynamics, (Notes for Elementary Molecular Gasdynamics Lectures in the School of Aerospace Engineering, Georgia Institute of Technology) 1966.

17. Sherman, F. S., New Experiments on Impact-Pressure Interpretation in Supersonic and Subsonic Rarefied Air Streams, NACA Technical Note TN 2995, September, 1953.

18. Schlichting, H., Boundary Layer Theory, McGraw-Hill Book Co., Inc., New York, 4th ed., 1960.

OTHER REFERENCES

19. Comparin, R. A., Glaettli, H. H., Mitchell, A. E., and Mueller, H. R., "On the Limitations and Special Effects in Fluid Jet Amplifiers," Symposium on Fluid Jet Control Devices, American Society of Mechanical Engineers, 1962.

20. Dahl, A. I. (ed.), Temperature, Its Measurement and Control in Science and Industry, Vol. 3, Part 2, Reinhold Publishing Co., New York, 1962.

21. Denker, R. E., "Theoretical Analysis of Fluid Amplifier Design," Proceedings of the Harry Diamond Laboratories Fluid Amplification Symposium, Vol. II, 1964.

22. Glaettli, H. H., Muller, H. R., and Zings, R. H., "Remarks on the Limitations of Pure Fluid Elements," Proceedings of the Harry Diamond Laboratories Fluid Amplification Symposium, Vol. I, 1964.

23. Holmes, A. B. and Foxwell, J. E., "Supersonic Fluid Amplification with Various Expansion Ratio Nozzles," Proceedings of the Harry Diamond Laboratories Fluid Amplification Symposium, Vol. I, 1964.

24. Hougen, O. A. and Dodge, F. W., The Drying of Gases, Edward Brothers, Inc., Ann Arbor, Michigan, 1947.

25. Hrubecky, H. F. and Pearce, L. N., "Flow Field Characteristics in a Model Bi-Stable Fluid Amplifier," Proceedings of the Harry Diamond Laboratories Fluid Amplification Symposium, Vol. I, 1964.

26. Kane, E. D. and Maslach, G. J., Impact Pressure Interpretation in a Rarefied Gas at Supersonic Speeds, NACA Technical Note TN 2210, October, 1950.

27. Kary, S., Winston, E. T., and Hawes, P., "The Response of a Bistable Fluid Amplifier to a Step Input," Proceedings of the Harry Diamond Laboratories Fluid Amplification Symposium, Vol. I, 1964.

28. Page, R. H., Hill, W. G., and Kessler, T. J., Reattachment of Two-Dimensional Supersonic Turbulent Flows, ASME Technical Paper No. 67-FE-20, 1967.

29. Pai, S. I., Fluid Dynamics of Jets, D. Van Nostrand Company, New York, 1954.

30. Sawyer, R. A., "The Flow Due to a Two-Dimensional Jet Issuing Parallel to a Flat Plate," Journal of Fluid Mechanics, Vol. 9, December, 1960.

31. Sawyer, R. A., "Two-Dimensional Reattaching Jet Flows Including The Effects of Curvature on Entrainment," Journal of Fluid Mechanics, Vol. 17, December, 1963, pp. 481-498.

32. Shapiro, A. H., The Dynamics and Thermodynamics of Compressible Fluid Flow, The Ronald Press Co., New York, 1953.

33. Shih, C., "Flow Characteristics in a Supersonic Fluid Amplifier," Advances in Fluidics, American Society of Mechanical Engineers, New York, 1967, p. 129.

34. Warren, R. W., "Some Parameters Affecting the Design of Bistable Fluid Amplifiers," Symposium on Fluid Jet Control Devices, American Society of Mechanical Engineers, 1962.

35. Yalamanchili, J., Experimental Investigation of Supersonic Fluid Amplifier Performance Characteristics, Honeywell, Inc. Systems and Research Division Document 6D-F-502, Vol. A, 1966.

VITA

Daniel Charles Anderson, Jr. was born in New Orleans, Louisiana on November 7, 1943. He attended Louisiana public schools in Caddo Parish and Lincoln Parish, and he graduated from Ruston High School, Ruston, Louisiana in June 1961. He entered the Louisiana Polytechnic Institute in September, 1961 and graduated with a Bachelor of Science degree in Mechanical Engineering in June 1965. Mr. Anderson was married in 1963 to the former Fredrica Carol Lee. In September, 1965 he entered the Georgia Institute of Technology and completed the requirements for a Master of Mechanical Engineering degree in March, 1967. During the summer of 1965 he was employed by the Atlantic Refining Company, Houston, Texas, and during the summer of 1967 he was employed at the Lockheed-Georgia Company, Marietta, Georgia. Since March, 1967 he has continued to pursue the Doctorate degree in the School of Mechanical Engineering.